

AD-A142 464

DETECTION OF SEVERE WEATHER BY FAA (FEDERAL AVIATION  
ADMINISTRATION) RADARS(U) JOHNS HOPKINS UNIV LAUREL MD  
APPLIED PHYSICS LAB E B DOBSON ET AL. SEP 79

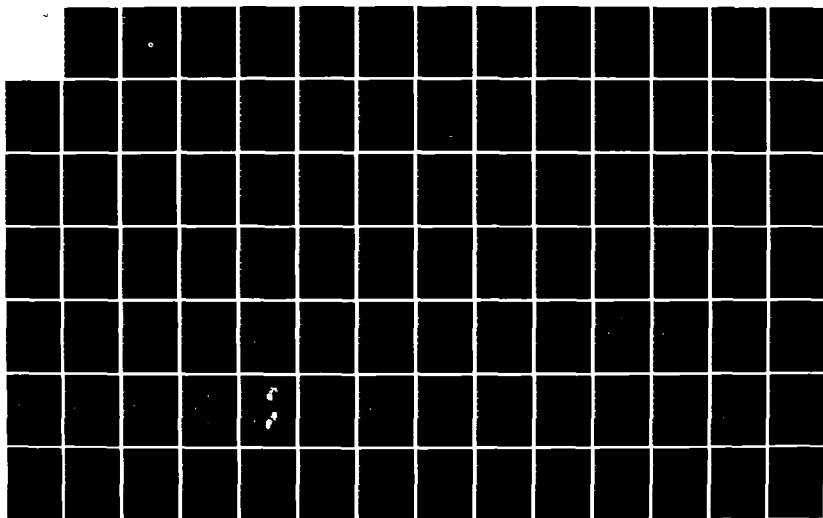
1/2

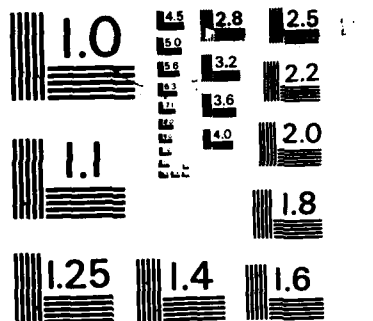
UNCLASSIFIED

FAA-RD-79-91 DOT-FA74WA-3423

F/G 17/9

NL





MICROCOPY RESOLUTION TEST CHART  
NATIONAL BUREAU OF STANDARDS - 1963 - A

9

# DETECTION OF SEVERE WEATHER BY FAA RADARS

ELLA B. DOBSON

FREDA L. ROBISON

ABRAHAM ARNOLD

THOMAS G. KONRAD

The Johns Hopkins University • Applied Physics Laboratory  
Laurel, Maryland 20810



SEPTEMBER 1979

FINAL REPORT

104  
A

Document is available to the U.S. public through  
the National Technical Information Service,  
Springfield, Virginia 22161.

Prepared for

**U.S. DEPARTMENT OF TRANSPORTATION**  
**FEDERAL AVIATION ADMINISTRATION**  
Systems Research & Development Service  
Washington, D.C. 20590

84 06 26 036

AD-A142 464

DTIC FILE COPY

NOTICE

This document is disseminated under the sponsorship of the Department of Transportation in the interest of information exchange. The United States Government assumes no liability for its contents or use thereof.

1. Report No. FAA-RD-79-91	2. Government Accession No. A142 464	3. Recipient's Catalog No.	
4. Title and Subtitle Detection of Severe Weather by FAA Radars		5. Report Date September 1979	6. Performing Organization Code
7. Author(s) Ella B. Dobson, Freda L. Robison, Abraham Arnold, Thomas G. Konrad		8. Performing Organization Report No.	
9. Performing Organization Name and Address The Applied Physics Laboratory The Johns Hopkins University Johns Hopkins Road Laurel, Maryland 20810		10. Work Unit No. (TRAIS)	11. Contract or Grant No. Tasks DOT FA74WA-3423; X-D & X-E
12. Sponsoring Agency Name and Address U.S. Department of Transportation Federal Aviation Administration Systems Research and Development Service Washington, D. C. 20590		13. Type of Report and Period Covered Final Report April 1977 - May 1979	
14. Sponsoring Agency Code FAA/ARD-243		15. Supplementary Notes	
16. Abstract A A need exists to improve the radar weather display available to air traffic controllers. In support of this objective, theoretical and corresponding empirical investigations were performed to validate the feasibility of using FAA radars (both terminal and enroute) as the sensors to provide the improved input for the weather displays. The theoretical investigation consisted of a computer simulation in which empirical weather data and the parameters of the FAA and NWS radars were used as inputs. By varying the position in range and height of reflectivity profiles, the amount of reflectivity that should be received by the various radars was computed and used to determine values of reflectivity for comparison purposes. The empirical program consisted of measurements by FAA and NWS radars of the power received from the same storms. This information was also converted into reflectivity values for comparison purposes. Both the theoretical and empirical results indicate the FAA radars (when operated in a mode optimized for weather detection) should be capable of providing improved input for use in the display of severe weather in support of air traffic control. NOTE: Varying amounts of equipment modifications and/or additions would be required (depending on the model FAA radar) for simultaneously obtaining optimized displays of aircraft and calibrated weather.			
17. Keywords Weather Radar Radar Reflectivity Severe Weather Weather Detection		18. Distribution Statement Document is available to the U.S. public through the National Technical Information Service, Springfield, Virginia 22161.	
19. Security Classif. (of this report) Unclassified	20. Security Classif. (of this page) Unclassified	21. No. of Pages 169	22. Price

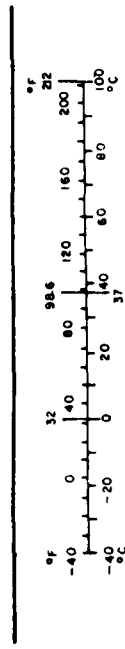
# METRIC CONVERSION FACTORS

## Approximate Conversions to Metric Measures

Symbol	When You Know	Multiply by	To Find	Symbol
<b>LENGTH</b>				
in	inches	2.5	centimeters	cm
ft	feet	30	centimeters	cm
yd	yards	0.9	meters	m
mi	miles	1.6	kilometers	km
<b>AREA</b>				
in <sup>2</sup>	square inches	6.5	square centimeters	cm <sup>2</sup>
ft <sup>2</sup>	square feet	0.09	square meters	m <sup>2</sup>
yd <sup>2</sup>	square yards	0.8	square meters	m <sup>2</sup>
ac	square miles	2.6	square kilometers	km <sup>2</sup>
	acres	0.4	hectares	ha
<b>MASS (weight)</b>				
oz	ounces	28	grams	g
lb	pounds	0.45	kilograms	kg
	short tons (2000 lb)	0.9	tonnes	t
<b>VOLUME</b>				
teaspoon	teaspoons	5	milliliters	ml
fluid ounce	fluid ounces	30	milliliters	ml
cup	cup	0.24	liters	l
quart	quarts	0.95	liters	l
gallon	gallons	3.8	liters	l
cu ft	cubic feet	0.03	cubic meters	m <sup>3</sup>
cu yd	cubic yards	0.76	cubic meters	m <sup>3</sup>
<b>TEMPERATURE (exact)</b>				
°F	Fahrenheit temperature	5/9 (after subtracting 32)	Celsius temperature	°C

## Approximate Conversions from Metric Measures

When You Know	Multiply by	To Find	Symbol
<b>LENGTH</b>			
millimeters	0.04	inches	in
centimeters	0.4	inches	in
meters	3.3	feet	ft
meters	1.1	yards	yd
kilometers	0.6	miles	mi
<b>AREA</b>			
square centimeters	0.16	square inches	in <sup>2</sup>
square meters	1.2	square yards	yd <sup>2</sup>
square kilometers	0.4	square miles	mi <sup>2</sup>
hectares (10,000 m <sup>2</sup> )	2.5	acres	ac
<b>MASS (weight)</b>			
grams	0.035	ounces	oz
kilograms	2.2	pounds	lb
tonnes (1000 kg)	1.1	short tons	
<b>VOLUME</b>			
milliliters	0.03	fluid ounces	fl oz
liters	2.1	pints	pt
liters	1.06	quarts	qt
liters	0.26	gallons	gal
cubic meters	35	cubic feet	ft <sup>3</sup>
cubic meters	1.3	cubic yards	yd <sup>3</sup>
<b>TEMPERATURE (exact)</b>			
°C	Celsius temperature	9/5 (then add 32)	Fahrenheit temperature



\* 1 in. = 2.54 (exact). \* 1 ft. = 0.3048 (exact). Conversions and more data in Tables, see NBS Mon. Pub. 286, Units of Weights and Measures, Pt. 1, p. 25. SO Catalog No. C13 11-286

DETECTION OF SEVERE WEATHER BY FAA RADARS

Final Report

EXECUTIVE SUMMARY



BACKGROUND

Federal Aviation Administration (FAA) air traffic controllers need up-to-the-minute weather information to vector aircraft when severe storm conditions are in the neighborhood. Storm positions, although available elsewhere from Weather Service radars, are frequently unavailable in a timely manner to the FAA under present operating conditions. The FAA terminal and enroute radars are intentionally operated in such a manner to maximize the detection and tracking of aircraft and to minimize the "clutter" of storms. The FAA recognizing the need to improve the radar weather display available to its air traffic controllers initiated studies designed to investigate the feasibility of an improved weather display capability using modified FAA air traffic control (ATC) radars.

APPROACH TO PROBLEM

Experiment

Experiments were performed by the FAA to investigate the possibility that the FAA radars might be reconfigured or modified to yield improved weather data along with aircraft data. Two experiments were carried out in the summer of 1977 in Oklahoma and Louisiana in which ARSR-1D and ASR-8 radars measured storm intensities simultaneously with Weather Service WSR-57 radars. The WSR-57 radars were used as a standard against which the FAA radars were compared.

Simulation

The experiments performed in Oklahoma and Louisiana tested the weather detection capabilities of two FAA radars. In order to extend the knowledge gained in the test to other FAA radars and to guide the interpretation of the experimental data,

a computer simulation was performed that used empirical weather data and the parameters of the FAA radars as inputs. The simulation involved positioning reflectivity profiles (i.e., reflectivity vs height) at various ranges and computing the amount of power that would be received from that range by a given FAA radar.

### Comparisons

#### Empirical - WSR-57 vs FAA

WSR-57 and FAA radar signal levels were recorded on video tape from which digitized magnetic tapes of the storm data were made. These digitized signals were used along with measured calibrations to compute reflectivity (Z) values in plan position indicator (PPI) format. After geometrical collocation of the data from the two radars, PPI displays that were contoured using the National Weather Service reflectivity levels were compared. In addition, comparisons were made of the amount of spatial area measured by each radar for a given level.

#### Simulation vs Empirical

To compare the empirical results to the simulation, WSR-57 measured reflectivity profiles from several storms were chosen and run through the simulation program to predict what the FAA radar should have measured for each profile. These simulated values were then compared to what the FAA radar actually measured.

### RESULTS

#### Simulation

##### Terminal

The simulation results show that the ASR-8 low beam and ASR-5 radars, whose normal operating range is 60 nmi (111 km), will on the average detect reflectivity levels that are within 3 dBZ of the WSR-57 when the maximum gain of the radars is positioned with the -3 dB point on the horizon. On the average, the FAA radars and the WSR-57 will underestimate the maximum. Operating at ranges less than 60 nmi, the FAA terminal radars are not seriously affected by lack of beamfilling storms or earth



curvature. The closest simulation range was 11 nmi (20 km), so that all results are for ranges 11 nmi and greater. No attempt was made to examine weather detection at clutter ranges, therefore, based on the simulation, no statement can be made regarding the adverse effects of close-in clutter on the detection of severe weather.

### Enroute

The ARSR-2/3 and ARSR-1D enroute radars on the average measure reflectivities that range between 5 to 10 dBZ down from the maximum reflectivity for ranges between 20 and 240 km when the maximum gain is positioned at 1° elevation. The ARSR-2/3 with a 4° (3 dB) beamwidth in general measure reflectivities closer to the maximum than the ARSR-1D with a 6° (3 dB) beamwidth. The wider beamwidths decrease the ability to measure the maximum because as the storm profile moves out in range a smaller percentage of the beam is filled due to the width of the beam at greater ranges and earth curvature. These beamfilling effects also cause the WSR-57 to measure less than the maximum. For the maximum gain positioned at 1°, the WSR-57 is approximately 5 dBZ below the maximum at 240 km.

In addition to beamfilling and earth curvature effects, the effects of integration within the beam at a given range also contribute to the measurement of reflectivity values by both the enroute and WSR-57 radars that are less than the maximum. At most ranges, the beam contains not only the maximum but values less than the maximum. At long ranges for storm profiles with the maximum at the surface the radar may not illuminate the maximum because it is below the horizon. For this reason, the enroute radars measure values closer to the maximum for storms that have the maximum reflectivity at an altitude considerably above the surface.

Positioning of the enroute radars with the -3 dB gain on the horizon reduces the reflectivity measurement, compared to 1° positioning, by approximately 1 dBZ for the ARSR-2 at 240 km and 3 dBZ for the ARSR-1D at the same range. At close in ranges

(i.e., less than 80 km) the ARSR-1D can be expected to measure reflectivities closer to the maximum with the -3 dB point on the horizon than it does with maximum gain at 1°. This is because the storm maximum can be expected to be illuminated more often with the higher gain position. At 1° elevation the maximum antenna gain is below the maximum unless the storm maximum is on the surface.

### Experimental

#### Terminal

Analysis of the terminal data were not included in this report because of difficulties encountered primarily in calibration, and data recording. Nonetheless, the successful check of the ARSR-1D against the WSR-57 leads to the conclusion that results of the simulation of the terminal radar are indeed valid, i.e., that the ASR radars will also give an accurate measure of storm intensity beyond the ground clutter regions.

#### Enroute

Six storm cells detected by the ARSR-1D radar and the WSR-57 were analyzed from recorded video signals. These storms were 55 (30) to 185 km (100 nmi) in range from the radar. The storm contours as seen by both radars were found to be similar in shape, location of the maximum, and in the area of the contoured levels. On the average, however, a difference of approximately 4 dB was found between the measured reflectivity values for the two radars. The source of this difference has not been found but it may well lie in the calibration of one or both of the radars or possibly in the positioning of the maximum gain of the ARSR-1D. Since this difference is not believed to be fundamental it can easily be taken into account in the future by calibration.

Overall comparisons for the six storm cells analyzed from the Oklahoma experiment showed that the ARSR-1D always measured contour levels similar to the WSR-57. The ARSR-1D beam-width appears to have little effect on the measurement of storms within 185 km. However, the simulation indicated that measurements

made by the enroute radars beyond approximately 240 km (130 nmi) should have a statistical correction applied to partially correct for the effects of beamfilling, earth curvature, and integration. Such a correction cannot be exact because storm height is not known in real time, however, it would enable the position and potential intensity of storms at long ranges to be more accurately displayed for controller use. That is, if a storm is detected at 300 km (162 nmi), for example, a knowledge of the beamwidth at that range would indicate that the maximum reflectivity in the storm must be above a certain threshold.

#### MTI

Moving Target Indicator (MTI) data were analyzed from the Oklahoma experiment. The analysis indicated that MTI as it is presently configured on the ARSR-1D will not provide accurate storm reflectivity estimates. This is attributed to limiting in the MTI receiver because of the small dynamic range and due to the unpredictability of storm paths with respect to the radar (i.e., radial vs tangential).

#### Simulation vs Experiment

Simulated ARSR-1D reflectivities when compared to measured ARSR-1D reflectivities gave a mean difference of 1.2 dBZ with a 4.5 dBZ deviation about that mean. A linear least squared fit gave a slope of .9 and an intercept of 5.1. The general agreement is considered good.

#### OVERALL CONCLUSIONS

The following conclusions are made based on the results from this study.

- (1) All ARSR radars can be used to measure and display meaningful weather data when operated in a mode optimized for weather detection within 240 km. This conclusion is based on both experimental results from the ARSR-1D and simulated results. The 240 km range restriction is imposed because beyond this range the effects of earth curvature, partially filled beams, and integration greatly degrade the estimates of storm intensity.

(2) All ARSR radars and the WSR-57 will, in general, underestimate the maximum reflectivity with the amount of underestimation dependent on storm range and position of the maximum in altitude. For storms with maximum reflectivity on the ground the underestimation increases with increasing 3 dB beamwidth. Thus, the WSR-57 with the 2 degree beam should be closer to the maximum. When the maximum is positioned at high altitudes the ARSR radars should detect the storm intensity more accurately than the WSR-57 radar in a normal scan mode (i.e., .5° or 1° elevation angle). This result is significant since there is evidence that severe storms have maximum intensity at higher altitudes during the period of peak development.

(3) The ARSR and the WSR-57 radars measure a reflectivity closer to an average of the total profile reflectivity (i.e.,  $\langle Z \rangle$ ) than to the maximum.

(4) The ARSR MTI systems as they are presently configured are not suitable for accurate weather measurement.

(5) At ranges greater than 240 km the ARSR radars should have a statistical correction factor applied to the received signal to account for partial beamfilling, earth curvature and integration effects. It should be noted that the WSR-57 should also have such correction if operated beyond this range. The exact nature of this statistical correction would have to be determined based on a study of average heights and profiles of severe storms. Since such a correction factor would be statistical in nature, it would not eliminate all reflectivity measurement errors at long ranges but rather reduce them.

(6) The simulation indicates that the ASR-8 low beam and ASR-5 are capable of detecting weather accurately within their normal operating range and outside the limits of ground clutter (i.e., MTI area). This statement assumes an operating mode which is suitable for detecting weather (i.e., linear polarization and  $R^{-2}$  STC curve).

(7) The ASR-8 high beam is not suitable for weather detection when operated as the sole source of the measurement. However,

when it is used in a range gating mode with the low beam and restricted to close-in ranges, it may measure reflectivity as accurately as the low beam. The reason for restriction of the high beam to short ranges is that its maximum gain is positioned at a higher elevation angle which causes it to illuminate the upper portions of storms at shorter ranges than the low beam. The high beam is operationally utilized at close-in ranges to minimize the reception of ground clutter. This improves MTI and weather reflectivity over ground-clutter performance.

(8) The location and strength of reflectivity echoes should aid air traffic controllers in determining areas of intense precipitation. It should be noted, however, that research studies concerning turbulence associated with thunderstorms have not established a clear relationship between intense reflectivity areas and turbulent areas. In fact, areas of significant turbulence have been observed to exist in the clear air outside the areas of reflectivity associated with the thunderstorm. Based on such studies, the recommended criteria is for aircraft to avoid higher reflectivity (46 dBZ and above - levels 4, 5, and 6) storm cores by 10 to 15 miles. Also, it can be said that high reflectivity areas (50 dBZ and above - levels 5 and 6) will contain intense precipitation and often aircraft damaging hail. Therefore, if reflectivity data is properly interpreted, such displayed information could materially assist the air traffic controllers.

NOTE: Varying amounts of equipment modifications and/or additions would be required (depending on the model FAA radar) for simultaneously obtaining optimized displays of aircraft and calibrated weather.

## TABLE OF CONTENTS

	<u>Page No.</u>
Executive Summary	iii
List of Figures	xii
Acknowledgements	xiv
1.0 Introduction	1
2.0 Simulation	3
2.1 Method of Simulation	3
2.2 Parameters for Comparison	9
2.2.1 WSR Reflectivity ( $Z_{WSR}$ )	9
2.2.2 Maximum Reflectivity ( $Z_{MAX}$ )	9
2.2.3 Total Reflectivity ( $\langle Z \rangle$ )	9
2.3 Computer Program	10
2.4 The FAA Radars	10
2.5 Empirical Weather Data	12
2.6 Discussion of Simulation Results	12
2.6.1 Individual Profiles - Terminal	14
2.6.2 Individual Profiles - Enroute	16
2.6.3 Mean Reflectivity for Profile Set	22
3.0 Experiments	31
3.1 New Orleans - Slidell	31
3.2 Oklahoma City - Norman	33
4.0 Data Reduction - Enroute	36
4.1 Digitizing Raw Data	36
4.2 Calibration - ARSR-1 and WSR-57	36
4.3 Averaging	38
4.4 Computation of Reflectivity	38

Table of Contents (continued)

	<u>Page No.</u>
4.5 Overlapping Pulse Volumes	41
4.6 Contouring and Area Calculation	42
5.0 Data Analysis - Enroute	45
5.1 Contour Comparison	45
5.2 Storm Cell Comparison (contours)	45
5.3 Area Comparisons	58
5.4 Comparison with the Simulation	58
5.5 Comparison of MTI and Log Video Data	61
6.0 Data Reduction and Analysis - Terminal	66
7.0 Interpretation of Results	67
7.1 Enroute Radars	67
7.2 Terminal Radar	68
8.0 Conclusions	69
9.0 Reference	72
 Appendix A - The Computer Program	
Appendix B - FAA Radar Gain Patterns	
Appendix C - ATC Enroute Weather Detection	
Appendix D - The Effect of Ground Reflections on Weather Reflectivity Measurements	

## LIST OF FIGURES

	<u>Page No.</u>
Figure 2-1. Sketch of a typical shaped beam antenna illumination of a storm.	4
Figure 2-2. Three typical reflectivity profiles.	13
Figure 2-3. Simulated reflectivity for ASR-8 and WSR-57 - Profile A.	15
Figure 2-4. Simulated reflectivity for ASR-8 and WSR-57 - Profile B.	17
Figure 2-5. Simulated reflectivity for ASR-8 and WSR-57 - Profile C.	18
Figure 2-6. Simulated reflectivity for ARSR-1D, ARSR-2, and WSR-57 - Profile A.	20
Figure 2-7. Simulated reflectivity for ARSR-1D, ARSR-2, and WSR-57 - Profile B.	21
Figure 2-8. Simulated reflectivity for ARSR-1D, ARSR-2, and WSR-57 - Profile C.	23
Figure 2-9. Mean reflectivity vs range for ASR-8, ASR-5, and WSR-57.	25
Figure 2-10. Mean reflectivity vs range for ASR-8, ASR-5, and WSR-57. Maximum gain positioned with -3 dB point on the horizon.	26
Figure 2-11. Mean reflectivity vs range for ARSR-1D, ARSR-2, and WSR-57.	28
Figure 2-12. Mean reflectivity vs range for ARSR-1D, ARSR-2, and WSR-57. Maximum gain positioned with -3 dB point on the horizon.	29
Figure 3-1. Relative locations of radars in Oklahoma and Louisiana experiments.	32
Figure 4-1. Calibration curves for ARSR-1D and WSR-57.	37
Figure 4-2. Illustration of overlapping pulse volumes for WSR-57 and ARSR-1D in Oklahoma.	43



List of Figures (continued)

Page No.

Figure 5-1.	B-scan showing reflectivities in a rectangular array of range and azimuth. Range is in nautical miles and azimuth is in degrees.	46
Figure 5-2.	Storm cell 1 - ARSR-1D and WSR-57 contoured reflectivity. .5° azimuth and 782 meter range resolution.	49
Figure 5-3.	Storm cell 1 - ARSR-1D and WSR-57 contoured reflectivity. 2° azimuth and 782 meter range resolution.	50
Figure 5-4.	Contoured WSR-57 measured reflectivity showing three elevation angles.	52
Figure 5-5.	Storm cell 2 - ARSR-1D and WSR-57 contoured reflectivity. .5° azimuth and 782 meter range resolution.	53
Figure 5-6.	Storm cell 3 - ARSR-1D and WSR-57 contoured reflectivity. .5° azimuth and 782 meter range resolution.	54
Figure 5-7.	Storm cell 3A - ARSR-1D and WSR-57 contoured reflectivity. .5° azimuth and 782 meter range resolution.	55
Figure 5-8.	Storm cell 4 - ARSR-1D and WSR-57 contoured reflectivity. .5° azimuth and 782 meter range resolution.	56
Figure 5-9.	Example of contoured reflectivity showing two levels.	57
Figure 5-10.	Storm cell 5 - ARSR-1D and WSR-57 contoured reflectivity.	59
Figure 5-11.	Ratio of ARSR-1D area to WSR-57 area at a level vs level number.	60
Figure 5-12.	Measured ARSR-1D reflectivity vs simulated ARSR-1D reflectivity for 18 WSR measured profiles.	62
Figure 5-13.	ARSR-1D measured reflectivity vs WSR-57 profile maximum at the same azimuth and range as the ARSR-1D measurement for 18 WSR measured profiles.	63
Figure 5-14.	Comparison of MTI and log video contours.	65

#### ACKNOWLEDGEMENTS

Grateful acknowledgement is given to Mr. Bill Goodchild and Mr. Robert Oliver of NAFEC who conducted the experiments at Oklahoma and Louisiana, respectively. Without the digitized data provided by them, the analysis would not have been possible. Thanks to Messrs. K. Coonley and I. D. Goldman of the FAA for helpful discussions and suggestions throughout this work. Thanks also to all the APL personnel who worked with us in this effort. Particularly Mr. Isadore Katz and Mr. John P. Berry. This work was performed under Federal Aviation Administration Contract DOT-FA74W-3423, Tasks X-D and X-E.

## DETECTION OF SEVERE WEATHER BY FAA RADARS

### Final Report

#### 1.0 INTRODUCTION

During certain seasons in various parts of the country severe storms occur which do great damage to life and property. These storms quite often are cells which contain intense precipitation, hail, strong updrafts and down drafts, and turbulent wind conditions. The tops of these convective storms may exceed 18 km (59 kft) and several such cells may occur aligned in squall lines over an extended range. It is well known that such storms present hazardous conditions for aircraft flying in their vicinity; therefore, the warning to pilots and air traffic controllers of the exact location and intensity of severe storms is necessary for aircraft safety. The avoidance of storm areas by wide areal avoidance is not economically feasible. A more viable approach would be to isolate those areas with most probable severe weather, and control around those areas only, thus reducing time and fuel cost. Radar, which has been used for this purpose by the National Weather Service (NWS) for many years, is the best tool available at present for measuring storm intensity remotely. The Federal Aviation Administration (FAA), recognizing the need to improve the radar weather display available to its air traffic controllers, initiated studies designed to investigate the feasibility of an improved weather display capability using FAA air traffic control (ATC) radars.

In April of 1977 the Applied Physics Laboratory (APL) was given the task of evaluating, through theoretical and experimental analysis, the detection and display capability of the Federal Aviation Administration's surveillance radars. These radars have the sensitivity to detect weather but are, in general, operated in a mode unsuitable for weather detection. That is, to maximize aircraft detection air traffic controllers usually operate with moving target indicator (MTI) and a sensitivity time control (STC) curve equivalent to an  $R^{-4}$  range correction or a special adjusted shape that depends upon siting conditions.

During periods of precipitation they may also operate with circular polarization. All of these modes are adverse to calibrated weather detection. In addition the FAA radars have wide-shaped antenna beams in the vertical in order to obtain altitude coverage. Wide-shaped beams are not generally used for weather detection. Considering these aspects of FAA radar operation and characteristics along with other problems, it was necessary to analyze their ability to detect intense weather.

The problem was approached in two parts. The first part was a simulation of detection using radar parameters and empirical weather data measured by weather research radars. The second part consisted of two experiments performed in Oklahoma and Louisiana, respectively. The Oklahoma test was run to test the reflectivity measurement capabilities of an enroute radar and the Louisiana test was run to test the terminal radar capabilities. In both cases an FAA radar measured and recorded weather data simultaneously with a NWS radar. The purpose of the experiments was to compare the optimized FAA radar measurement of weather reflectivity with that of the NWS radars which routinely use radar for weather tracking and forecasting.

This report presents the results of both parts of this study. It is intended that the results be used to determine the necessary operational and/or physical changes that must be made to FAA radars for maximizing weather detection. No evaluation of these changes or design of display equipment is included in this study.

## 2.0 SIMULATION

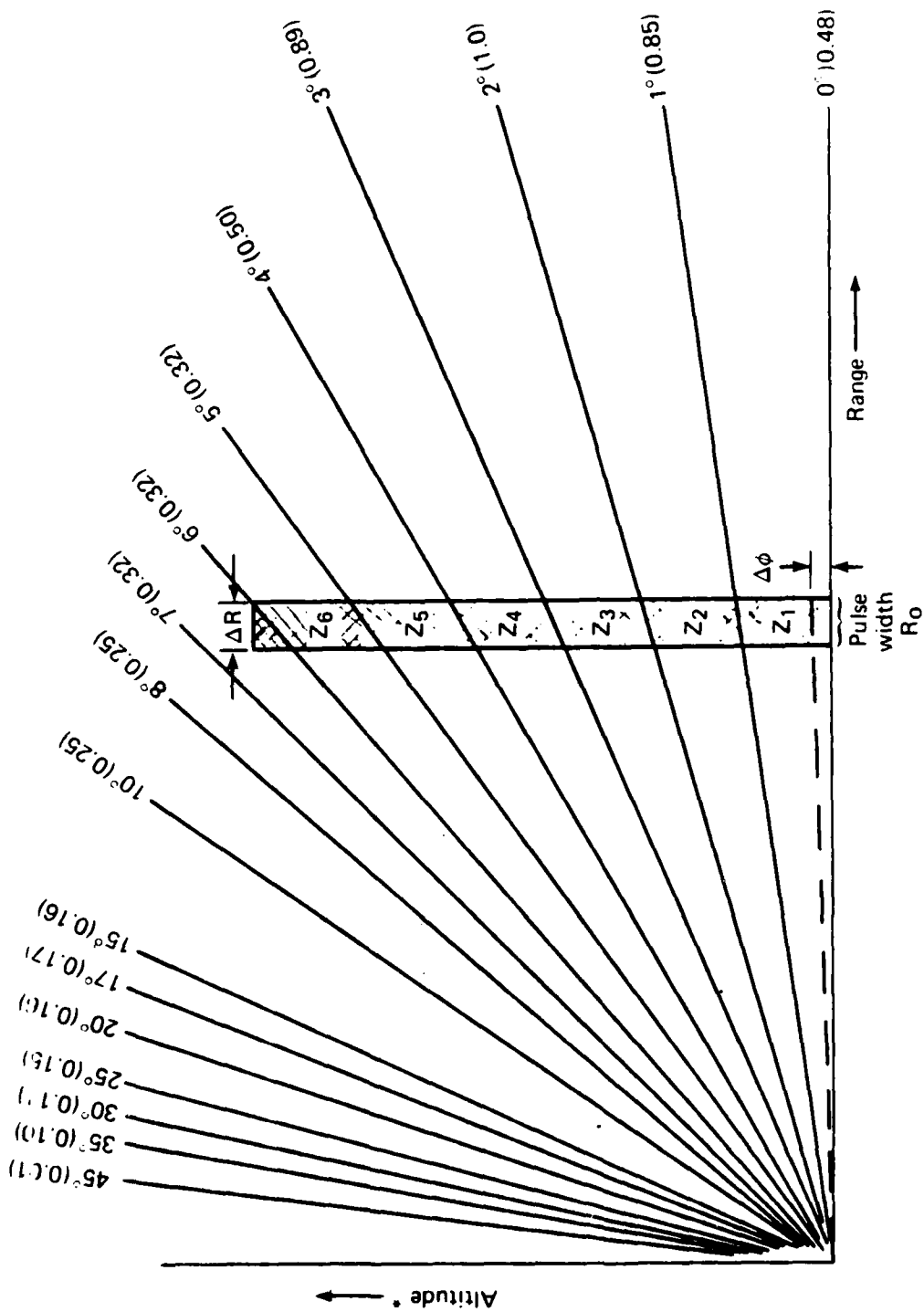
The experiments were performed to test two types of radars, the ARSR-1D and the ASR-8. The tests were run in specific locations and thus the storms were not necessarily representative of a wide variety of storms throughout the country. Therefore, a simulation study was designed which would predict the detection capability of weather by many FAA radars for various empirical reflectivity profiles measured throughout the country.

These weather detection simulations for both the enroute and terminal radars, using measured radar data and real gain patterns as inputs, provided insight which assisted in the interpretation of the results of the two experiments. This in turn allowed certain deductions to be made for other FAA radar types operating in different geographical locations.

### 2.1 Method of Simulation

The general approach to this simulation was to use the radar equation, radar parameters, and empirical radar reflectivity profiles to predict the received signal from a storm at various radar ranges. Because of the shape of the vertical gain pattern of the surveillance radars, the computational procedure will be discussed in detail.

Consider the sketch in Figure 2-1. Shown here are a series of elevation angles with an indicated reflectivity profile at some range,  $R_0$ . Assume that the profile has some range depth,  $\Delta R$ , and values of  $Z_1$  as a function of altitude. The sketch shows a typical shaped beam antenna illumination of a storm by indicating in parenthesis at each elevation angle the one way antenna gain relative to the maximum antenna gain. The illumination of any elemental volume,  $v_1$ , has associated with it a gain depending on the height or elevation angle. This changing gain, as given by the true antenna pattern, must be considered in the simulation. We designed the simulation by asking two questions: The first is, what power,  $P_r$ , will be received by the radar given that it



\* Altitude scale expanded approximately 8 times the range scale

Figure 2-1. Sketch of a typical shaped beam antenna illumination of a storm. Hatched areas indicate small volumes used in simulation. At each elevation angle the one way antenna gain relative to maximum antenna gain is indicated in parenthesis. Antenna tilt is 2°.

has detected a certain profile at a given range? Secondly, given a predicted power received, what is the radar reflectivity to be associated with it? We will proceed with the equations and methods of computation to answer these questions.

The weather radar equation can be expressed in several different ways, we have chosen the form given by Battan (1973). Consider the power received from an elemental volume.

$$P_r(\phi_i) = \frac{P_t G_T(\phi_i) G_R(\phi_i) \lambda^2}{(4\pi)^3 R^4} L_T \sum_{i=1}^n \sigma_i \quad (2.1)$$

where

- $P_t$  - peak transmitted power
- $R$  - slant range to the midpoint of the elemental volume
- $G_T(\phi_i), G_R(\phi_i)$  - transmit and receive gains over the elemental volume centered at angle  $\phi_i$  as given by the real measured antenna pattern
- $L_T$  - represents all system losses including receiver, antenna, and atmospheric
- $\sum \sigma_i$  - sum of all scatterers within the pulse volume  $v_i$ .

To simulate what the FAA radar antenna will measure, we will divide the precipitation volume into small volumes,  $v_i$ , defined by the horizontal beamwidth,  $\theta$ , the vertical angular element,  $\Delta\phi$ , and pulsewidth,  $c\tau/2$ .

Since we are calculating the small volumes as indicated by the stippled areas in Figure 2-1, the volume is given by

$$v_i = \pi \left( \frac{R}{2} \Delta\phi \right) \left( \frac{R}{2} \theta \right) \left( \frac{c\tau}{2} \right) = \frac{\pi}{4} R^2 \Delta\phi \theta \left( \frac{c\tau}{2} \right) \quad (2.2)$$

where

- $\theta$  - azimuthal beamwidth
- $\Delta\phi$  - is a small elevation angle increment
- $c\tau/2$  - range resolution
- $\tau$  - pulsewidth

In radar meteorology these scatterers ( $\sigma_i$ ) are in general assumed to be spheres of various diameters and the sum of their cross sections is denoted by  $Z$ .

$$\sum_{\text{vol}} \sigma_i = \frac{\pi^5}{\lambda^4} |K|^2 Z_i \quad (2.3)$$

where  $|K|^2$  is a function of index of refraction of ice or water. So that if we substitute (2.2) and (2.3) for  $\sum_{i=1}^n \sigma_i$  in Eq. (2.1) we get

$$P_r(\phi_i) = \left\{ \frac{P_t \pi^3 \theta c\tau |K|^2 L_T}{512 \lambda^2} \right\} \frac{G_T(\phi_i) G_R(\phi_i) Z_i \Delta\phi}{R^2} \quad (2.4)$$

or

$$P_r(\phi_i) = \frac{K_p G_T(\phi_i) G_R(\phi_i) Z_i \Delta\phi}{R^2} \quad (2.5)$$

Where  $K_p$  is the expression in brackets.

We will use Eq. (2.5) to compute the power at constant ranges for angles  $\phi_i$  across the vertical beam. The total power measured by the shaped-beam radar at any range,  $R$ , is then given by,

$$P_r(R) = \sum_{i=1}^M \frac{K_p G_T(\phi_i) G_R(\phi_i) Z_i \Delta\phi}{R^2} \quad (2.6)$$

where there are  $M$  increments of size  $\Delta\phi$  used in the computation.



This  $P_r(R)$  value as computed from Eq. (2.6) represents the simulated received power from the total pulse volume at range,  $R$ . We desire to compute a reflectivity,  $Z$ , value using  $P_r(R)$ . In order to do this let us write the radar equation in an integral form

$$P_r(R) = \frac{P_t \pi^2 |K|^2 L_T}{64 R^4 \lambda^2} \int_{\text{vol}} G_T(\phi) G_R(\phi) Z(R) dV \quad (2.7)$$

This equation is similar to Eq. (2.1) and is written in this manner in Eq. (2.7) to stress the  $\int G_T G_R Z(R) dV$ . To solve for  $Z(R)$  exactly given a single value of  $P_r(R)$ , it is necessary to solve the integral equation or know the  $Z$  profile from which the  $P_r(R)$  was measured. In real life we will have no knowledge of the real  $Z$  profiles, so an assumption is made to compute what we call an "effective reflectivity". The assumption is that  $Z$  is constant with height. If  $Z$  is a constant we can take  $Z$  out of the integral in (2.7) to obtain

$$P_r(R) \approx \frac{P_t \pi^2 |K|^2 L_T}{64 R^4 \lambda^2} Z_{\text{eff}} \int_{\text{vol}} G_T(\phi) G_R(\phi) dV \quad (2.8)$$

Note that  $Z_{\text{eff}}$  should not be confused with the "equivalent reflectivity",  $Z_e$ , usually used in radar meteorology.

The  $\int_{\text{vol}} G_T G_R dV$  can be expressed as a summation assuming that the gain pattern is available as a function of elevation angle

$$\int_{\text{vol}} G_T(\phi) G_R(\phi) dV \approx \frac{\pi}{4} R^2 \theta \frac{c\tau}{2} \sum_{i=1}^N G_T(\phi) G_R(\phi) \Delta\phi \quad (2.9)$$

So that (2.8) becomes

$$P_r(R) = \left\{ \frac{P_t \pi^3 |K|^2 \theta \frac{c\tau}{2} L_T}{256 \lambda^2} \right\} \frac{1}{R^2} Z_{eff} \sum_{i=1}^N G_T(\phi_i) G_R(\phi_i) \Delta\phi$$

The summation of gains in the equation above are performed over the antenna pattern from the horizon to the top of the pattern in elevation. If the pattern is divided into N equal angle increments the summation goes from 1 to N. Solving for  $Z_{eff}$

$$Z_{eff} = \frac{R^2 P_r(R)}{K_p \sum G_T(\phi_i) G_R(\phi_i) \Delta\phi} \quad (2.10)$$

We have chosen to use the integrated gain of the real antenna pattern in the computation of  $Z_{eff}$  for the FAA radars. Had we chosen to use the conventional equation,  $Z_{eff}$  would be computed by

$$Z_{eff} = \frac{R^2 P_r(R) 2 \ln 2}{K_p G_{MAX}^2 \phi} \quad (2.11)$$

where  $\phi$  is the 3 dB elevation beamwidth and  $2 \ln 2$  is the Probert-Jones correction for the FAA radar. It should be emphasized that while (2.11) could have been used for computation of  $Z_{eff}$  from the simulated power received, the integrated gain had to be used in the computation of  $P_r(R)$  to adequately describe a true power received. Equations (2.11) and (2.10) will essentially yield the same  $Z_{eff}$  when the  $\sum G_T(\phi_i) G_R(\phi_i) \Delta\phi$  in Eq. (2.10) is integrated from the -3 dB point on the horizon. This is not the case, however, for such an integration when the -3 dB is not on the horizon.

## 2.2 Parameters for Comparison

Up to now, only a simulated  $Z_{\text{eff}}$  has been discussed. Some method is needed to interpret this  $Z_{\text{eff}}$  in terms of true storm intensity. To do this there must be something with which to compare the  $Z_{\text{eff}}$ . Three quantities have been chosen for comparison with  $Z_{\text{eff}}$ . For clarity we will refer to these as (1)  $Z_{\text{WSR}}$ , (2)  $Z_{\text{MAX}}$ , and (3)  $\langle Z \rangle$ .

### 2.2.1 WSR Reflectivity ( $Z_{\text{WSR}}$ )

$Z_{\text{WSR}}$  is obtained by simulating what a  $2^\circ$  narrow beam radar would measure if it were positioned at  $1^\circ$  elevation angle. This quantity is obtained in exactly the same manner as the  $Z_{\text{eff}}$  except that a  $2^\circ$  Gaussian beam pattern and WSR-57 radar parameters were used.

### 2.2.2 Maximum Reflectivity ( $Z_{\text{MAX}}$ )

$Z_{\text{MAX}}$  is the maximum reflectivity in a profile and will be used to determine how well it is represented by  $Z_{\text{eff}}$ .

### 2.2.3 Total Reflectivity ( $\langle Z \rangle$ )

The several measures of  $Z$  used for comparison with  $Z_{\text{eff}}$  in the simulation ( $Z_{\text{WSR}}$  and  $Z_{\text{MAX}}$ ) are quantities that, in principle, are observable by a suitable radar (Weather Service radar and maximum reflectivity by a narrow-beam radar). There is a heuristic value in introducing another  $Z$ , which is independent of a radar and dependent only on the  $Z$  profile. We call this "total  $Z$ " (denoted as  $\langle Z \rangle$ ), where  $\langle Z \rangle$  refers to the storm profile itself. This quantity is defined as

$$\langle Z \rangle = \frac{1}{h} \int_0^h Z(h) dh$$

where  $h$  is height.

The three quantities discussed above will be the primary quantities used for comparison of  $Z_{eff}$ . However, others will be discussed in later sections as they arise.

### 2.3 Computer Program

Computer programs were written for the Hewlett-Packard 9825 computer to perform the simulation and mean reflectivity analysis. The main features of the programs which should be emphasized are: (1) The simulated power received is computed at  $.10^\circ$  elevation angle increments along the  $Z(h)$  profile using the gain appropriate to that height,  $h$ , and summed to the top of the storm, (2) The simulated power received from the FAA radar is turned into a  $Z_{eff}$  using Eq. (2.10), (3)  $Z_{WSR}$  is computed in a manner similar to  $Z_{eff}$  using the WSR-57 gain pattern, (4) Each profile is positioned in range at 20 km increments.

The simulation program computed the three variables,  $Z_{MAX}$ ,  $Z_{WSR}$ , and  $Z_{eff}$ , for 37 profiles and computed the difference between the first two and  $Z_{eff}$ . Another program was then used to compute the mean difference between these parameters and their correlation.

### 2.4 The FAA Radars

Six radar types were considered in the simulation. The nominal radar parameters for these radars are shown in Table 1. The antenna gain patterns for each of the radars is given in Appendix B. The main characteristics of all FAA radars are their wide-shaped vertical beams and narrow Gaussian horizontal beams. They all utilize MTI for ground clutter cancellation and may employ various other weather clutter rejection methods such as circular polarization CFAR, etc. In the case of the ASR-8 and ARSR-3, there are two beams on the radars called high and low beams. During normal operations the high beam and low beam are often used in a range gating mode. Transmission occurs via the low antenna beam and reception is achieved on either the low or high beam.

Table 1  
RADAR CHARACTERISTICS

	ARSR-1D	ARSR-2/1E	ARSR-3	ASR-8	ASR-4/5/6/7	WSR-57
Frequency (MHz)	1280 - 1350	1280 - 1350	1250 - 1350	2700 - 2900	2700 - 2900	2700 - 2900
Peak Power (kW)	500 or 4000	500 or 4000	5000	1500	425	500*
Pulse Repetition Rate (s <sup>-1</sup> )	360	360	310 - 365	1030	1200	164 (long pulse)
Pulse Width (μs)	2	2	2	.6	.83	4
Noise Figure (dB)	<4	<4	4 (Lo Beam)	4	4	8
Subclutter Visibilit. (dB)	27	27	23	28	25	(no MTI)
Cancellation Ratio	33 (dB)	33 (dB)	40 (dB)	34 (dB)	30 (dB)	(no MTI)
Minimum Detectable Signal (dBm)	-113 (1) -116 (2) -111 (3)	-113 (1) -116 (2) -111 (3)	-115 (4) -113 (5) -112 (3)	-110 (4) -109 (5) -108 (3)	-106 (1) -104 (3)	-109 (1)
Antennas which may be used with each radar	ARSR-1D	ARSR-2 (FA 7000)	ARSR-3 Lo Hi	ASR-8 Lo Hi	ASR-4/5/6/7	WSR
Beam Tilt Adjustment (deg)	-1 to +5	-1 to 5	-1 to 5	-0 to 5	-2 to 7	-10 to 45
Antenna Rotation Speed (rpm)	6	6	5	12.5	15	3

	Antenna	Maximum Gain (dB)	Horizontal Beamwidth (deg)
(1) normal	ARSR-1	34.3	1.35
(2) integrated	ARSR-2 (FA 7000)	34.0	1.2
(3) MTI	ARSR-3 Lo	34.5	1.25
(4) log CFAR	Hi	33.5	1.25
(5) weather	ASR-8 Lo	34.0	1.35
(6) log	Hi	34.0	1.35
	ASR-4/5/6/7	34.0	1.5
	WSR-57	38 - 40	2.2

\*During the Oklahoma experiment, NSSL operated this radar at approximately 370 kW peak.

The gain patterns for each of these radars were read at .5° elevation angle increments and recorded on HP 9825 cassette tapes for use in the program.

## 2.5 Empirical Weather Data

Many research groups have been involved in the study of thunderstorms using radar as a remote sensing tool to measure the intensity and spatial distribution of precipitation within storms. For this simulation, we have chosen profiles of radar reflectivity vs altitude from many of these researchers.

There were 37 profiles used in the simulation and the set contains basically three types such as those shown in Figure 2-2. They are: (A) The reflectivity is constant from the ground to some altitude and decreases with altitude from that point to the top of the storm. (B) The reflectivity is lower on the ground than it is aloft. (C) The reflectivity is maximum on the ground and decreases gradually to the top of the storm. The shape of these profiles may be indicative of the type of storm although little research has been done to determine this.

Some of the profiles are of thunderstorms with hail. The size that hail reaches can be much greater than raindrop sizes. Such hail with a coating of water will produce an especially high return (reflectivity is proportional to the sixth power of a linear dimension). The profiles used in the simulation were taken from thunderstorms for the most part because it is primarily these storms that are potentially dangerous to aircraft.

## 2.6 Discussion of Simulation Results

In the simulation, 37 reflectivity profiles were analyzed as mentioned previously. In this section the three shown in Figure 2-2 will be used for discussion along with the ARSR-2 and ASR-8 radars. Profile A was positioned in range and a simulated detection by the ARSR-2 and ASR-8 radars was computed. In addition, the parameters  $Z_{WSR}$  and  $\langle Z \rangle$  were computed.

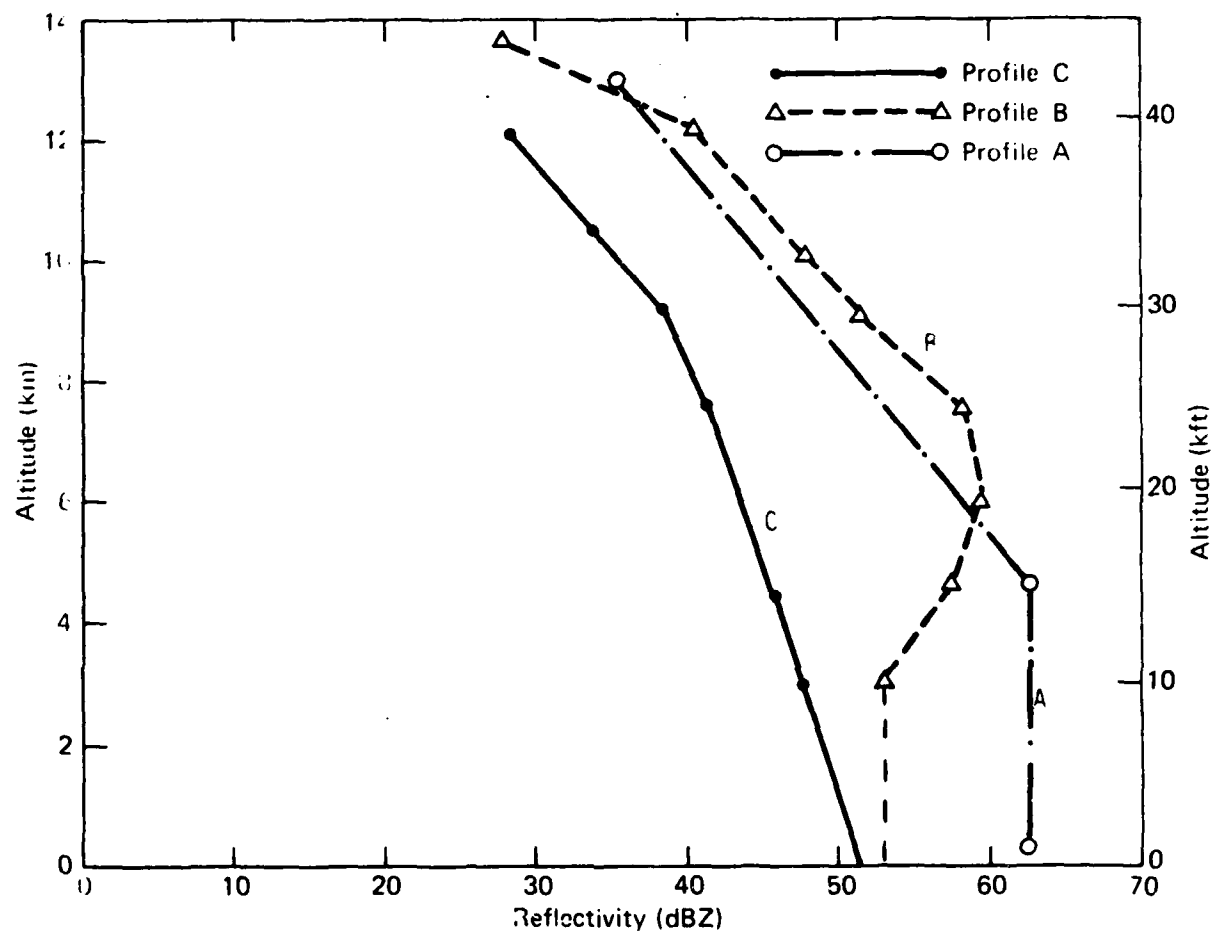


Figure 2-2. Three typical reflectivity profiles.

Reflectivity, as a function of range, is shown for profiles A, B, and C and the various radars in Figures 2-3 through 2-8. Two radar positions are shown for the ARSR-2. One is with the position of maximum gain (PMG) at  $1^\circ$  and the other with PMG such that the -3 dB point of the gain pattern is on the horizon, PMG at  $2^\circ$ . The ARSR-1 is shown for a  $1^\circ$  PMG.

#### 2.6.1 Individual Profiles - Terminal

The values of the reflectivity calculated for the ASR-8 low beam at  $1^\circ$  PMG, using profile A, lie within 3 dBZ of the maximum at all ranges and are within 2 dBZ of  $\langle Z \rangle$ , as can be seen in Figure 2-3. The ASR-8 low beam positioned at  $2.5^\circ$  PMG measured a reflectivity within 4 dBZ of the maximum at all ranges. The WSR-57 measures the profile within 1 dBZ at all ranges.

The 3 dB beamwidth of the radars and the portion of the vertical profile being illuminated determines the radar's estimate of reflectivity. Profile A is constant from the ground to 4.6 km (15 kft) and decreases at 3 dBZ per km from this height to 13 km (43 kft). Therefore, the WSR-57 ( $1^\circ$  PMG) is illuminating only the maximum at ranges less than 111 km (60 nmi). The ASR-8 low beam ( $1^\circ$  PMG) starts to illuminate the upper portion of the storm at approximately 69 km (37 nmi) and therefore measures a reflectivity lower than the maximum beyond this range. As the storm moves out in range more of the upper portion is illuminated and the ASR-8 low beam reflectivity decreases further from the maximum. The ASR-8 high beam ( $4.5^\circ$  PMG) starts to drop below the maximum at an even shorter range for the same reason. In addition, the ASR-8 high beam ( $4.5^\circ$  PMG) has only a portion of the beam filled starting at approximately 100 km (54 nmi) range and so for this radar at  $4.5^\circ$  PMG the reflectivity is also being reduced due to partial beamfilling. The same thing applies to the ASR-8 high beam ( $6^\circ$  PMG) with a greater effect on the reflectivity measure.

Good overall reflectivity performance is achievable by range gating of the ASR-8 high and low beams as a function of



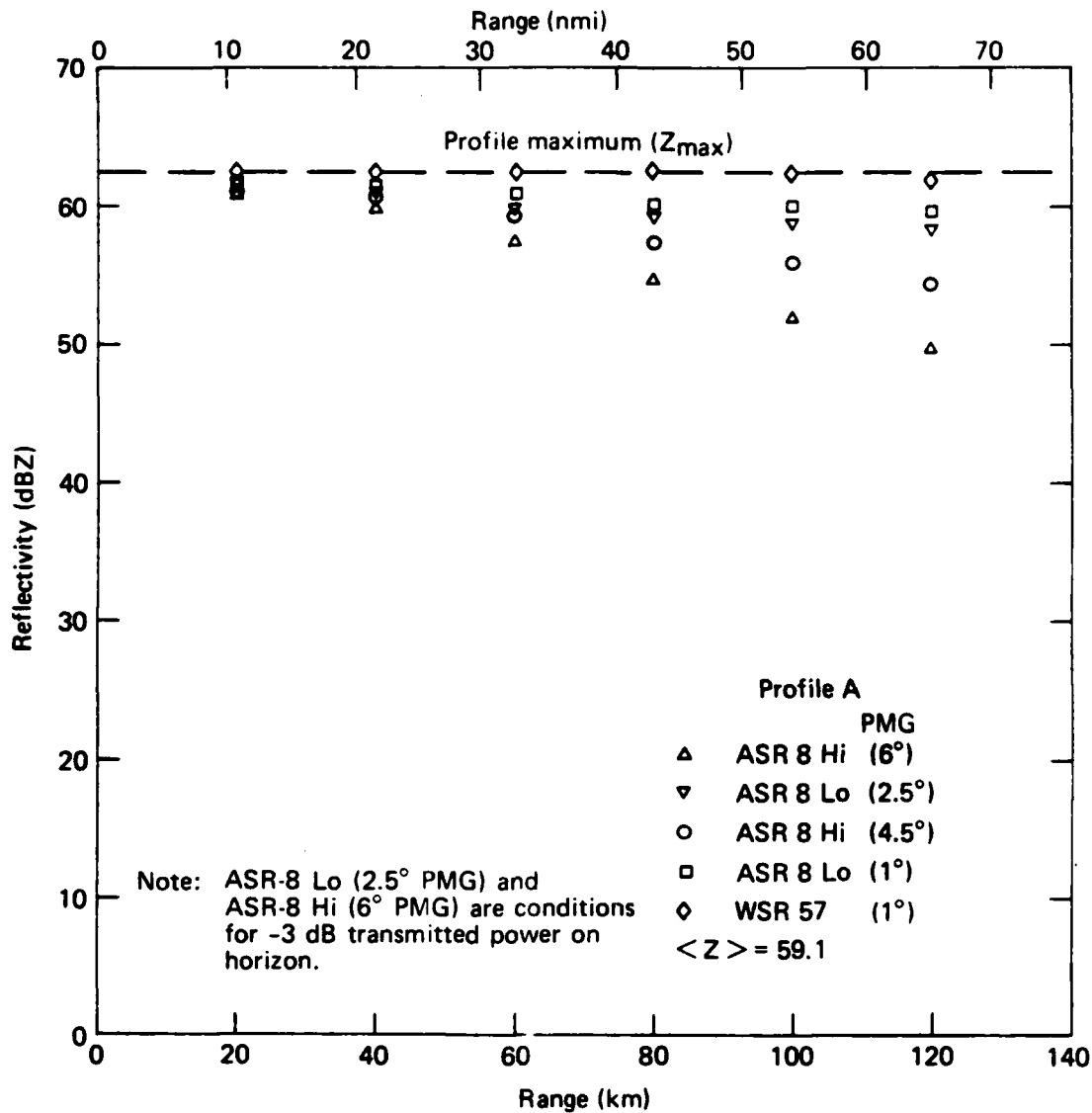


Figure 2-3. Simulated reflectivity for ASR-8 and WSR-57 - Profile A.

azimuth (RAG) such that the high beam is only utilized at close-in ranges when necessary to minimize the reception of ground clutter. This permits improvements in MTI and weather reflectivity performance.

The results from profile B, shown in Figure 2-4, show a different effect. In this case the profile has its maximum reflectivity at 6.2 km (20 kft) height. The terminal radars with wider beams illuminate the maximum at shorter ranges than the WSR-57 with its 2° beam. However, because the reflectivity is less than the maximum below 6 km the reflectivity averaged over the beam is less than the maximum for all radars at all ranges. The ASR-8 high beam (6° PMG) falls off from the maximum more at 120 km because the beam is partially filled.

The reflectivities for profile C shown in Figure 2-5 have a trend very similar to those of profile A. This should be expected since profile C has its maximum on the ground and the maximum is illuminated starting at very short ranges.

It should be noted that for all three profiles,  $\langle Z \rangle$  is less than the maximum because it is an effective average over the total profile. In addition, values of reflectivity for the various radars are closer to  $\langle Z \rangle$  than the maximum. Notable exceptions exist due to the particular spatial relationships for profile A between the storm's maximum, the points of the maximum antenna gains, and the antenna vertical beam shape. In general, radars do not illuminate profiles that are constant with respect to reflectivity within the beam (as is the case for profile A), hence all radars including the WSR-57 measure values of reflectivity closer to  $\langle Z \rangle$  than to the maximum.

#### 2.6.2 Individual Profiles - Enroute

The FAA enroute radars and the WSR-57 are affected by partial beamfilling and earth curvature. The results in Figures 2-6 through 2-8 show this effect rather vividly. Because these effects cause increasing error with increasing range on all three

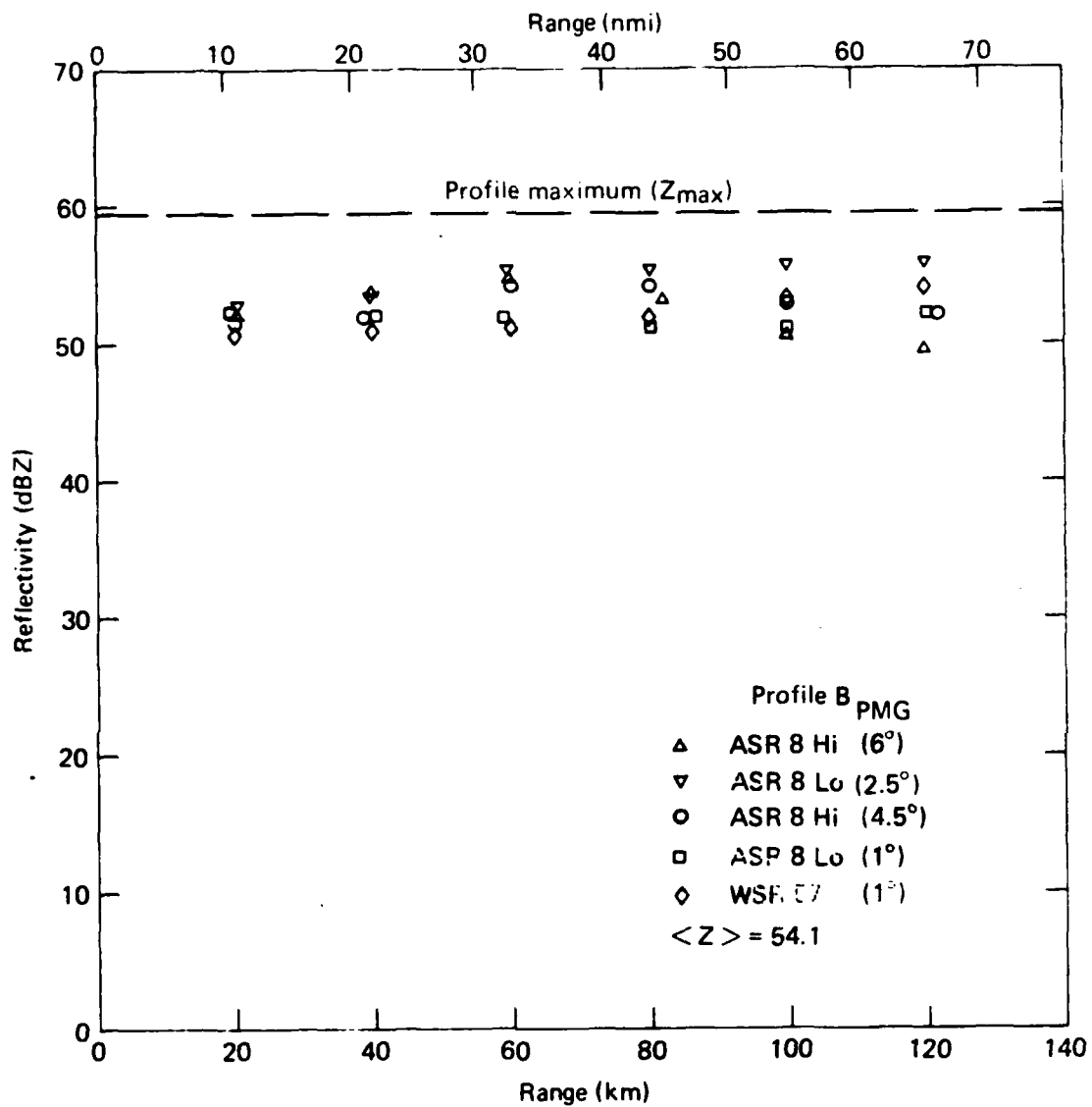


Figure 2-4. Simulated reflectivity for ASR-8 and WSR-57 - Profile B.

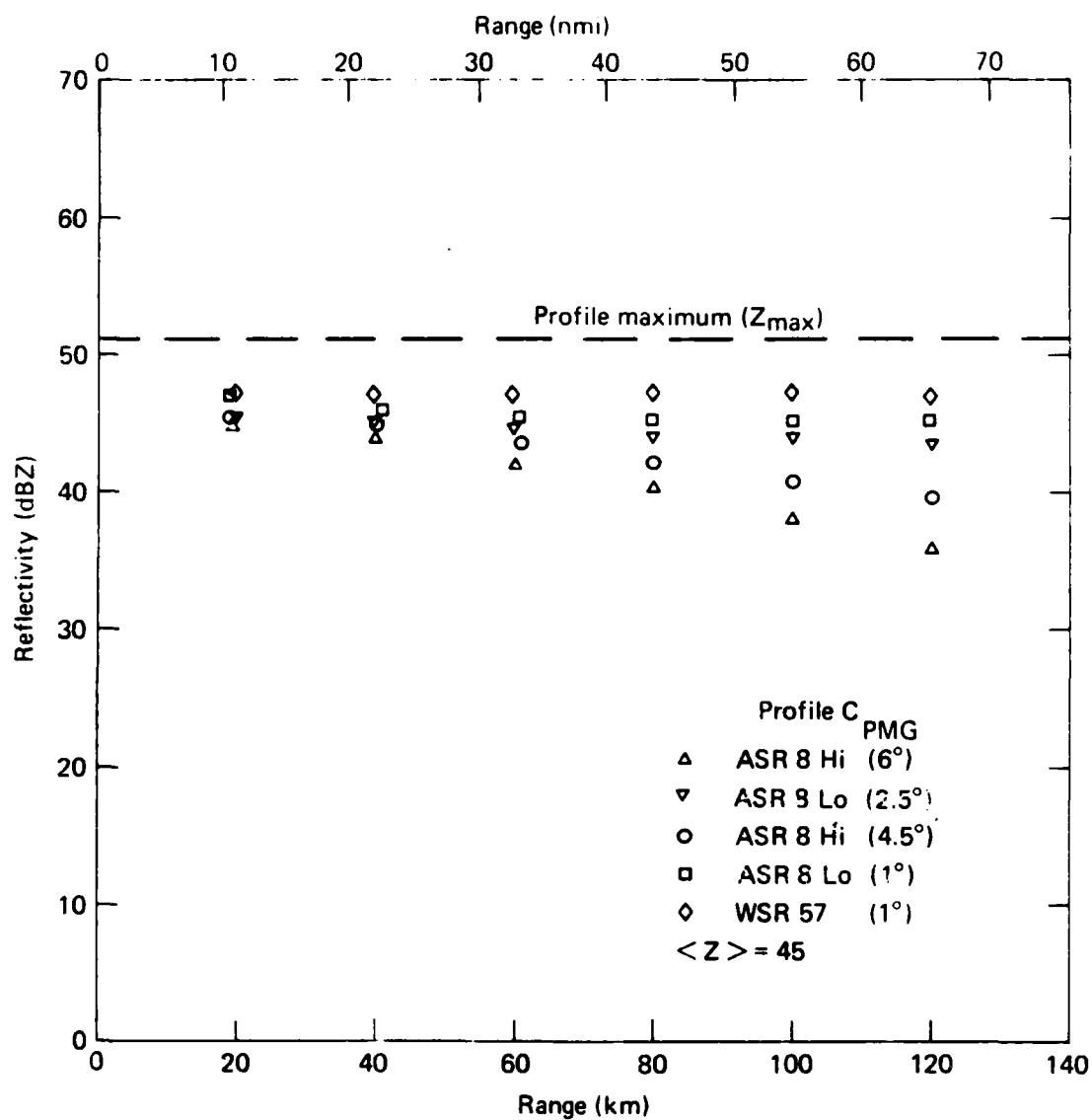


Figure 2-5. Simulated reflectivity for ASR-8 and WSR-57 - Profile C.

profiles, we will restrict discussion of the results to ranges less than approximately 240 km (130 nmi). This 240 km range is close to the normal operating range of the WSR-57.

Consider the results of profile A in Figure 2-6. Inside of 120 km (64.8 nmi) the ARSR-2 (1° and 2° PMG) is within about 4 dBZ of the maximum. Beyond this range the ARSR-2 reflectivity at 2° PMG decreases more rapidly than the ARSR-2 at 1° PMG. The ARSR-1D at 1° PMG has a steady fall off from the maximum out to 240 km and measures reflectivities comparable to the ARSR-2 (2° PMG) at 240 km. The WSR-57 also falls off from the maximum starting at approximately 140 km.

The relative effects of illuminating the total profile A, and beamfilling can be illustrated by considering the reflectivity measurements at 200 km (107.9 nmi) in Figure 2-6. The ARSR-1D (1° PMG) is about 75% filled and is illuminating the profile from about 2.3 km (7.5 kft) to the top. The reflectivity measured by the ARSR-1D (1° PMG) at 200 km is 56 dBZ or approximately 6.5 dBZ down from the maximum. About 1.2 dBZ of this difference can be attributed to partial beamfilling while the rest is due to averaging of the profile within the beam above the horizon. Similar reasoning can be used for the behavior of ARSR-2 reflectivity measures.

Profile B results are shown in Figure 2-7. As with the terminal radars, the wider beams of the enroute radars illuminate the maximum at shorter ranges than the WSR-57. However, as mentioned in previous discussion of this profile (i.e., terminal case), all radars fall short of measuring the maximum at all ranges. Regardless of the effects of earth curvature or partial beamfilling, there is no range inside of 240 km where only the maximum value is within the beam. Therefore an averaged quantity is measured. The ARSR-2 (1° PMG) measures values 7 dBZ down from the maximum at 40 km as compared to 8 dBZ down by the WSR-57. The ARSR-2 (1° PMG) reflectivities increase from this range up to

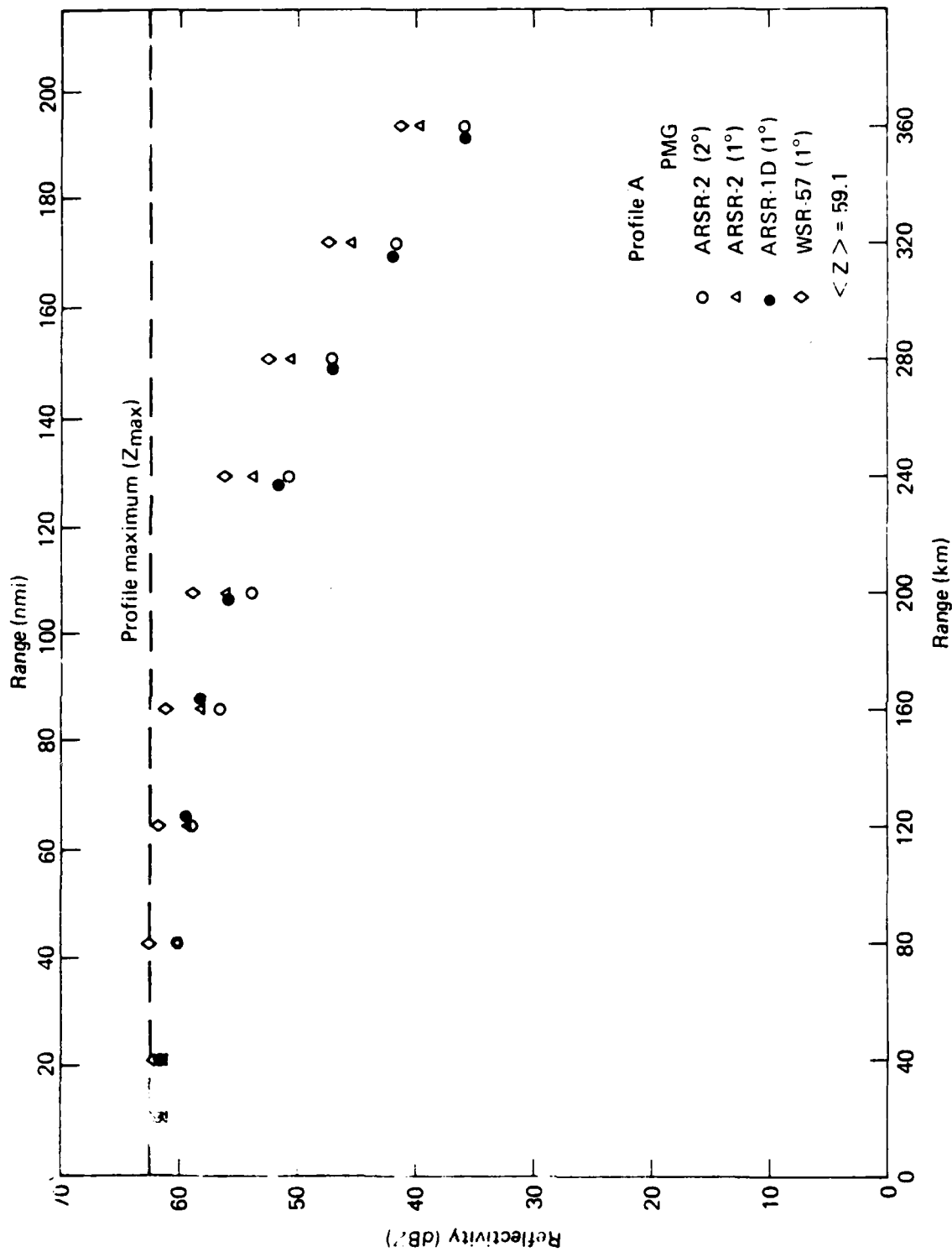


Figure 2-6. Simulated reflectivity for ARSR-1D, ARSR-2, and WSR-57 - Profile A.

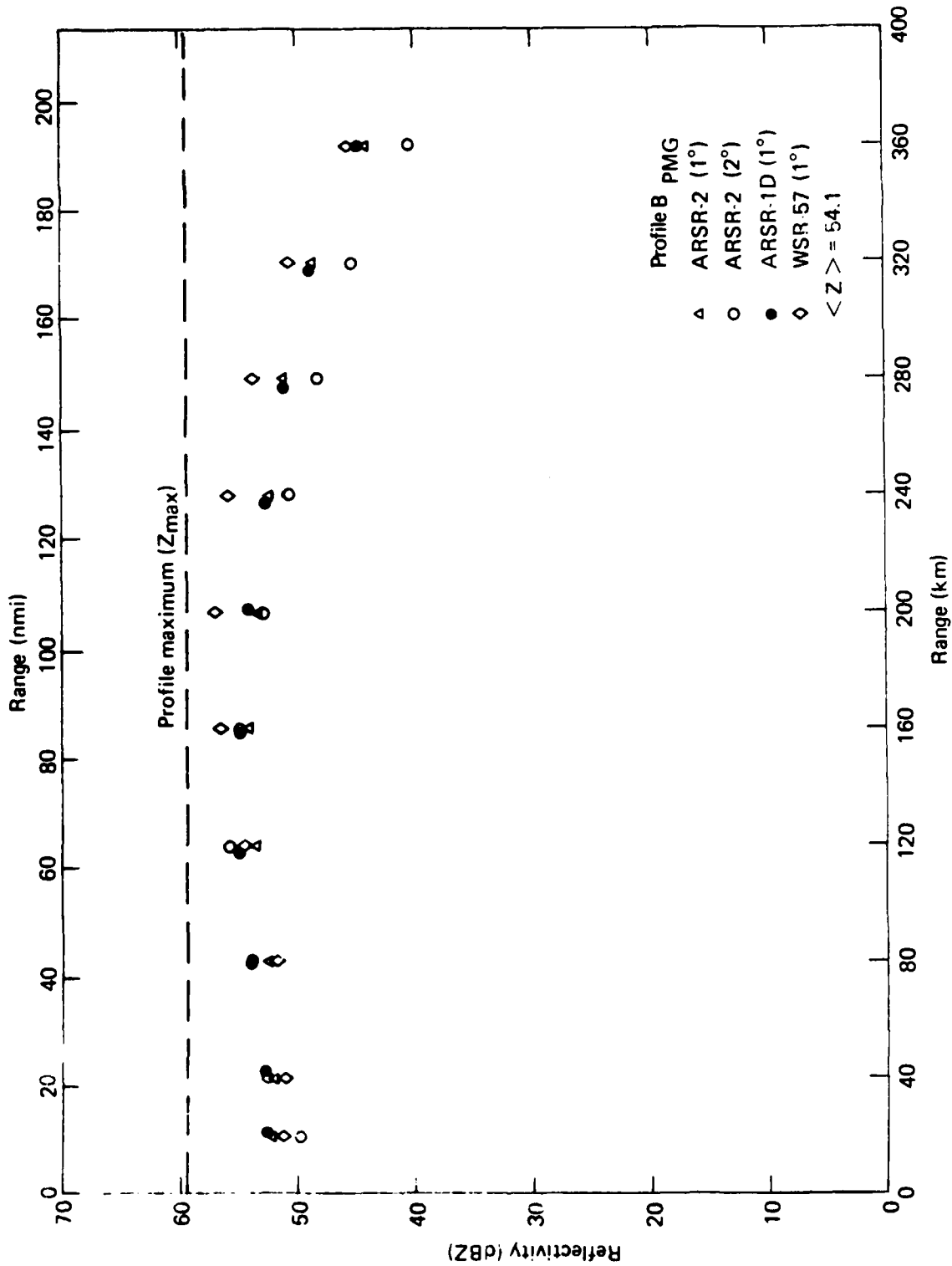


Figure 2-7. Simulated reflectivity for ARSR-1D, ARSP-2, and WSP-57 - Profile B.

a value which is 5 dBZ below the maximum at 160 km and decrease from this point on. The ARSR-2 (2° PMG) measures within 3.5 dBZ of maximum at 120 km. The ARSR-1D (1° PMG) measures within 4 dBZ of maximum at 120-160 km. The range at which the particular radar's reflectivity is closest to the maximum varies depending on the width and position of the beam. The WSR-57 measures closest to the maximum at 200 km where it is within 2 dBZ because its full narrower beamwidth illuminates the best portion of the profile at that range.

The results of profile C shown in Figure 2-8 indicate that none of the radars measure the maximum exactly at any range. Again, this is because an average of the total profile within the beam is being measured rather than the maximum. This is evidenced by the fact that the radars measure values closer to  $\langle Z \rangle$  than to the maximum. The general trend in reflectivity values from profile C is a decrease with range attributed to the portion of the profile being illuminated, partial beamfilling and earth curvature. The amount of the decrease depends on the range and the particular radar making the measurement.

Results from the ARSR-3 have not been included in Figures 2-6 through 2-8 because the  $Z_{eff}$  values are, in general, within 1 dBZ of the ARSR-2 at the same PMG.

#### 2.6.3 Mean Reflectivity for Profile Set

The data chosen for the profile set used in this study reflects research data from the various parts of the United States. It does not represent a statistical sample. Storm research using radars is still in the early stages with respect to a statistical model or models representative of various areas of the country. Therefore, the reason for discussing the mean reflectivity for 37 profiles is not for universal application of the results in a statistical sense. Rather the presentation of the mean for the profile set allows a convenient method of discussing average results a given radar would produce. The profile



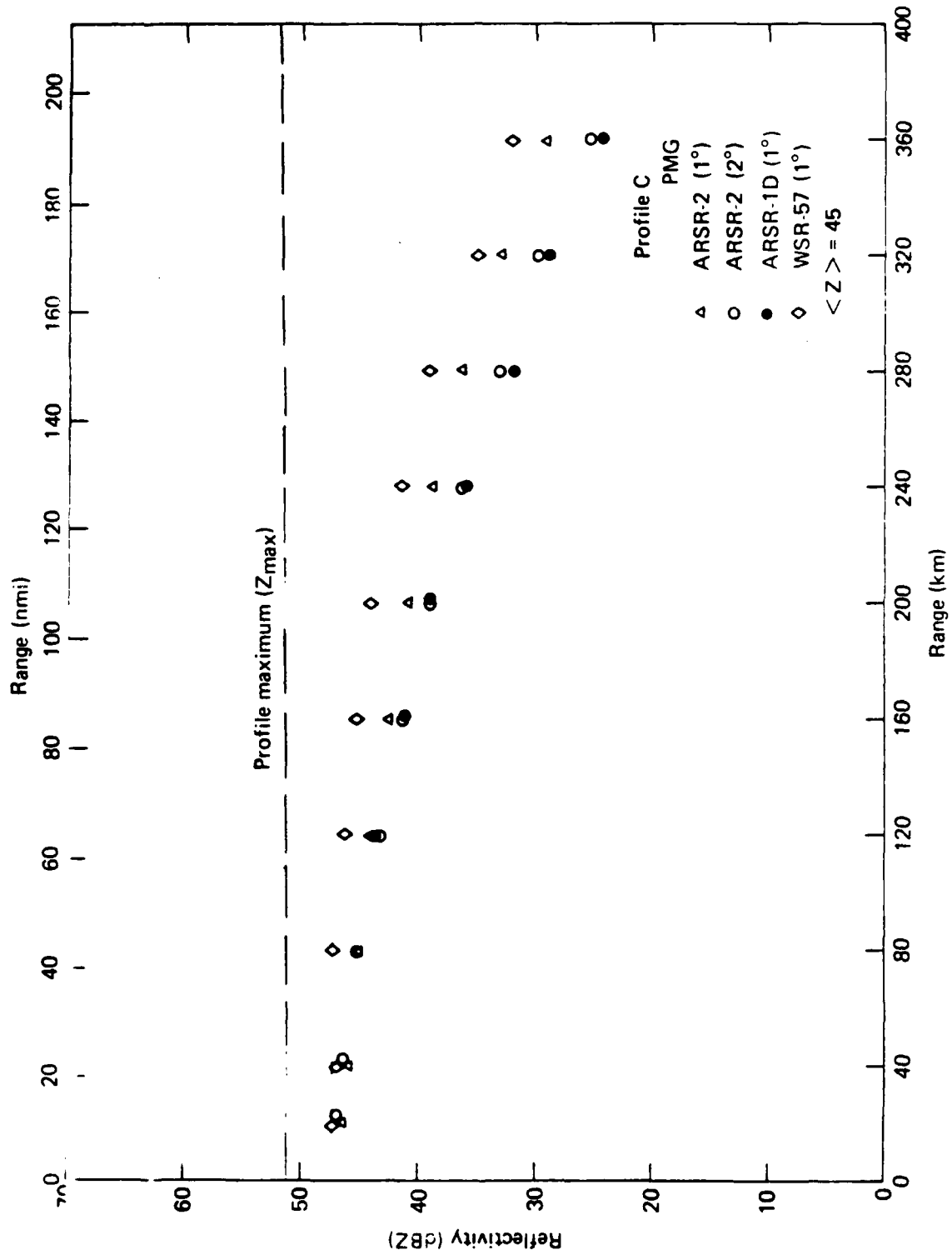


Figure 2-8. Simulated reflectivity for ARSP-1D, ARSP-2, and WSR-57 - Profile C.

set does include a wide range of reflectivities, shapes, and maximum altitudes. However, none of the profiles have maximum reflectivities less than 30 dBZ and it is highly improbable that a storm cell with maximum reflectivity less than 30 dBZ is severe.

The procedure for obtaining the mean reflectivities discussed in this section is as follows: (1) results such as those shown in Figure 2-6 were computed for each of the thirty-seven profiles. That is, a  $Z_{\text{eff}}$  and  $Z_{\text{WSR}}$  were computed as a function of range for each profile. (2) A  $Z_{\text{MAX}}$  and  $\langle Z \rangle$  were obtained for each profile. (3) The mean reflectivities were then obtained by averaging the 37  $Z_{\text{eff}}$  values at each range and the 37  $Z_{\text{WSR}}$  values at each range. (4)  $\overline{\langle Z \rangle}$  and  $\overline{Z_{\text{MAX}}}$  are quantities obtained from averaging the 37 values of  $\langle Z \rangle$  and  $Z_{\text{MAX}}$ , respectively. To interpret  $\overline{Z_{\text{MAX}}}$  in terms of the radars one can say that if a given radar at some range had measured  $Z_{\text{MAX}}$  exactly for all 37 profiles, then its mean reflectivity would be equal to  $\overline{Z_{\text{MAX}}}$ . Therefore, comparing the mean reflectivities of the data to  $\overline{Z_{\text{MAX}}}$  gives an indication of the average performance of the radar in measuring maximum reflectivities for the profile set.

The ASR-8 Low and ASR-5 have very similar gain patterns so it should be expected that the results would be similar. The data show (see Figs. 2-9 and 2-10) that on the average for the profile set the ASR-8 low and ASR-5 (outside the MTI area) are within 1 dBZ of  $\overline{\langle Z \rangle}$  at all ranges for 1° PMG and within 1.5 dBZ of  $\overline{\langle Z \rangle}$  for 2.5° PMG (-3 dB on horizon). On the average these two radars underestimate  $\overline{Z_{\text{MAX}}}$  by between 3 and 4 dBZ at 1° PMG and up to 5 dBZ at 2.5° PMG at terminal ranges. The WSR-57 underestimates  $\overline{Z_{\text{MAX}}}$  by between 2 and 3 dBZ and is within 1.5 dBZ of  $\overline{\langle Z \rangle}$  for 1° PMG. It should be noted that a 1° PMG for the WSR-57 is the same as the -3 dB point on the horizon.

The ASR-8 high beam is positioned such that at both antenna tilt positions analyzed there is a greater decrease in reflectivity with range than for the corresponding ASR-8 low beam. The ASR-8 low beam provides a much better reflectivity

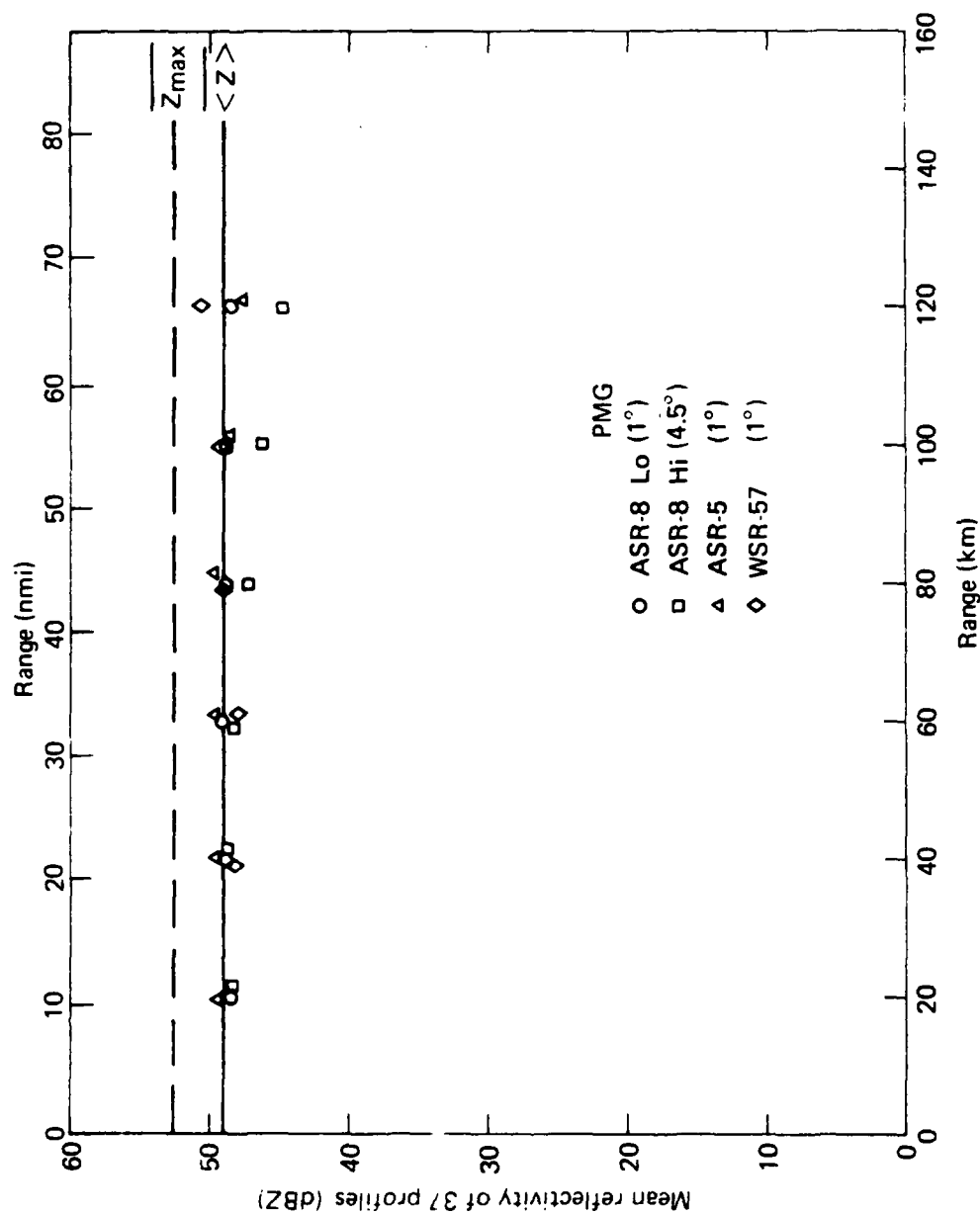


Figure 2-9. Mean reflectivity vs range for ASR-8, ASR-5, and WSR-57.

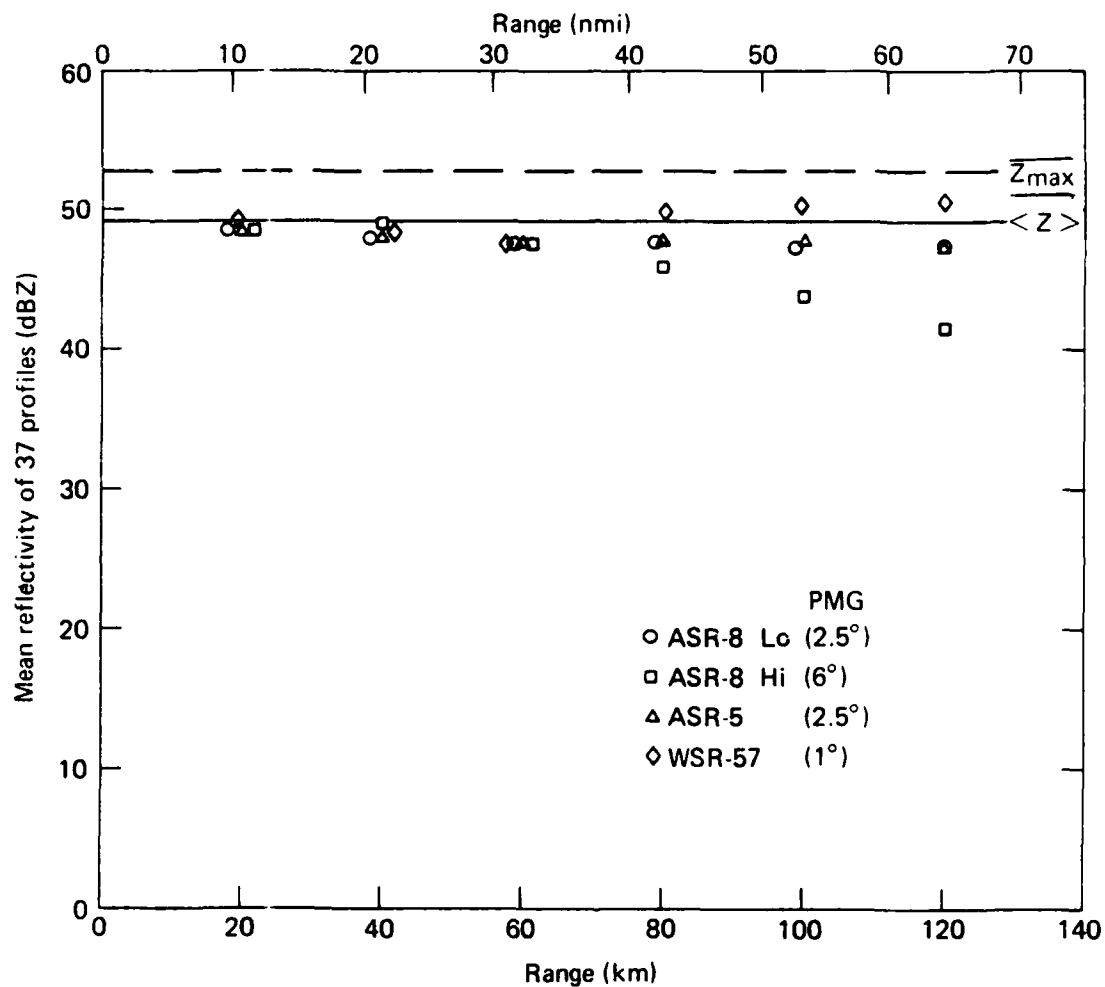


Figure 2-10. Mean reflectivity vs range for ASR-8, ASR-5, and WSR-57. Maximum gain positioned with -3 dB point on horizon.

measure than the ASR-8 high beam at all ranges greater than 60 km (32.4 nmi). Refer to Section 2.6.1 for range gating of ASR-8 beams to achieve overall improvements in the MTI and weather performance.

The mean reflectivities which are shown in Figures 2-11 and 2-12 for the enroute radars reflect the influence of the 3 dB beamwidth as a function of range. At ranges less than about 80 km (43.2 nmi) the ARSR-1D with its 6° beamwidth illuminates a larger portion of the storms than the WSR-57 and ARSR-2 at both beam positions considered. This larger beam is advantageous in those cases where the storms peak at altitude. Inside 80 km, this is reflected in the ARSR-1D reflectivity values which are closer to  $\overline{Z}_{MAX}$  than the other two radars. For example, with the -3 dB point on the horizon (Figure 2-12) at 80 km the differences between  $\overline{Z}_{MAX}$  for the ARSR-1D, ARSR-2, and WSR-57 are respectively, 1.2, 3.0, and 4.0 dBZ. As the range increases the ARSR-2 and the WSR-57 measure closer to the  $\overline{Z}_{MAX}$  than the ARSR-1D with the estimate of  $\overline{Z}_{MAX}$  degrading increasingly with range for all the radars. At 240 km (129.6 nmi), the ARSR-1D, ARSR-2, and WSR-57 are on the average 12, 8, and 4.5 dBZ low in the measurement of  $\overline{Z}_{MAX}$ .

The data in Figure 2-12 show that on the average for the profile set, the ARSR-1D at 3° PMG is 12 dBZ down from  $\overline{Z}_{MAX}$  and the ARSR-2 at 2° PMG is 8 dBZ down from  $\overline{Z}_{MAX}$  at 240 km, while the WSR-57 at 1° PMG is 4.5 dBZ down from  $\overline{Z}_{MAX}$  at 240 km. The ARSR-2 at 2° PMG is about 4 dBZ down and the ARSR-1D at 3° PMG is about 8 dBZ down from  $\langle Z \rangle$  at 240 km range as compared to only 1 dBZ down from  $\langle Z \rangle$  at 240 km by the WSR-57 at 1° PMG. This may not be as serious as it sounds, because knowing that the potential for this exists, average corrections vs range can be made. In other words, unlike meteorological research where accurate dBZ measures are needed for computation of rain rate and the dynamics of atmospheric physics, the controllers require a knowledge of location and potential severity of storms.

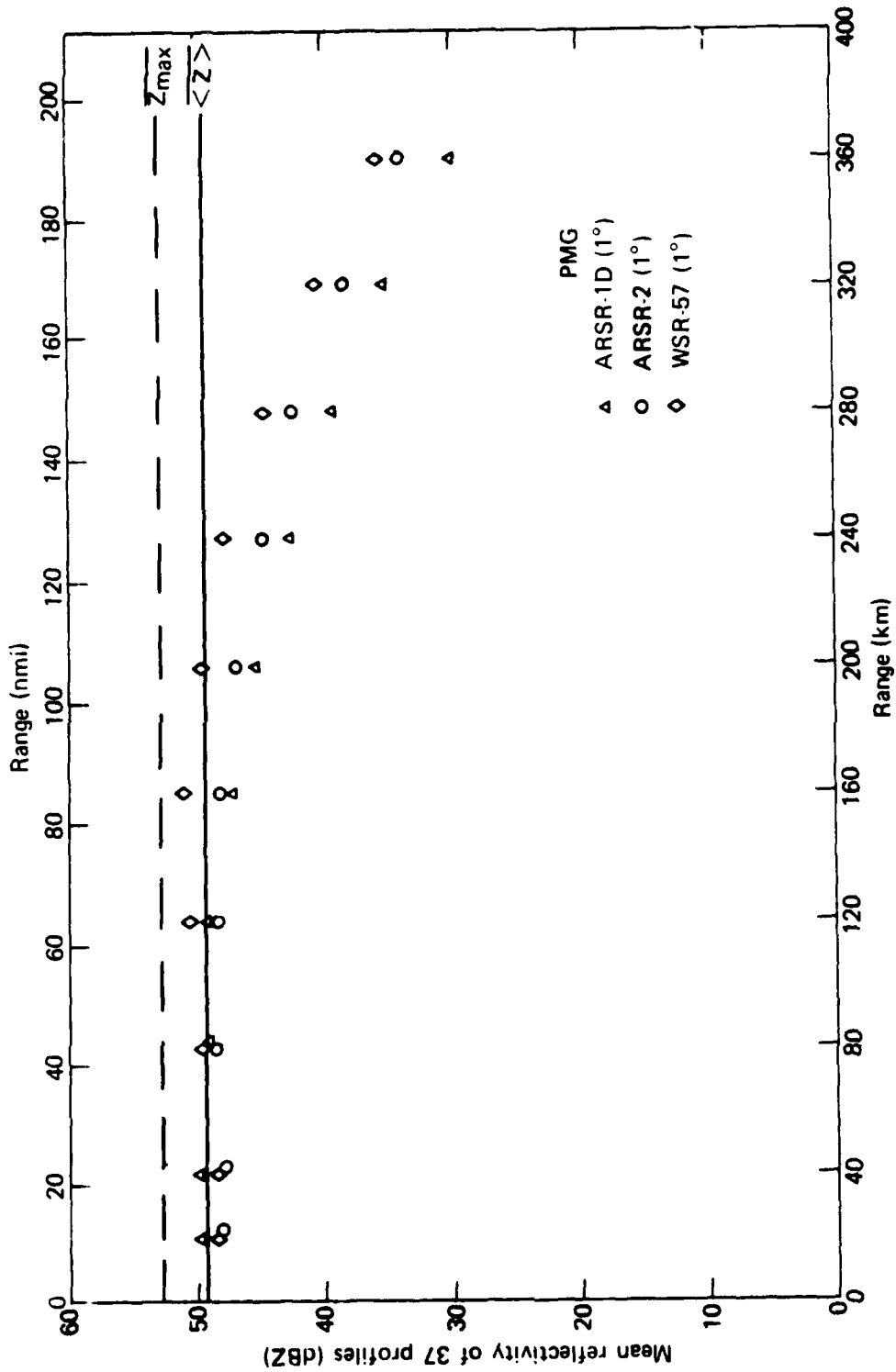


Figure 2-11. Mean reflectivity vs range for ARSR-1D, ARSR-2, and WSR-57.

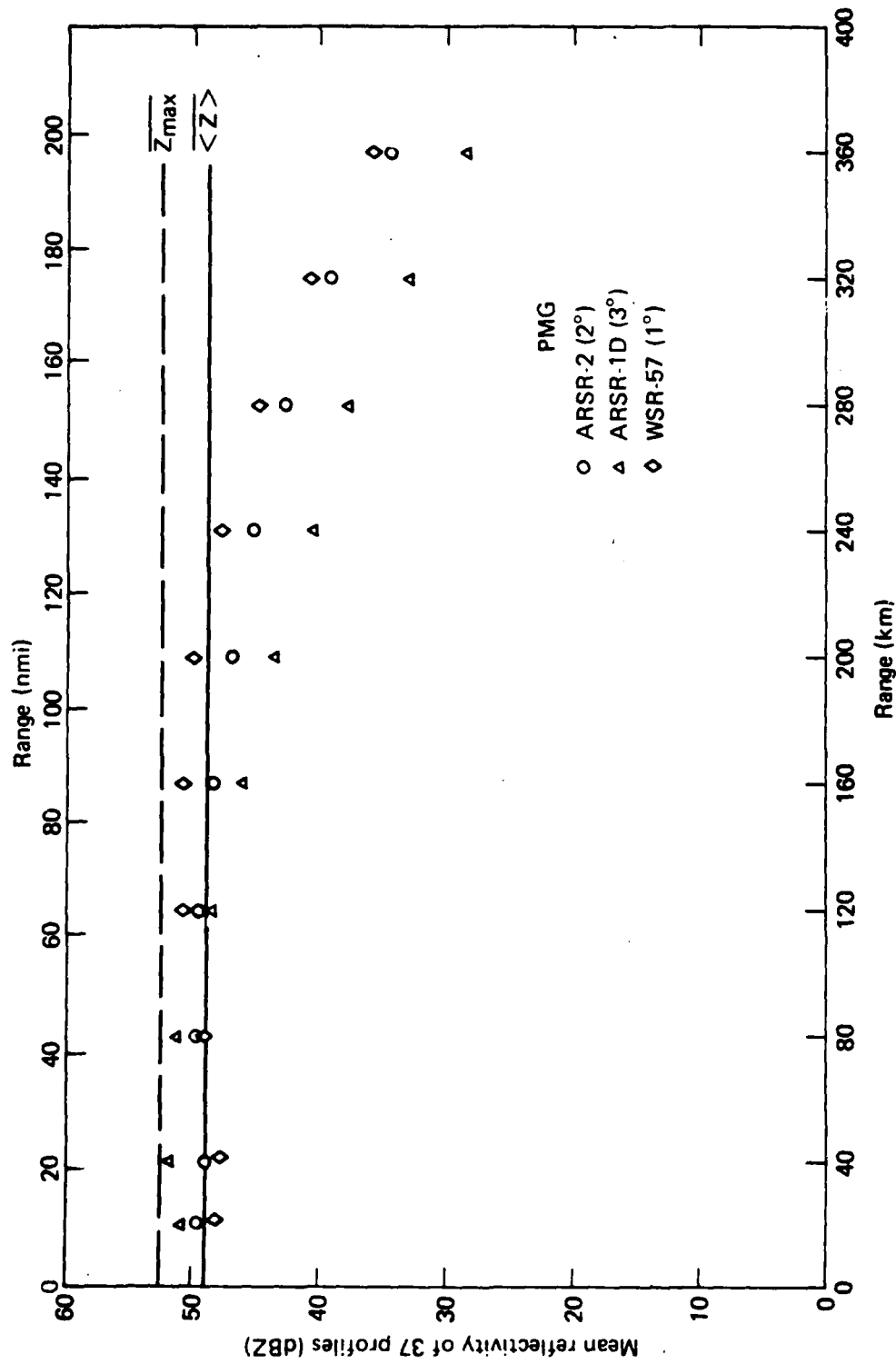


Figure 2-12. Mean reflectivity vs range for ARSR-1D, ARSR-2, and WSR-57. Maximum gain positioned with -3 dB point on the horizon.

The ARSR-3 results were not included in Figures 2-11 and 2-12 because they are within 0.5 dBZ of the ARSR-2 at all ranges.

It should be noted that the simulated power received was calculated based on the direct power only that would be received for the selected antenna tilt angle (i.e., no consideration for ground reflected energy).  $Z_{eff}$  was calculated based on the free space antenna pattern for the selected tilt angle (i.e., integration of the power above the horizon without regard to ground reflections).

It was recognized that both  $Z_{eff}$  (calculated) and  $Z_{eff}$  (calculated) for the simulation would be altered to some extent because of the amount of energy added to the pattern above the horizon due to ground reflections. The magnitude of the reflected energy at each elevation angle above the horizon is a function of antenna height, wavelength, and coefficient of reflection of the ground. In order to establish bounds on this effect a separate worst case analysis was performed on the effect of ground reflections assuming a coefficient of reflection ( $\rho$ ) equal to 1. The results of this analysis are discussed in Section 5.2 in conjunction with the experimental data but the results could be applied to the simulation as well. The discussion of the analysis is delayed until later. Based on this analysis, a general statement can be made that if the worse case (i.e.,  $\rho = 1$ ) applies, the ARSR-1D simulated reflectivities for a 1° PMG would be increased by 2 dBZ on the average between 40 km (21.6 nmi) and 160 km (86 nmi). The WSR-57 simulated reflectivities would not be increased at normal operational PMG's (above 0.5°).



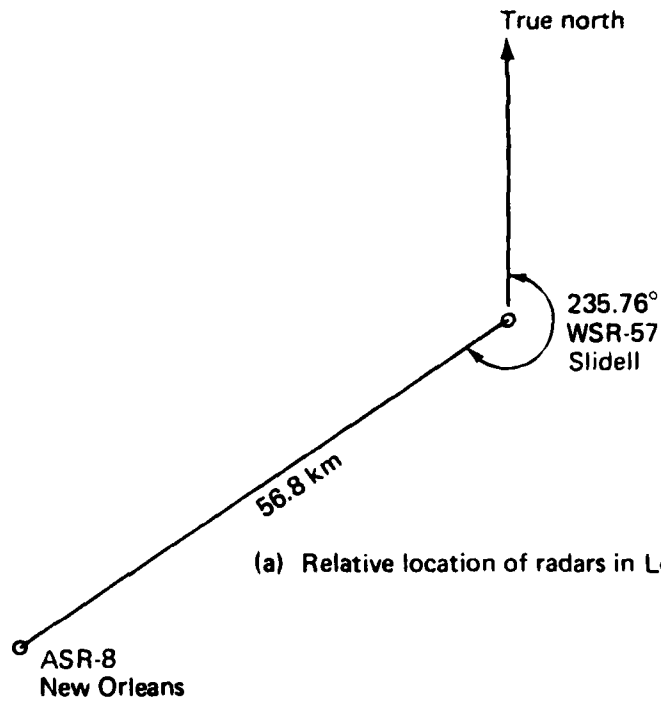
### 3.0 EXPERIMENTS

#### 3.1 New Orleans - Slidell

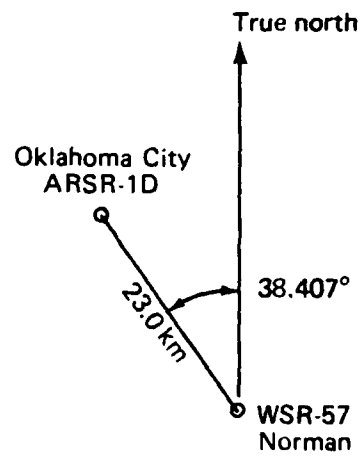
During August of 1977 an experiment was conducted in Louisiana to compare simultaneous weather detection by the FAA ASR-8 terminal radar at New Orleans International Airport (NOIA) and the NWS WSR-57 at Slidell, Louisiana. The relative location of the two radars is shown in Figure 3-1(a).

A video tape recorder was used at the WSR-57 site to record raw log video during a data run. A data run consisted of the antenna being scanned in a PPI mode at each of the following elevations to permit definition of vertical profiles: 1°, 5°, 9°, 13°, 11°, 7°, and 3°. At the beginning of each day a radar calibration was recorded on video tape at 3 dB power intervals and after each run, a short calibration of four power levels was recorded. No radar modifications were made at the WSR-57 site and the radar was operated exactly as the NWS operates it. The WSR-57 radar was available for the experiment only five minutes out of each half hour because it was an NWS operational facility.

At the ASR-8 site certain modifications were necessary in the receiver to detect orthogonal circular polarization on the standby channel of the radar, since the radar, in practical operation, often uses circular polarization which attenuates weather signals. This modification was the only major one; however, equipment was built to switch modes of the standby radar channel automatically during a data run and the  $R^{-2}$  STC curve was used instead of the usual  $R^{-4}$ . An automatic switching and recording sequence was necessary for the standby channel at NOIA to enable data collections which would later permit examination of various methods of optimizing the ASR-8 system for weather detection for comparison with the five minute WSR-57 data. A data run for the ASR-8 consisted of continual video tape recording of the log normal video and MTI video throughout a WSR-57 five minute data run, where the beginning of a run was signaled vocally via telephone.



(a) Relative location of radars in Louisiana test



(b) Relative location of radars in Oklahoma test

Figure 3-1. Relative locations of radars in Oklahoma and Louisiana experiments.

The ASR-8 has two feed horns. The low beam is used for transmit and receive and the high beam is used for receive only. An automatic sequence consisted of receiving four 360° scans of the low beam with no signal attenuation; four scans of low beam with the signal attenuated; four scans of high beam with no signal attenuation; and four scans of high beam with attenuation. The purpose for recording low beam and high beam in sequence was to investigate the feasibility of using the high and low beams in a range gating mode to aid in detection of weather over ground clutter. That is, if high beam detection at close ranges were sufficiently accurate, it could be used over ground clutter areas where its higher beam position reduces or avoids clutter. A switch would then be made to the low beam at ranges outside ground clutter. The attenuation was placed in the sequence to investigate the use of attenuation in more accurately measuring reflectivity values with MTI particularly when received with ground clutter. Since the MTI receiver dynamic range is small, higher reflectivities and weather returns with strong ground clutter saturate the MTI receiver. It was hoped that attenuation would bring higher signals out of saturation and permit more accurate measurements of weather reflectivity. On some occasions this automatic sequence was replaced in a data run with other changes of standby radar channel operation to collect data for analysis concerning the effect of specific radar circuitry on weather detection and calibration, such as MTI velocity response.

Calibration levels were recorded for the ASR-8 in a manner similar to the WSR-57.

Data runs were recorded on several days during the test. At the end of the experiment the data were carried to NAFEC to be digitized and sent to APL for processing and analysis.

### 3.2 Oklahoma City - Norman

This experiment was conducted during September and October of 1977 to compare the ARSR-1D, located at Oklahoma City,

detection of weather to the WSR-57, located at Norman. The relative locations of these radars is shown in Figure 3-1(b). The experiment is described in detail in Appendix C.

In an operation similar to the Louisiana experiment a video tape recorder was used to record MTI and raw log normal video signal at the ARSR-1D site. A video tape recorder was also used at the WSR-57 site to record raw log video. Antenna elevation information was also recorded along with radar calibration signals. A data run consisted of scanning the WSR-57 in stepped elevation sequences while the ARSR scanned continuously in various operational configurations. The elevation sequences at Norman depended on the range of the storm and were either 0°, 2°, 4°, etc., to the top of the storm or 1°, 5°, 9°, ..., 7°, 3°, 0°. No modifications were made to WSR-57 and it was used in its usual operational mode.

The ARSR-1D at Oklahoma City is a radar normally used for teaching so that at certain times it could be dedicated to the experiment. No automatic sequence of modes was run in this test. Rather various radar configurations were run depending on the rain conditions and the configurations to be tested. The configurations for which data were recorded are shown in Table 2.

Table 2  
APSR CONFIGURATIONS  
Oklahoma Test

Configuration	1	1.5	2	3	6	7	8	9	10	12	14	15
Part	1	1	1	2	1	2	1	1	1	2	1	2
Polarization LP*	✓		✓	✓	✓	✓	✓	✓	✓	✓	✓	✓
Switch CP**		✓	✓						✓	✓		
RF Cable	✓	✓	✓	✓	✓	✓	✓	✓	✓	✓	✓	✓
STC	✓	✓	✓	✓	✓	✓	✓	✓	✓	✓	✓	✓
Attenuation	0 dB	✓	✓	✓	✓	✓	✓	✓	✓	✓	✓	✓
10 dB												
20 dB								✓				
Velocity Pot	0			✓								
Mid	✓		✓									
Max		✓		✓	✓	✓	✓	✓	✓	✓	✓	✓

\*Linear Polarization

\*\*Circular Polarization

NOTE: These configurations were taken from Table 1 of Appendix C. The configuration numbers are not sequential because some planned tests were eliminated before the experiment began.

#### 4.0 DATA REDUCTION - ENROUTE

Video was recorded for simultaneous observations of storms by the ARSR-1D and the WSR-57 in order to compare the reflectivities measured by each radar. Power levels along with azimuth and elevation information were digitized and recorded on tape for six selected storm cells. These data were then processed via a computer program. The method of data reduction will be discussed here.

##### 4.1 Digitizing Raw Data

The data on both the ARSR tapes and the WSR-57 tapes were digitized at range intervals of .869  $\mu$ sec and at the individual pulse repetition frequencies. The ARSR has a prf of 360 with a 6 rpm scan rate which results in a digitized data resolution of 130 meters in range and  $.1^\circ$  in azimuth. The corresponding resolution for the WSR-57 is 130 meters (.869  $\mu$ sec) and  $.11^\circ$  since it has a long pulse prf of 164 and scan rate of 3 rpm. The equipment used to digitize the ARSR-1D and WSR-57 data is limited in the number of data points that can be digitized. Therefore, the size of the storm cell digitized varies depending on its position. Those storms where the majority of the cell could be digitized were digitized provided they met all other criteria in terms of intensity, height, etc. The sizes of cells digitized can be seen in the figures of Section 5.

##### 4.2 Calibration - ARSR-1 and WSR-57

Calibration curves were digitized for the ARSR and WSR-57. The power levels recorded on other days were then checked from the analog signal to be certain no significant changes occurred from day to day. These calibration curves for mean power levels averaged over the entire digitized signal are shown plotted in Figure 4-1. The ARSR calibration was recorded with the STC curve in the system, therefore, the power levels were digitized at a range beyond the influence of the STC curve.

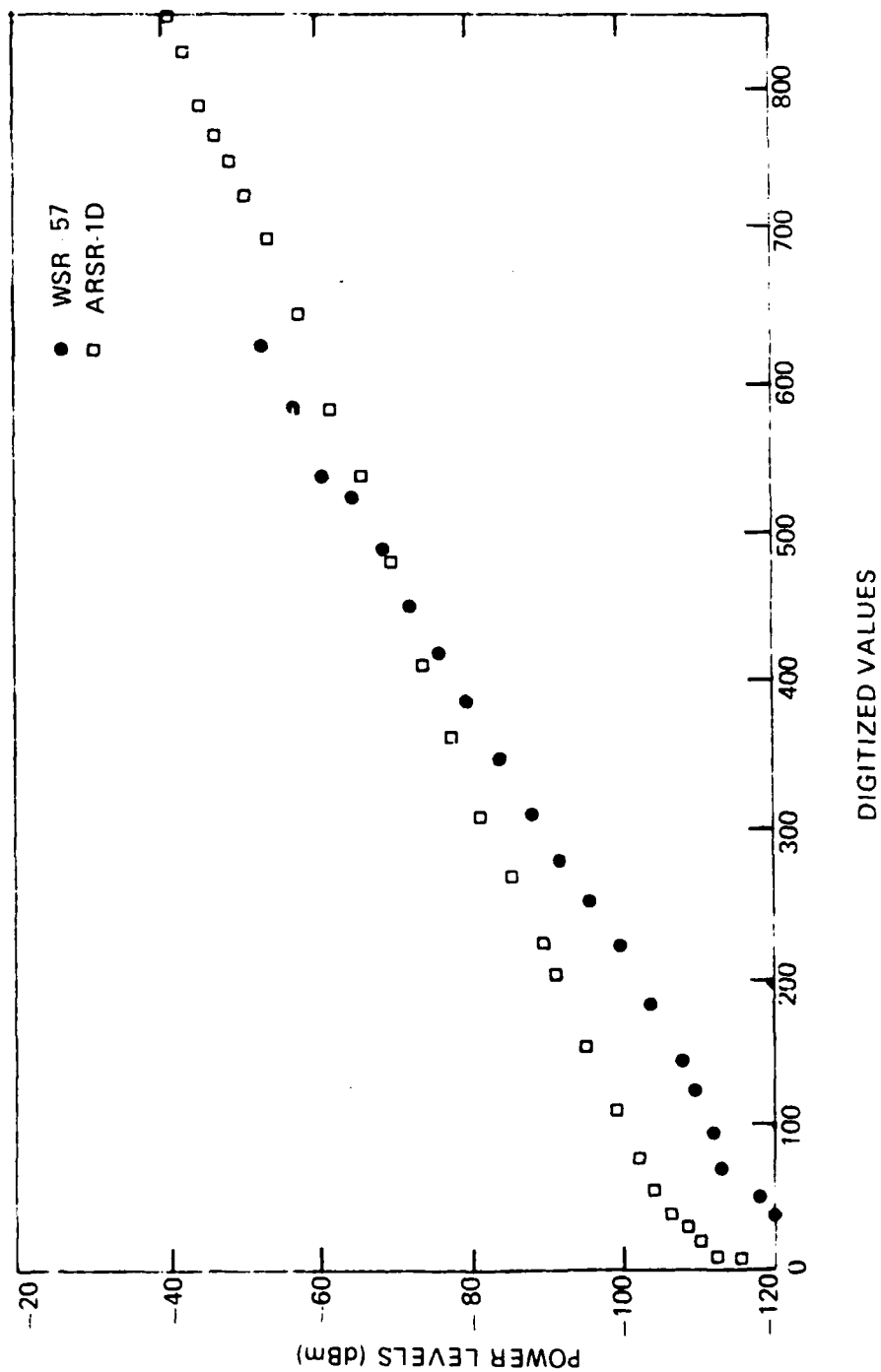


Figure 4-1. Calibration curves for ARSR-1D and WSR-57

The WSR-57 was recorded before injection of the STC signal, so that it was not a factor. The mean noise level which was obtained by averaging a digitized noise sample from the same time period was removed from both the curves. The received power from the sun was recorded on video tape for each of the radars as an additional calibration check but the signals have not been digitized to date.

#### 4.3 Averaging

The computer program was designed to read a scan of ARSR data from the tape and average I samples in range and J samples in azimuth, where I and J were inputs to the program and varied. The averaging was done in tape units (i.e., digitized values between 0 and 1024) and a statistical correction factor was applied to the radar equation to correct for log averaging. Similarly, a scan from the WSR was read from a tape and averaged for I and J samples. It was these averaged values that were used for computing reflectivity and comparing areas of colocated reflectivity. For the WSR-57 the samples were averaged in elevation and range for one portion of the analysis.

#### 4.4 Computation of Reflectivity

The simulation section of this report discussed the form of the radar equations used for the ARSR in this analysis. This equation using the integrated gain is given below (conversion factors: 1852 meters = 1 nautical mile;  $10^{18} \text{ mm}^6 = 1 \text{ m}^6$ ):

$$Z_{\text{eff}} (\text{mm}^6/\text{m}^3) = \frac{3.43 \times 10^{24} R^2 P_r}{K_{\text{ARSR}} \sum G^2(\phi_i) \Delta\phi} \quad (4.1)$$

$$K_{\text{ARSR}} = \frac{P_t \pi^3 |K|^2 \theta \frac{c\tau}{2} L_T}{256 \lambda^2}$$

where  $P_t$  and  $P_r$  are in watts;  $\theta$  is in radians;  $\tau$  is in seconds;  $\lambda$  is in meters; and  $R$  is in nautical miles.



Table 3 lists the parameter values for the two radars. The ARSR system losses are included in the calibration and the only loss included in the computation is -2.54 dB for log averaging. Included also is a correction of .7 dB for the Gaussian shape horizontal beamwidth. This is a correction based on Probert-Jones correction for a conical or elliptical beam in the azimuthal beam only.

The values in Table 3 give a  $K_{\text{ARSR}}$  (with the loss stated above) of  $3.52 \times 10^7$ . The  $\sum G^2 \Delta\phi = 5.75 \times 10^5$ . Therefore,  $K_{\text{ARSR}} \sum G^2 \Delta\phi = 2.02 \times 10^{13}$ .

$$Z_{\text{eff}} (\text{mm}^6/\text{m}^3) = 1.7 \times 10^8 R^2 P_r \quad (4.2)$$

Where range is in nmi and power received is in milliwatts.

During the Oklahoma experiment the ARSR-1D was positioned with maximum gain at  $3/4^\circ$ . This positioning directs some energy onto the ground. Therefore, ground reflections may be present in the ARSR-1D power received. These ground reflections were studied and will be discussed later. However, in the computation of  $Z_{\text{eff}}$  presented herein, no attempt was made to correct for ground reflections. In general practice, for meteorological radars, calibration and reflectivity threshold levels are set without regard to antenna tilt. Therefore, it was decided to keep the computation of  $Z_{\text{eff}}$  as close as possible to procedures used in common practice by operating meteorological radars.

The radar equation used for the WSR-57 is the equation generally used in radar meteorology. As was discussed in the section on simulation, the WSR-57 can underestimate the maximum in a storm due to the antenna beamwidth and tilt; however, for sake of consistency with the radar meteorology community, we have analyzed the data using the conventional equation. The radar equation for the WSR 57 is:

Table 3  
RADAR PARAMETERS

Parameter	ARSR-1D	WSR-57
Peak transmitted power - $P_t$	4700 kW*	370 kW
Range resolution - $c\tau/2$	300 meters	600 meters
Maximum gain	34.3 dB	38.1 dB*
Integrated gain - $\sum G^2_{\Delta\phi}$ (integrated from -3 dB point)	57.6 dB	60.6 dB
Horizontal beamwidth	1.35°	2.0°*
Vertical beamwidth (half power)	~6° (shaped to 44°)	2.0°
Frequency	1335 MHz	2875 MHz*
Function of index of refraction of water - $ K ^2$	.93	.93
Correction for log averaging	2.54 dB	2.54 dB
Probert-Jones correction for Gaussian shaped antenna	0.7 dB (azimuth only)	1.4 dB

\*Values furnished by FAA, ARD-243

$$Z_e (\text{mm}^6/\text{m}^3) = \frac{3.43 \times 10^{24} R^2 P_r}{K_{\text{WSR}}} \quad (4.3)$$

$$K_{\text{WSR}} = \frac{P_t \pi^3 |K|^2 \theta \phi \frac{c\tau}{2} G_{\text{MAX}}^2 L_T}{(2 \ln 2) 256 \lambda^2}$$

where  $P_t$  and  $P_r$  are in watts;  $\theta$  and  $\phi$  are in radians;  $\tau$  is in seconds;  $\lambda$  is in meters; and  $R$  is in nautical miles.

Using the Parameters given in Table 3,  $K_{\text{WSR}} = 4.7 \times 10^{13}$  and

$$Z_e = 7.3 \times 10^7 R^2 P_r \quad (4.4)$$

where  $R$  is in nmi and power received is in milliwatts. Eqs. (4.2) through (4.4) were used to compute the results that are discussed in Sections 5 and 6. Neither  $K_{\text{ARSR}}$  or  $K_{\text{WSR}}$  contain atmospheric losses due to oxygen and water vapor because these losses are dependent on range. However, it should be mentioned that within the operating ranges for the storm cells analyzed, the relative difference between these losses for the ARSR (i.e., L-band) and the WSR (i.e., S-band) was, on the average, .3 dB.

#### 4.5 Overlapping Pulse Volumes

The computer program and its logic flow are discussed in Appendix A. However, since the determination of those areas for which the two radars overlap in space is important, we will discuss it here.

The relative position of the two radars was shown in Figure 3-1. Suppose at a point in the program we have averaged precipitation reflectivities for both radars along with ranges and azimuths to the center of the averaged areas for a selected

storm cell. We determine whether a given ARSR area was overlapped by a corresponding WSR-57 area. To do this we translate all WSR-57 range,  $R_{WSR}$ , and azimuths,  $\theta_{WSR}$ , to the ARSR-1D locations to obtain  $R'_{WSR}$  and  $\theta'_{WSR}$ . These  $R'_{WSR}$  and  $\theta'_{WSR}$  values are tested to see if they fall within some small area around the ARSR-1D coordinate  $R_{ARSR}$ ,  $\theta_{ARSR}$ . If  $R'_{WSR}$  and  $\theta'_{WSR}$  are within this tolerance area, the areas are assumed to be overlapping in space (see Figure 4-2). The variables  $\epsilon_R$  and  $\epsilon_{AZ}$  were inputs to the program and were chosen to give the maximum overlap. The amount of overlap varies from storm cell to storm cell and area to area depending on angular location of the data with respect to the two radars.

In the cases where WSR-57 elevation scans were averaged, the overlap was established for each scan and the reflectivities for a given area were averaged in elevation.

#### 4.6 Contouring and Area Calculation

The main IBM 360/91 program used for data reduction printed the mean reflectivities at each scan, the rms reflectivities, and the average reflectivities in dBZ for each scan of the WSR and ARSR. The printout was in B-scan display such as those shown in the next section, where range and azimuth are printed in a rectangular grid. These B-scans were then stored on a Hewlett-Packard 9825 calculator tape, from which a contoured PPI type display, using NWS reflectivity levels (see Table 4), was generated. In addition to the contours for each set of storm cell data, the area with a given reflectivity level was computed for each storm cell. For example, consider a level 2 which has reflectivities from 30 to 40 dBZ. All ARSR areas having reflectivities within this range were summed.

Illustration of ARSR and WSR overlapping areas

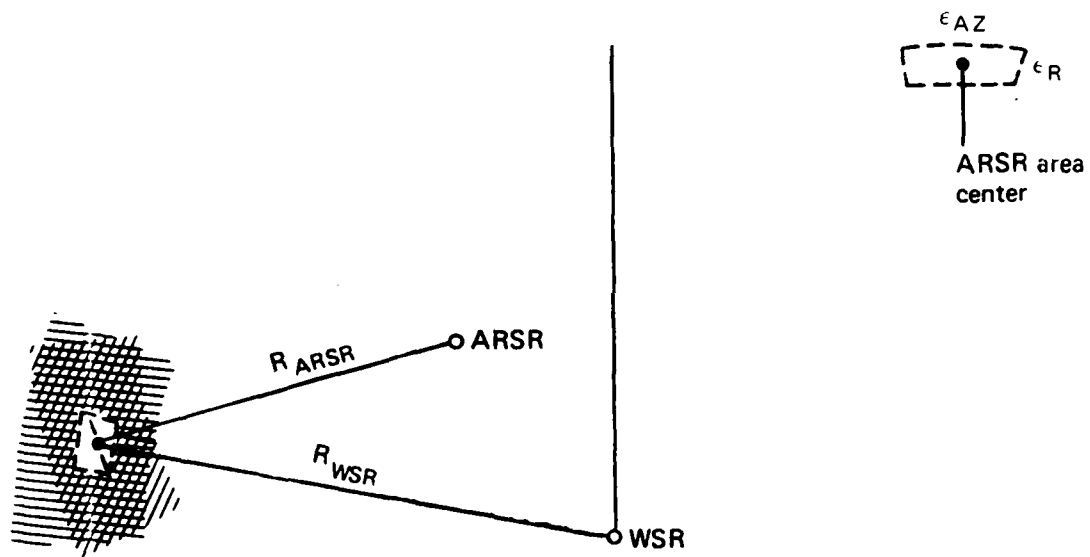


Figure 4-2. Illustration of overlapping pulse volumes for WSR-57 and ARSR-1D in Oklahoma.

Table 4

REFLECTIVITY LEVELS USED BY THE NATIONAL WEATHER SERVICE

NWS Level	Reflectivity (dBZ) (Z)
1	$Z < 30$
2	$30 \leq Z < 41$
3	$41 \leq Z < 46$
4	$46 \leq Z < 50$
5	$50 \leq Z < 57$
6	$Z \geq 57$

## 5.0 DATA ANALYSIS - ENROUTE

### 5.1 Contour Comparison

Of the data collected in Oklahoma, six storm cells were chosen for digitization and processing. These data were chosen due to storm height, intensity, and geometry. Other storm cells were available but they were not digitized by the FAA because of time limitations.

First the WSR-57 and ARSR-1D data were averaged and B-scan prints made to check the quality of data and geometric position of the radar echoes. These B-scans were then calibrated and printed with each radar in its respective coordinate system. Both of these stages of the data were for checking the data with PPI photographs for position and reflectivity levels. After assurance that the data were processable, they were run through the overlap program described previously. This program gives B-scans of each radar in the coordinate system of the ARSR-1D. A B-scan presents a distorted view of a PPI section (range and azimuth) because it presents polar coordinates in rectangular format. Nonetheless, it is a simple method of obtaining radar data in computer printout form. Figure 5-1 gives an example of this B-scan presentation. The data in these B-scans were processed on an IBM 360/91. These reflectivity levels were then put on a cassette tape where they were further processed to give storm cell contours, areas, etc.

### 5.2 Storm Cell Comparison (contours)

The B-scan plots in dBZ were analyzed for the six storm cells processed. The data indicated that on the average the ARSR-1D reflectivities were approximately 4 dBZ higher than the WSR reflectivities. No analytical justification for this overall difference in level could be found, however, explanations have been pursued. One possible source of this difference could be calibration error either in the WSR-57 or the ARSR-1D. This

MEAN VALUES												AZIMUTH --->											
34	34	34	35	35	35	36	36	36	37	37	37	37	38	38	38	39	39	39	40	40	40	40	
98.5	11	11	11	11	11	11	11	11	11	11	11	11	11	11	11	11	11	11	11	11	11		
98.0	11	11	11	11	11	11	11	11	11	11	11	11	11	11	11	11	11	11	11	11	11		
97.3	11	11	11	11	11	11	11	11	11	11	11	11	11	11	11	11	11	11	11	11	11		
96.7	11	11	11	11	11	11	11	11	11	21	21	23	23	21	11	11	11	11	11	11	11		
100.0	11	11	11	11	11	11	11	11	11	11	24	24	25	21	21	11	11	11	11	11	11		
100.4	11	11	11	11	11	11	11	11	11	11	26	26	25	24	24	11	11	11	11	11	11		
100.7	11	11	11	11	11	11	11	11	11	11	22	22	25	11	11	11	11	11	11	11	11		
101.1	11	11	11	11	11	11	11	11	11	11	26	26	26	20	20	11	11	11	11	11	11		
101.4	11	11	11	11	11	11	11	11	11	11	22	23	23	23	23	11	11	11	11	11	11		
101.8	11	11	11	11	11	11	11	11	11	11	22	24	24	22	22	11	11	11	11	11	11		
102.1	11	11	11	11	11	11	11	11	11	11	22	26	27	25	25	11	11	11	11	11	11		
102.5	11	11	11	11	11	11	11	11	11	11	22	24	26	28	28	11	11	11	11	11	11		
102.6	11	11	11	11	11	11	11	11	11	11	22	29	34	29	29	25	11	11	11	11	11		
102.8	11	11	11	11	11	11	11	11	11	11	24	29	30	32	31	31	22	11	11	11	11		
103.5	11	11	11	11	11	11	11	11	11	11	25	31	33	35	29	29	24	20	11	11	11		
103.9	11	11	11	11	11	11	11	11	11	11	24	29	34	34	33	33	29	22	11	11	11		
104.2	11	11	11	11	11	11	11	11	11	11	25	33	38	41	37	37	30	25	11	11	11		
104.5	11	11	11	11	11	11	11	11	11	11	33	39	42	42	42	37	27	23	11	11	11		
104.9	11	11	11	11	11	11	11	11	11	11	34	36	42	43	43	38	32	25	22	22	11		
105.2	11	11	11	11	11	11	11	11	11	11	25	25	35	33	39	39	40	29	24	11	11		
105.6	11	11	11	11	11	11	11	11	11	11	24	24	28	31	34	34	39	34	27	11	11		
106.0	11	11	11	11	11	11	11	11	11	11	11	11	11	11	27	27	33	23	32	23	11		
106.3	11	11	11	11	11	11	11	11	11	11	11	11	11	11	26	26	25	25	29	26	11		
106.7	11	11	11	11	11	11	11	11	11	11	11	11	11	11	25	25	26	26	28	24	11		
107.0	11	11	11	11	11	11	11	11	11	11	20	20	24	24	24	22	25	25	25	25	11		
107.4	11	11	11	11	11	11	11	11	11	11	11	11	11	11	24	24	32	31	31	21	11		
107.7	11	11	11	11	11	11	11	11	11	11	11	11	11	11	11	11	33	27	27	24	11		
108.1	11	11	11	11	11	11	11	11	11	11	11	11	11	11	20	20	30	32	27	27	11		
108.4	11	11	11	11	11	11	11	11	11	11	11	11	11	11	11	25	28	30	29	29	11		
108.8	11	11	11	11	11	11	11	11	11	11	11	11	11	11	11	23	23	26	27	24	11		
109.1	11	11	11	11	11	11	11	11	11	11	11	11	11	11	11	21	22	21	22	22	11		
109.5	11	11	11	11	11	11	11	11	11	11	11	11	11	11	11	22	27	27	23	11	11		
109.8	11	11	11	11	11	11	11	11	11	11	11	11	11	11	11	24	27	29	26	24	11		
110.2	11	11	11	11	11	11	11	11	11	11	11	11	11	11	11	11	22	22	27	11	11		
110.5	11	11	11	11	11	11	11	11	11	11	11	11	11	11	11	11	11	26	21	23	11		
110.9	11	11	11	11	11	11	11	11	11	11	11	11	11	11	11	11	25	27	26	25	11		
111.2	11	11	11	11	11	11	11	11	11	11	11	11	11	11	11	25	25	29	28	28	11		
111.6	11	11	11	11	11	11	11	11	11	11	11	11	11	11	11	11	11	22	29	25	11		
111.9	11	11	11	11	11	11	11	11	11	11	11	11	11	11	11	11	11	28	25	25	11		
112.3	11	11	11	11	11	11	11	11	11	11	11	11	11	11	11	11	23	23	22	22	11		
112.6	11	11	11	11	11	11	11	11	11	11	11	11	11	11	11	11	22	23	21	21	11		
113.0	11	11	11	11	11	11	11	11	11	11	11	11	11	11	11	11	11	11	11	11	11		
113.3	11	11	11	11	11	11	11	11	11	11	11	11	11	11	11	11	11	11	11	11	11		
113.7	11	11	11	11	11	11	11	11	11	11	11	11	11	11	11	11	11	11	11	11	11		
114.0	11	11	11	11	11	11	11	11	11	11	11	11	11	11	11	11	11	11	11	11	11		
114.4	11	11	11	11	11	11	11	11	11	11	11	11	11	11	11	11	11	11	11	11	11		
114.7	11	11	11	11	11	11	11	11	11	11	11	11	11	11	11	11	11	11	11	11	11		
115.1	11	11	11	11	11	11	11	11	11	11	11	11	11	11	11	11	11	11	11	11	11		

Figure 5-1. B-scan showing reflectivities in a rectangular array of range and azimuth. Range is in nautical miles and azimuth is in degrees.



error source can possibly be ascertained from sun strobe data which are available in video tape form but have not been digitized. Another suggested source comes from the fact that the maximum gain of the antenna was positioned at  $3/4^\circ$  elevation during the experiment. It is possible that this positioning could cause reflections from the surface which would increase the received power of the ARSR-1D. In order to obtain some indication of the magnitude of this effect, a theoretical analysis was performed with the PMG of the ARSR-1D at  $3/4^\circ$ . The analysis assumed that all energy directed to the ground would be reflected (i.e., a reflection coefficient = 1). Computations were performed at various ranges and the increase in total received power due to complete ground reflections determined. The results show (see Appendix D) that for the ARSR-1D the magnitude of the increased power is dependent on range and storm height. For storms with an altitude extent greater than 5 km (16.4 kft), the increase in power would vary as a function of range from near zero dBm at 40 km (21.6 nmi) to near 2.4 dBm at 200 km (110 nmi). A similar analysis for the WSR-57 positioned at  $0^\circ$  PMG would result in an increase as a function of range of approximately 3 dBZ from 40 km (21.6) to 160 km (86 nmi). A positioning of the WSR-57 at or above  $1/2^\circ$  PMG virtually eliminates any contribution from ground reflections.

In practice, there is no way to know exactly what the reflection coefficient is for various ranges and azimuths at an operating site. With this in mind the decision was made to make no adjustments to the experimental data due to ground reflections for either the ARSR-1D or the WSR-57 although the ARSR-1D was positioned with the PMG at  $3/4^\circ$  and the WSR was positioned at  $0^\circ$  for two storm cells.

As mentioned in Section 4.4, the conventional equation for computing WSR-57 reflectivity was used for the experimental data (i.e., maximum gain and  $2 \ln 2$  correction for beam shape). Had an integrated gain of the pattern for  $0^\circ$  PMG been used along with complete ground reflection (i.e.,  $\rho = 1$ ), the WSR-57

reflectivity values would not have changed because the 3 dB increase from ground reflections is cancelled by a 3 dB decrease from maximum gain to integrated gain. If the same thing had been done for the ARSR-1D integrating the gain pattern from the horizon with  $3/4^\circ$  PMG, an average decrease of 1 dBZ would result.

It appears that ground reflections cannot fully explain the discrepancy between the ARSR-1D data and the WSR-57 data. Despite this, the ARSR-1D reflectivity data presented has been lowered by 4 dBZ to permit meaningful side by side comparisons. It is felt that whatever the source of this bias error, it amounts to a calibration problem either in the ARSR-1D or the WSR-57 and can be accounted for in setting threshold levels. Thus it in no way degrades the capability of the ARSR-1D to measure weather.

In Figure 5-2 we observe a storm cell comparison centered at 38 nmi with respect to the ARSR-1D. This storm cell was recorded on September 28, 1977. The storm characteristics, as seen from three elevation scans through the WSR-57, indicated it had maximum reflectivities near the surface and decreased in intensity with altitude. The contours in Figure 5-2 represent an average of 5 digitized azimuth values and 6 digitized range values. These averaged quantities due to a digitization rate of .869  $\mu$ sec and the ARSR-1D scan rate result in  $.5^\circ$  azimuth and 782 meters range resolution. This  $.5^\circ$  resolution in azimuth is less than the ARSR-1D's  $1.35^\circ$  and the WSR-57  $2.0^\circ$  azimuthal beamwidths. This means that the values as presented do not represent spatially independent estimates. Averaging in azimuth up to the horizontal beamwidth does not substantially change the contours but does smooth the contours and reduces the area of maximum Z. This is shown in Figure 5-3 for storm cell 1 where both radars have been averaged over  $2^\circ$  of azimuth and 782 meters range. The general shape of the cells is the same in both Figures 5-2 and 5-3. Storm cell 1 (Figure 5-2) shows a level of 6 for the ARSR-1D; however, the WSR-57 does not show this. The other levels for this

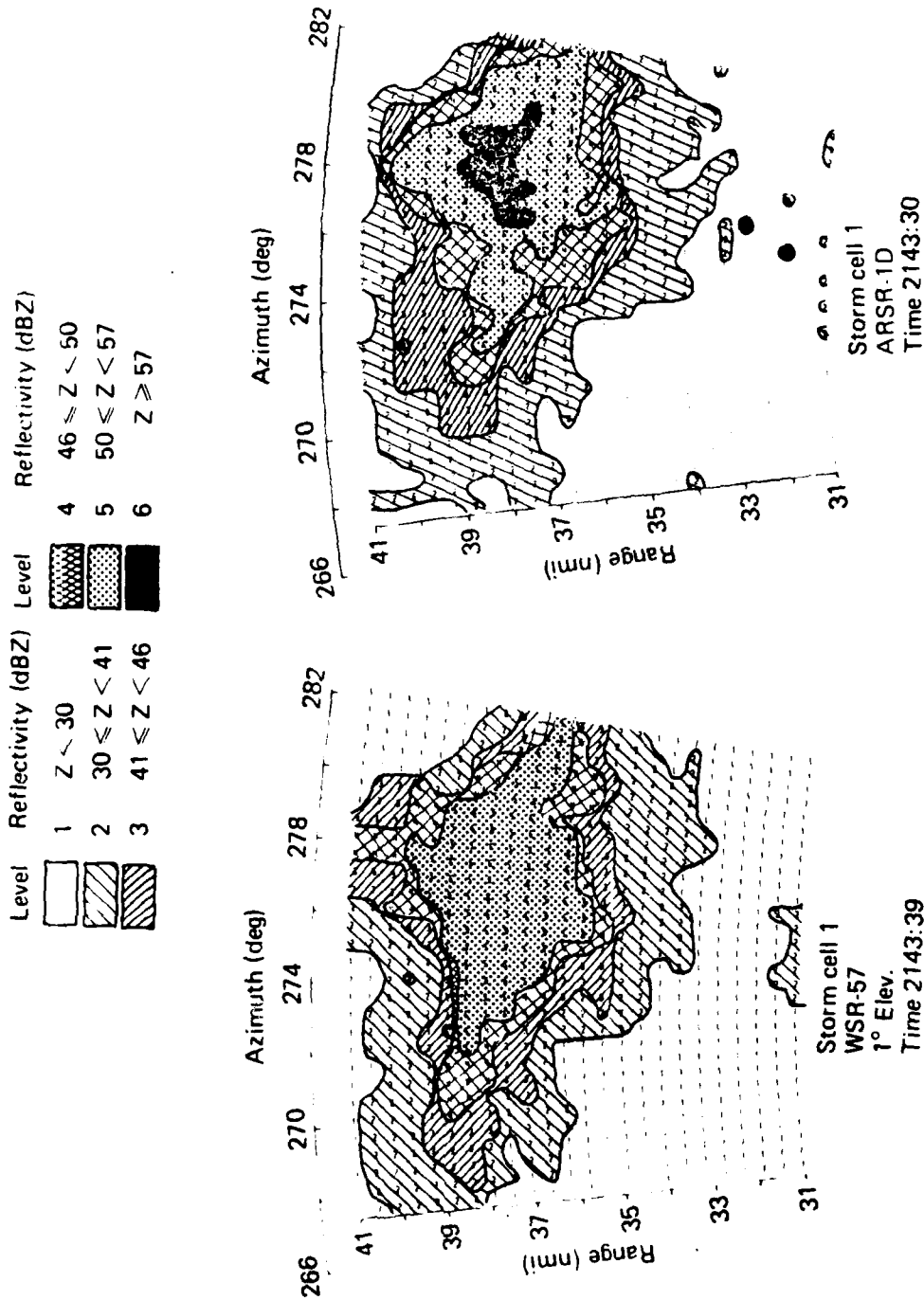


Figure 5-2. Storm cell 1 - ARSR-1D and WSR-57 contoured reflectivity.  
.5° azimuth and 782 meter range resolution.

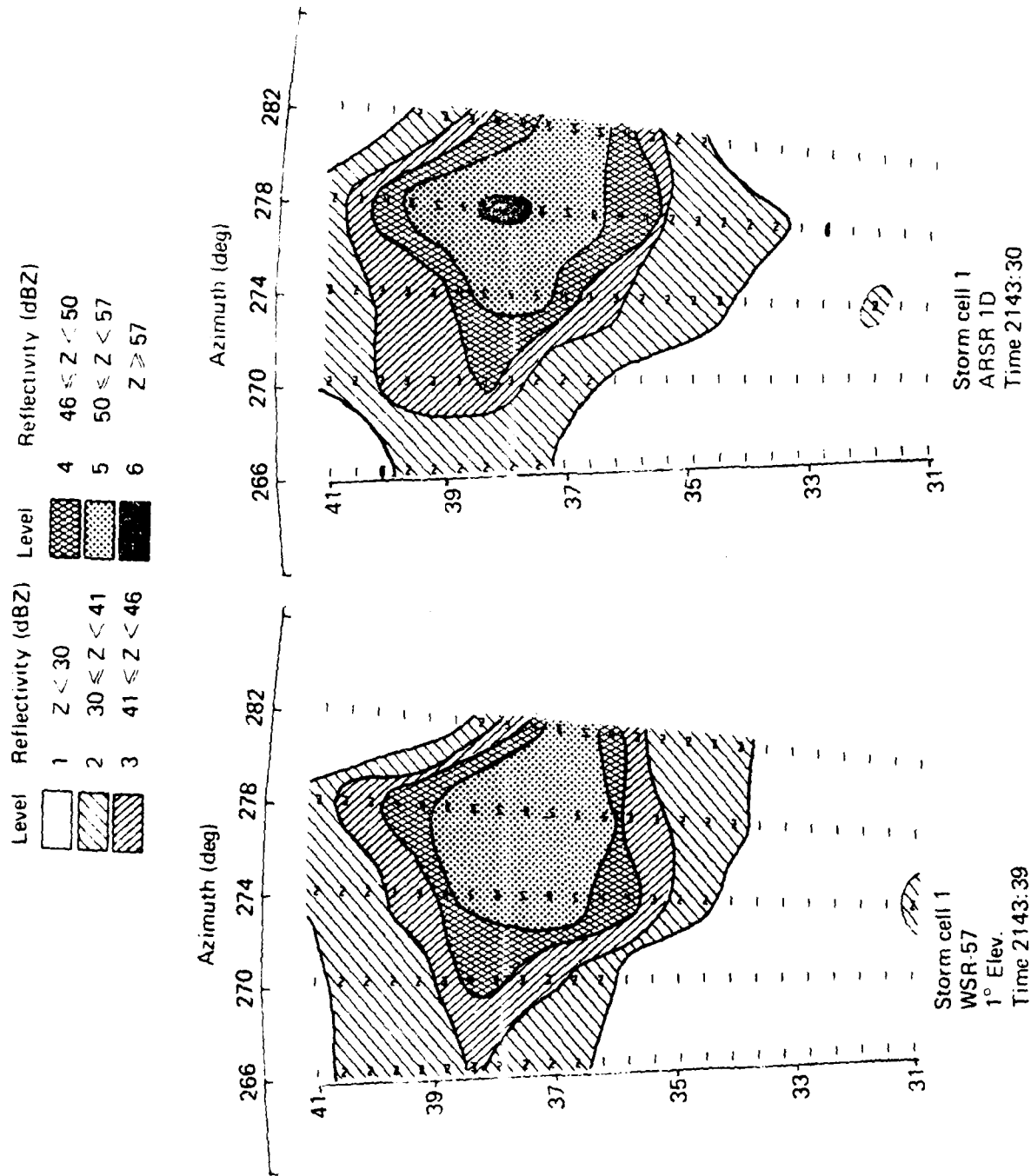


Figure 5-3. Storm cell 1 - ARSR-1D and WSR-57 contoured reflectivity.  
2° azimuth and 782 meter range resolution.

storm cell agree quite well. It is possible that this core was at altitude and existed for a very short period of time, which would mean that the WSR-57 possibly missed it at 1° elevation angle and it did not exist before and after when the WSR was scanning at higher elevations.

As mentioned previously, all cells were scanned in elevation (see Figure 5-4). Storm cell 1 had echoes up to 7°. The storm had its highest reflectivities at 1° elevation with the level of the core reflectivity decreasing about 3 dB at 3° and decreasing steadily from that point. The last echoes seen at 7° elevation and 39 nmi indicate a storm height between 8 and 10 km.

Storm cell 2 (see Figure 5-5) shows the detection of a cell at relatively long ranges (i.e., 185 km or 100 nmi). This cell is interesting because echoes showed on the WSR at only 1° elevation. This means that the storm did not extend above 9 km (29 kft). If we assume that the storm extended to 9 km, then the ARSR-1D with a 6° (3 dB) beamwidth has less than three quarters of the beam filled. The simulation in this case would predict the ARSR to be at least 1.2 dBZ below the WSR. This 1.2 dBZ would be difficult to see in the contours; however, there is no indication that the ARSR is lower. Instead the contours from the WSR and ARSR are approximately equal.

Storm cells 3 and 3A (Figures 5-6 and 5-7) are the same storm separated in time by about 4 minutes. Again the general shapes of echoes are similar. The ARSR area at level 2 seems to be smaller. It is judged that the information as presented by the ARSR-1D would be as helpful to air traffic controllers as that given by the WSR.

Figure 5-8 shows a rather large and complex storm cell. Again the similarities are apparent. This cell can be used to illustrate the possibility for implementation of a 2 level display by the FAA for controller use. Figure 5-9 illustrates where the

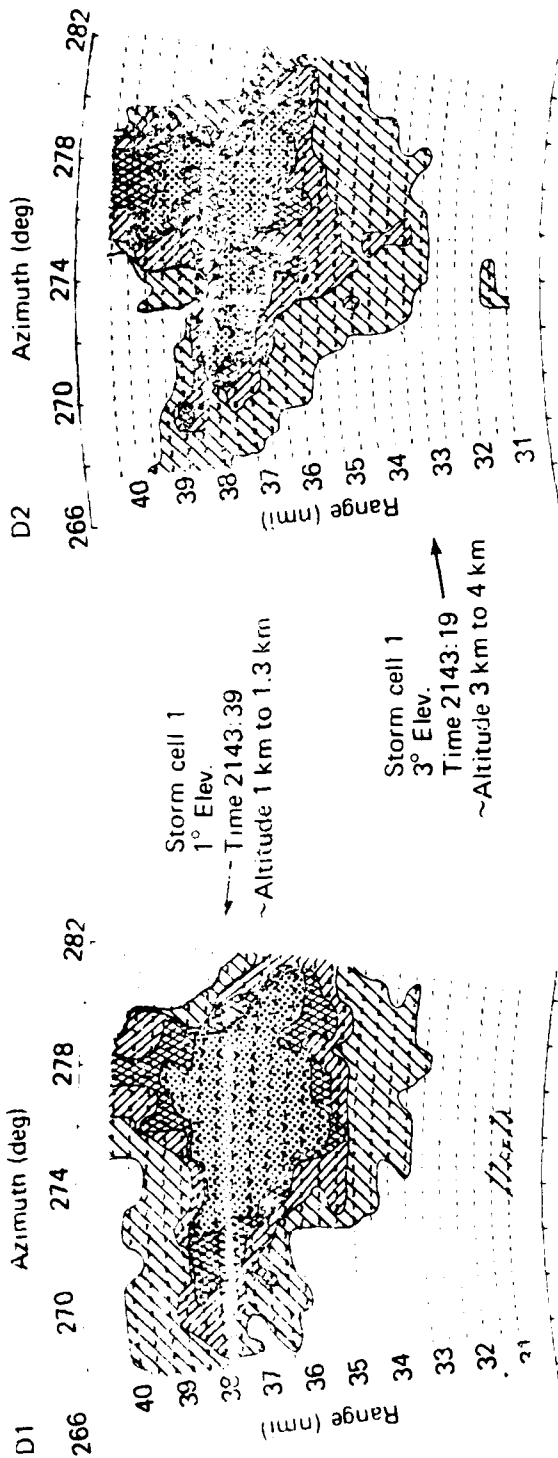


Figure 5-4. Contoured WSR-57 measured reflectivity showing three elevation angles.

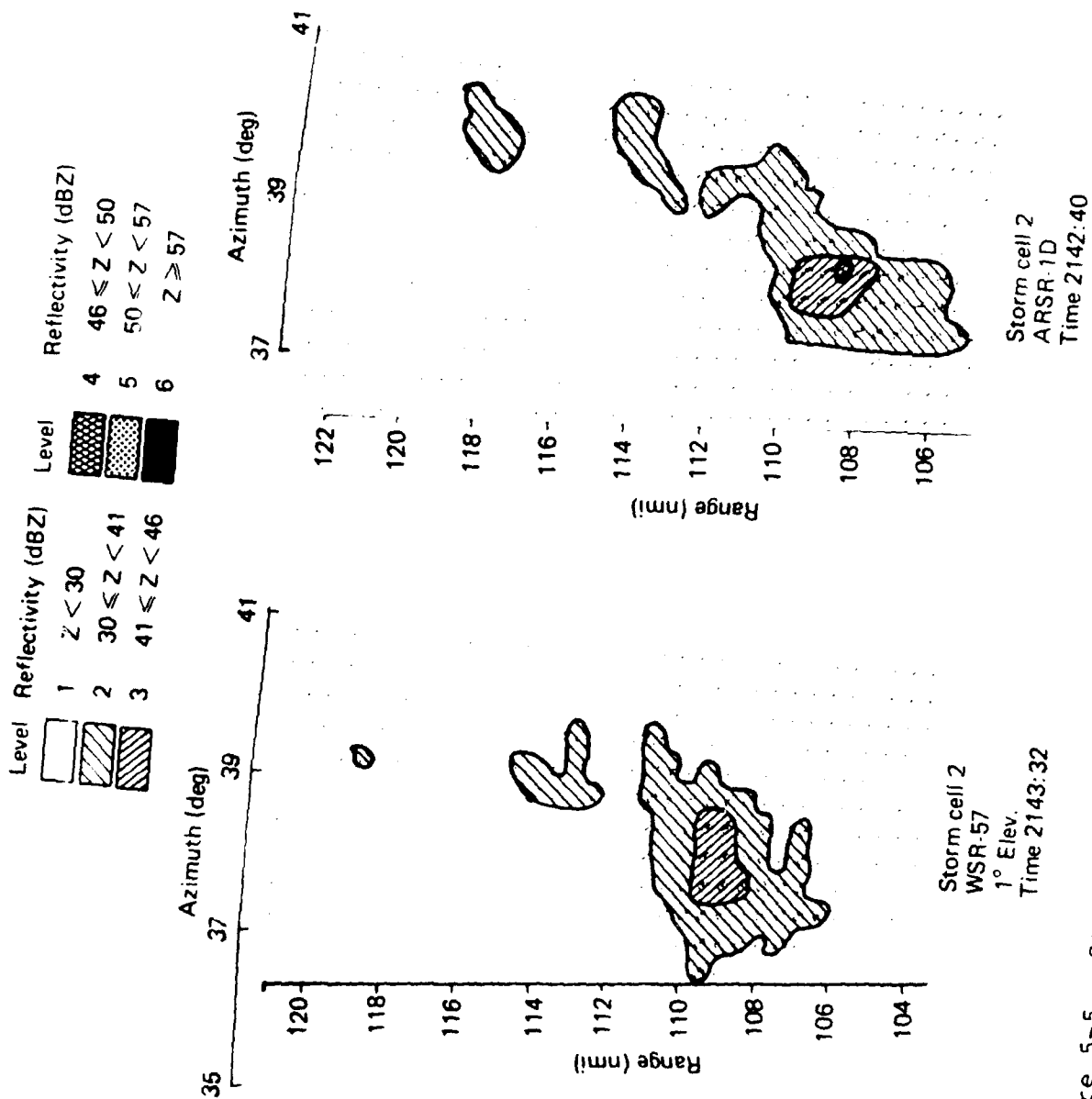
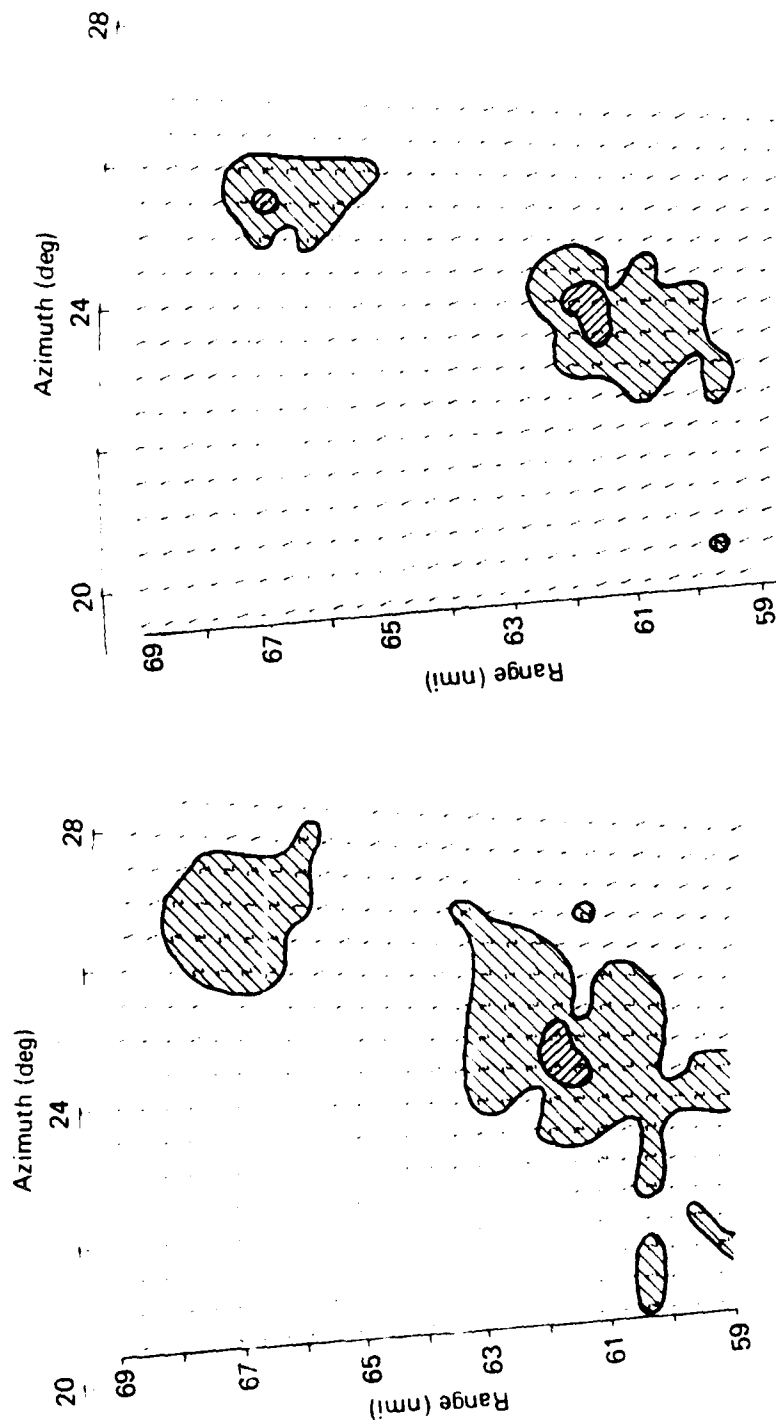
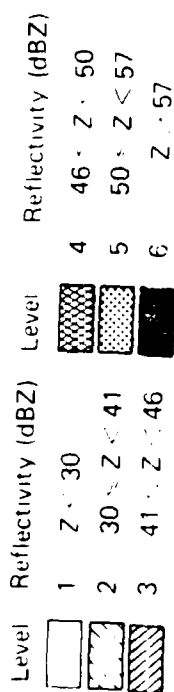


Figure 5-5. Storm cell 2 - ARSR-1D and WSR-57 contoured reflectivity.  
 .5° azimuth and 782 meter range resolution.



Storm cell 3  
WSR-57  
0 Elev.  
Time 1935:58

Storm cell 3  
ARSR-1D  
Time 1936:00

Figure 5-6. Storm cell 3 - ARSR-1D and WSR-57 contoured reflectivities. .5° azimuth resolution and 782 meter range resolution.



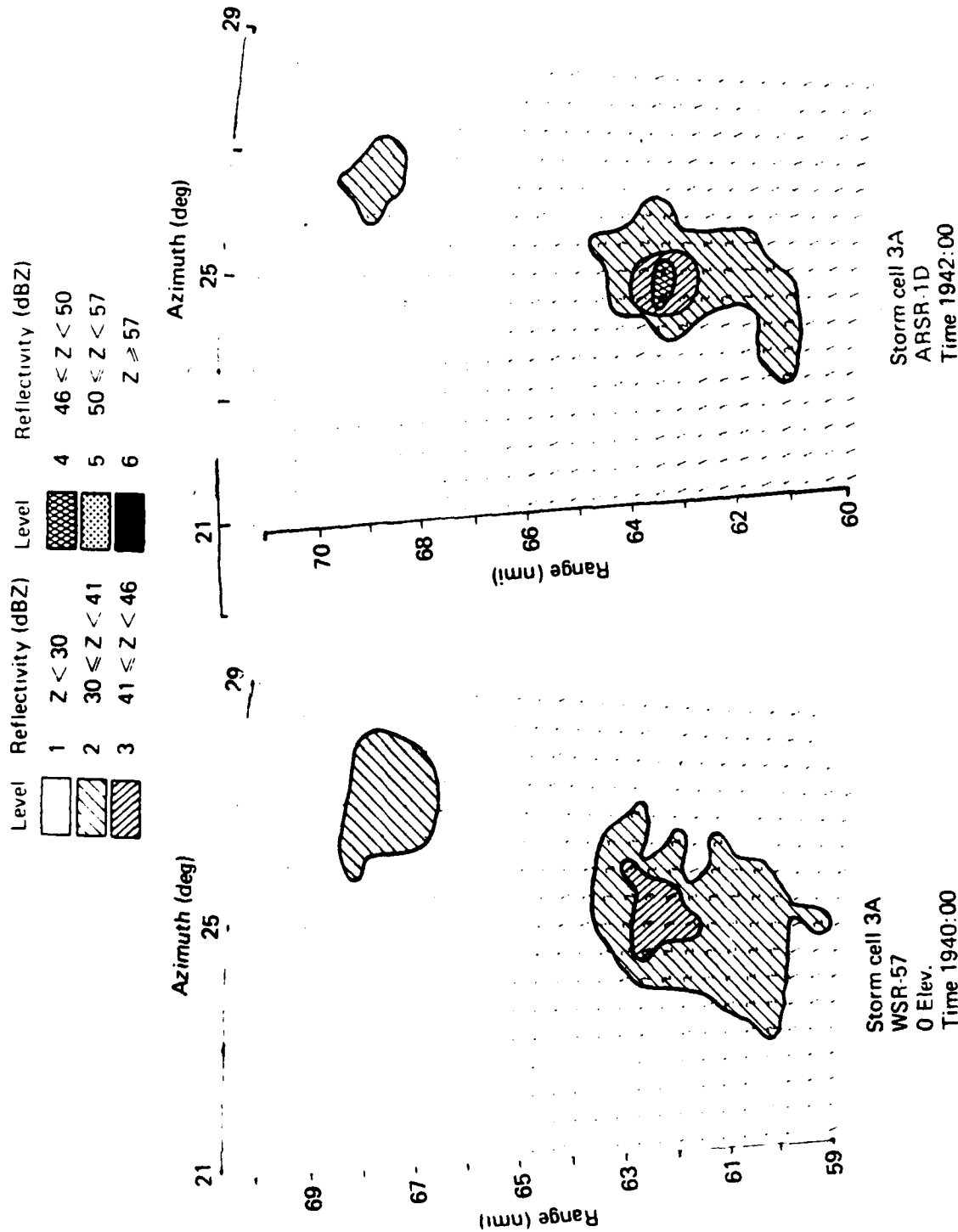


Figure 5-7. Storm cell 3A - ARSR-1D and WSR-57 contoured reflectivity. .5° azimuth and 782 meter range resolution.

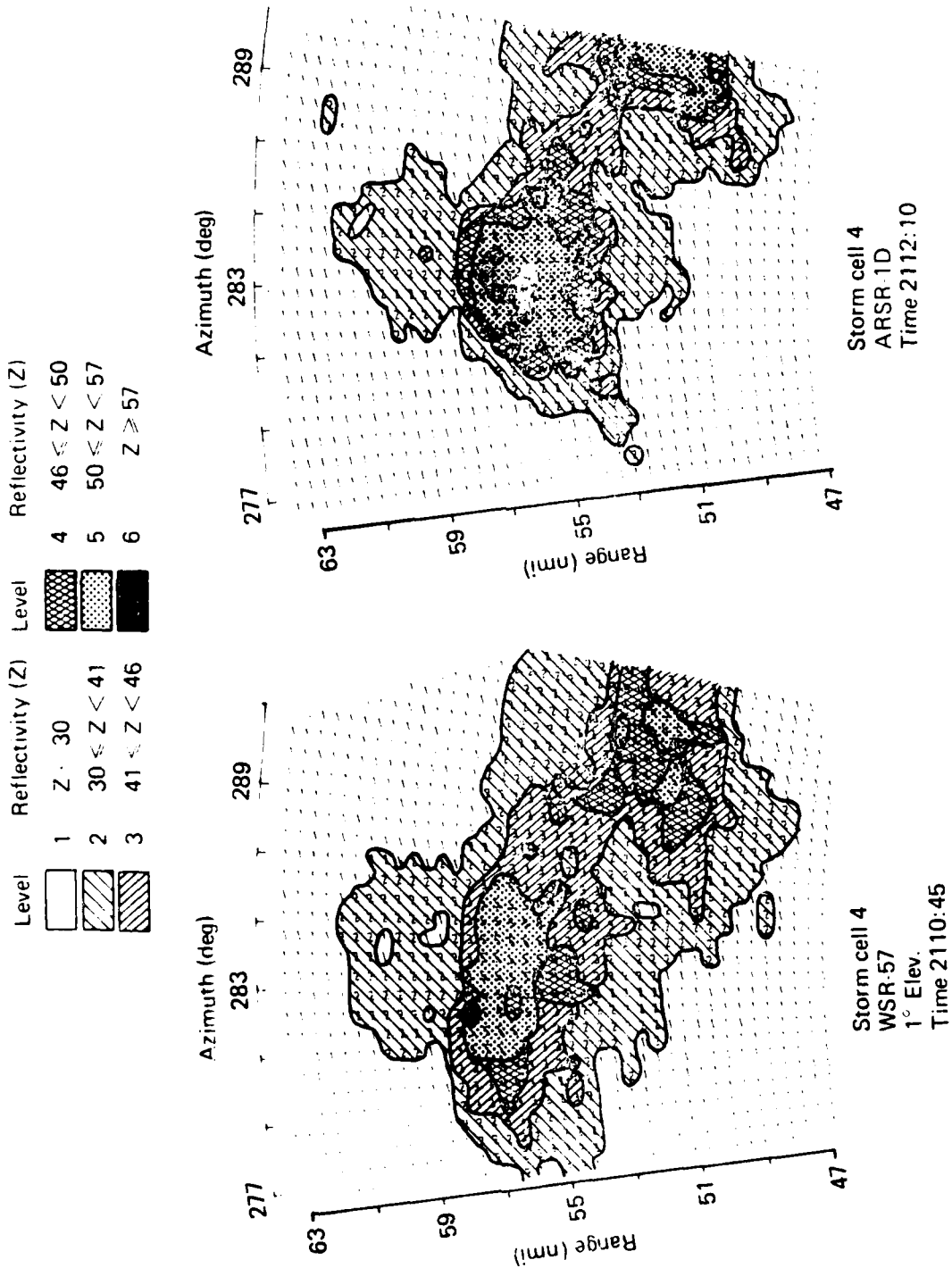


Figure 5-8. Storm cell 4 - ARSR-1D and WSR-57 contoured reflectivity.  
.5° azimuth and 782 meter range resolution.

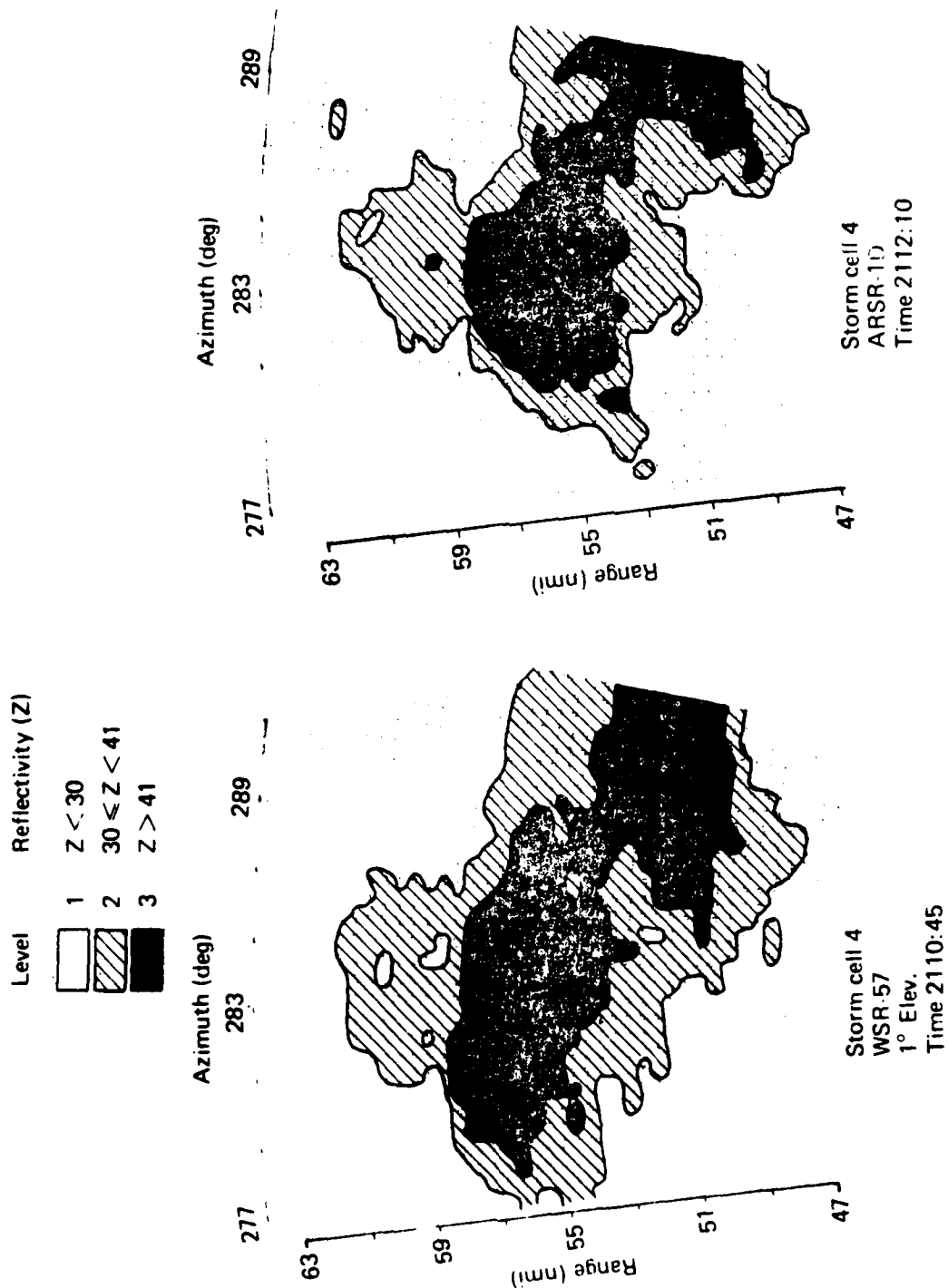


Figure 5-9. Example of contoured reflectivity showing two levels.

thresholds could be set for an installation; 30 dBZ (level 2) and 41 dBZ (level 3 and above). The information shown by the two radars would be virtually the same.

A stratiform rain condition is not, in general, hazardous to aircraft. However, storm cell 5 is shown (Figure 5-10) to indicate how this type rain might appear on the scope. There are no reflectivities above level 2 and the display appears patchy. In this particular rain, which actually is not an intense storm, there were no reflectivities above 37 dBZ. In general, this low level patchy signature is indicative of stratiform precipitation and is not difficult to recognize after seeing it several times.

### 5.3 Area Comparisons

To yield a measure of the comparability of the results from two radars, area comparisons were calculated. For a given storm cell, the area included at each level was computed for the two radars for all six cells. The ratios of the ARSR-1D area to the WSR area are shown in Figure 5-11. The level 1 indicated in this figure is different from the NWS level 1 in that it indicates dBZ values between 20 and 30 dBZ. There is quite a bit of scatter in the data. However, the mean is very close to 1.0. This result supports the comparability of the results.

### 5.4 Comparison with the Simulation

In theory the simulation indicates that, given the storm profile at some range, one can predict what the ARSR-1D should measure. We have chosen 18 profiles from the WSR measurements in several storms. This was done by taking an average reflectivity within a  $.7^\circ$  by 1 km area at each WSR elevation angle. This reflectivity was then assigned to an altitude corresponding to the mid-point of the WSR beam at that range. It should be noted that these profiles obtained from the WSR-57 are averages of the true profile. That is, the scatterers within the WSR-57  $2.0^\circ$  beam have been averaged. Technically, the ARSR-1D averaged the true profile over its beamwidth. Therefore, since

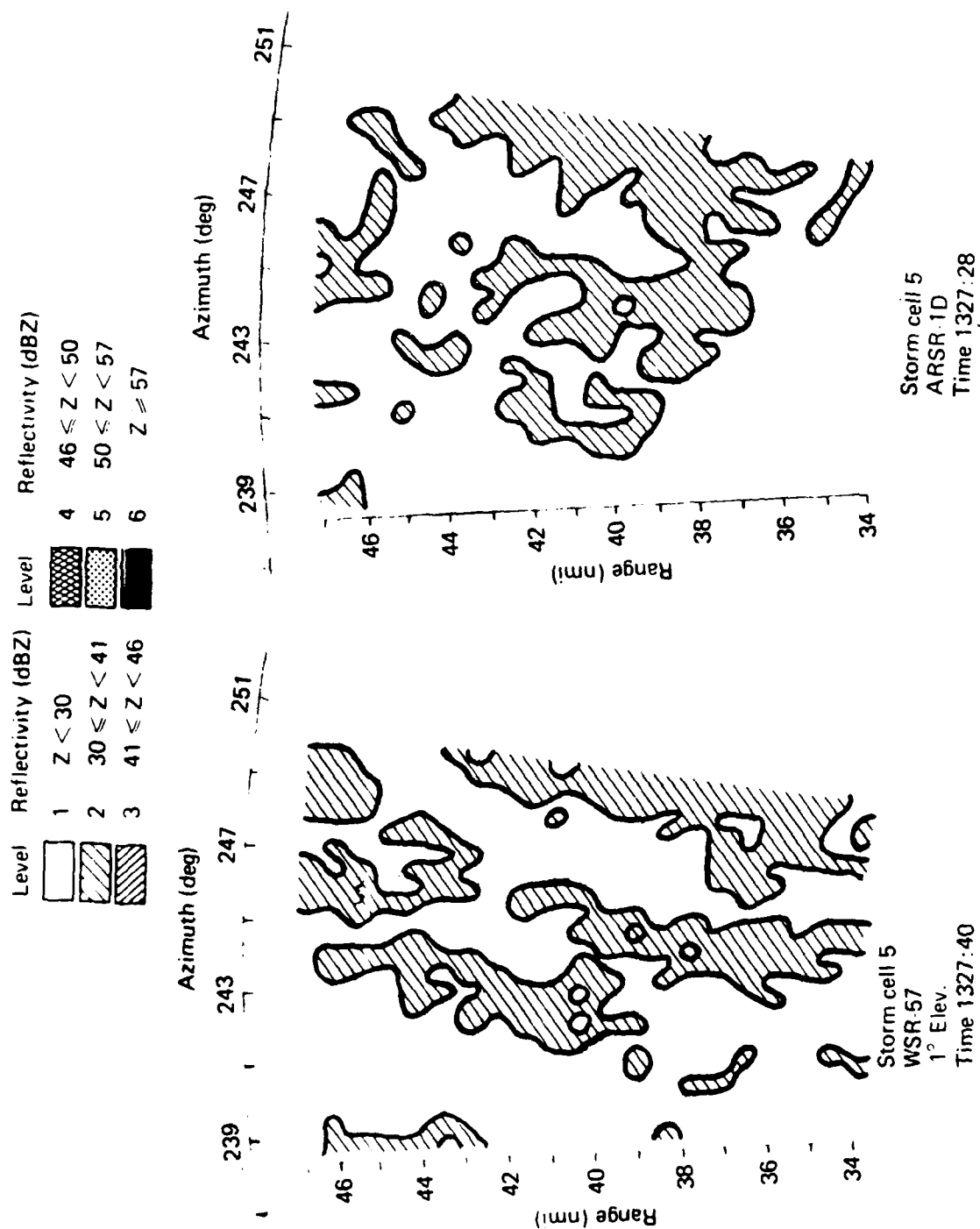


Figure 5-10. Storm cell 5 - ARSR-1D and WSR-57 contoured reflectivity.

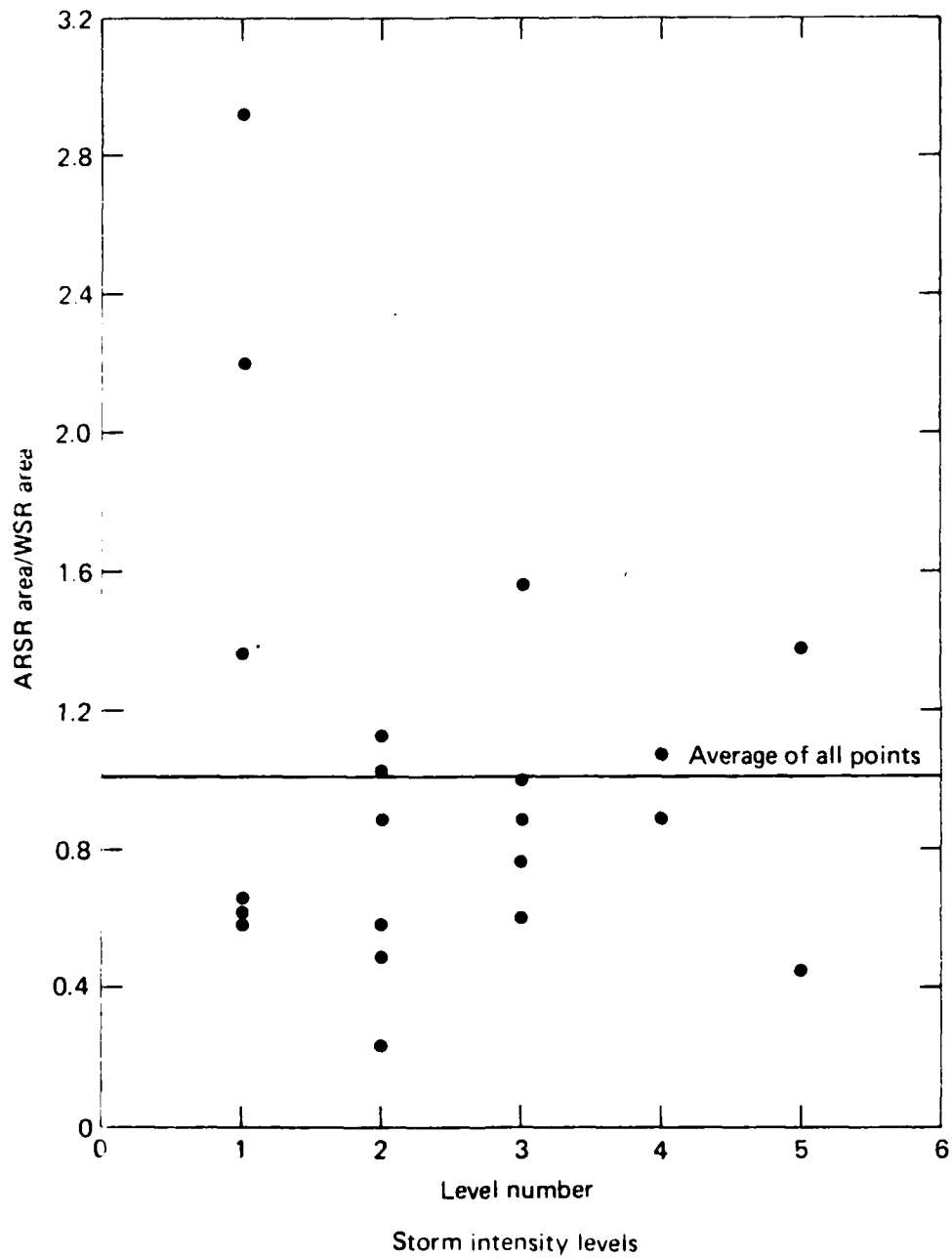


Figure 5-11. Ratio of ARSR-1D area to WSR-57 area at a level vs level number. The solid line is the average of all points.

the "true profile" was not put into the simulation, we should not expect the ARSR-1D measured reflectivity to be exactly equal to the simulation. However, the two reflectivities should be close if the simulation is representative of the actual ARSR-1D measurement. Figure 5-12 presents the results in a regression plot. Each profile was run through the simulation program and an ARSR reflectivity computed. There is a .89 correlation indicated. The linear regression equation gives a slope of .9 between the measured and the simulated ARSR values. Perfect agreement would be a slope of 1 and intercept of 0.

The ARSR-1D measured values were also compared to the maximum WSR measured reflectivities for the 18 profiles. These maxima were, in general, at the lowest elevation angle  $0^\circ$  or  $1^\circ$  for the WSR-57. Figure 5-13 gives these results. The slope of .97 and intercept of  $-.88$  from the regression are close to intercept 0 and slope 1 which perfect agreement would give.

#### 5.5 Comparison of MTI and Log Video Data

All reflectivity values previously discussed have been computed from log video. During the Oklahoma experiment Moving Target Indicator (MTI) data were also recorded. The MTI mode is used on FAA radars to eliminate fixed targets such as ground clutter. To accomplish this the velocity notch of the MTI filter is centered at zero velocity. As a result slowly moving weather targets may also be eliminated. However, in many thunderstorms internal velocities may be sufficiently high to fall in the pass band of the filter and allow the weather returns to be detected. For this reason MTI video data were recorded simultaneously with log video data. The resulting data showed that portions of storms were detected on MTI, however, the reflectivity measurements were not good for two reasons. On the edge of the storm cells, where reflectivities were below 30 dBZ, there were differences between MTI and log that were inconsistent. That is, the MTI at times measured patterns and reflectivities similar to the log video and other times they were dissimilar. In those areas

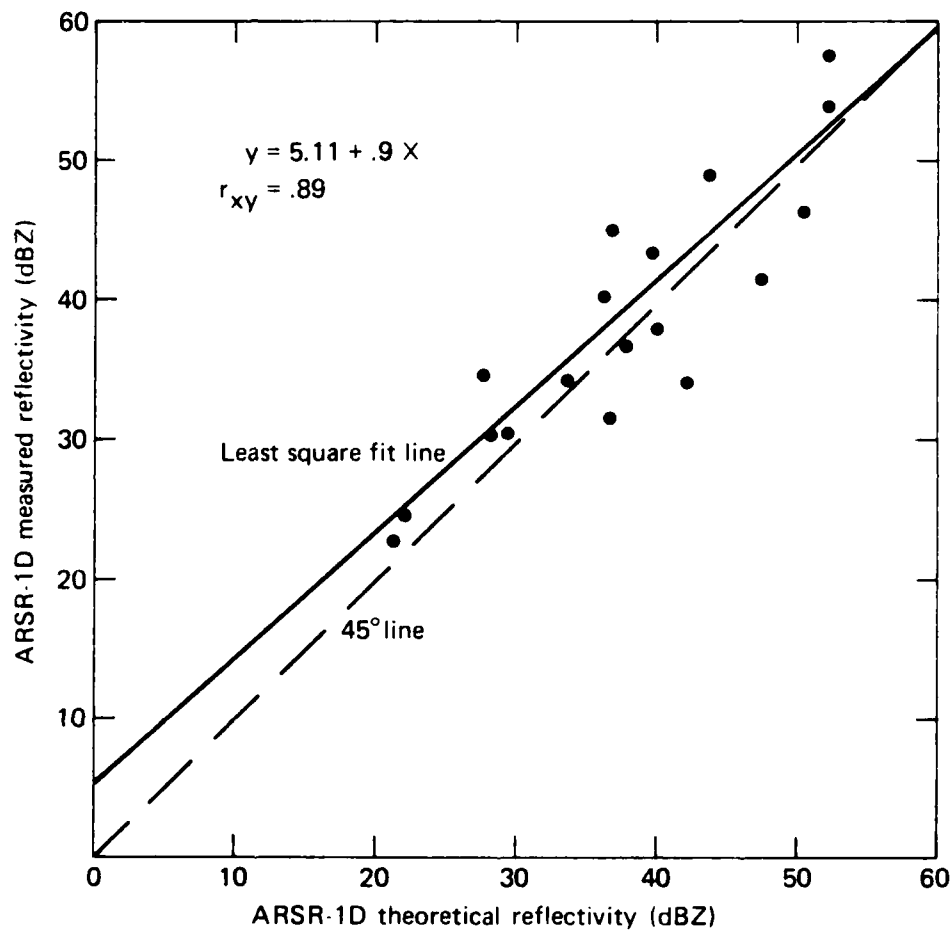


Figure 5-12. Measured ARSR-1D reflectivity vs simulated ARSR-1D reflectivity for 18 WSR measured profiles.



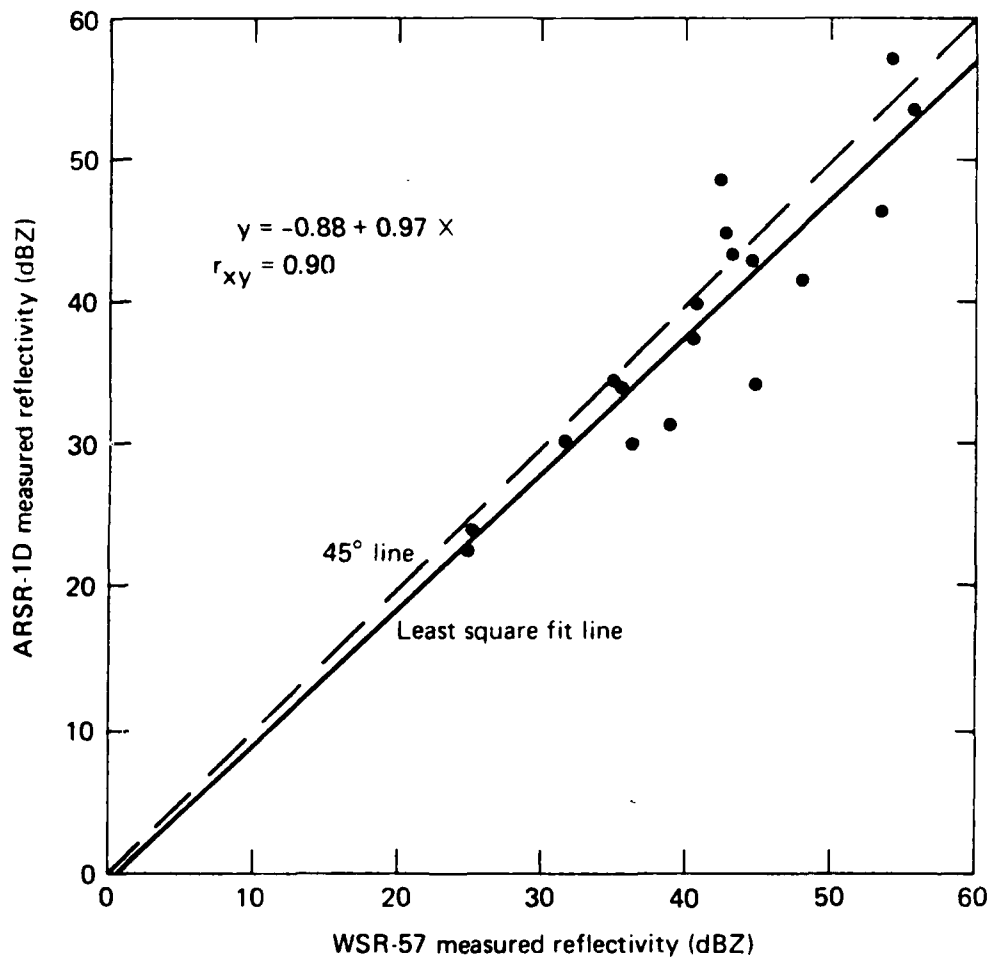
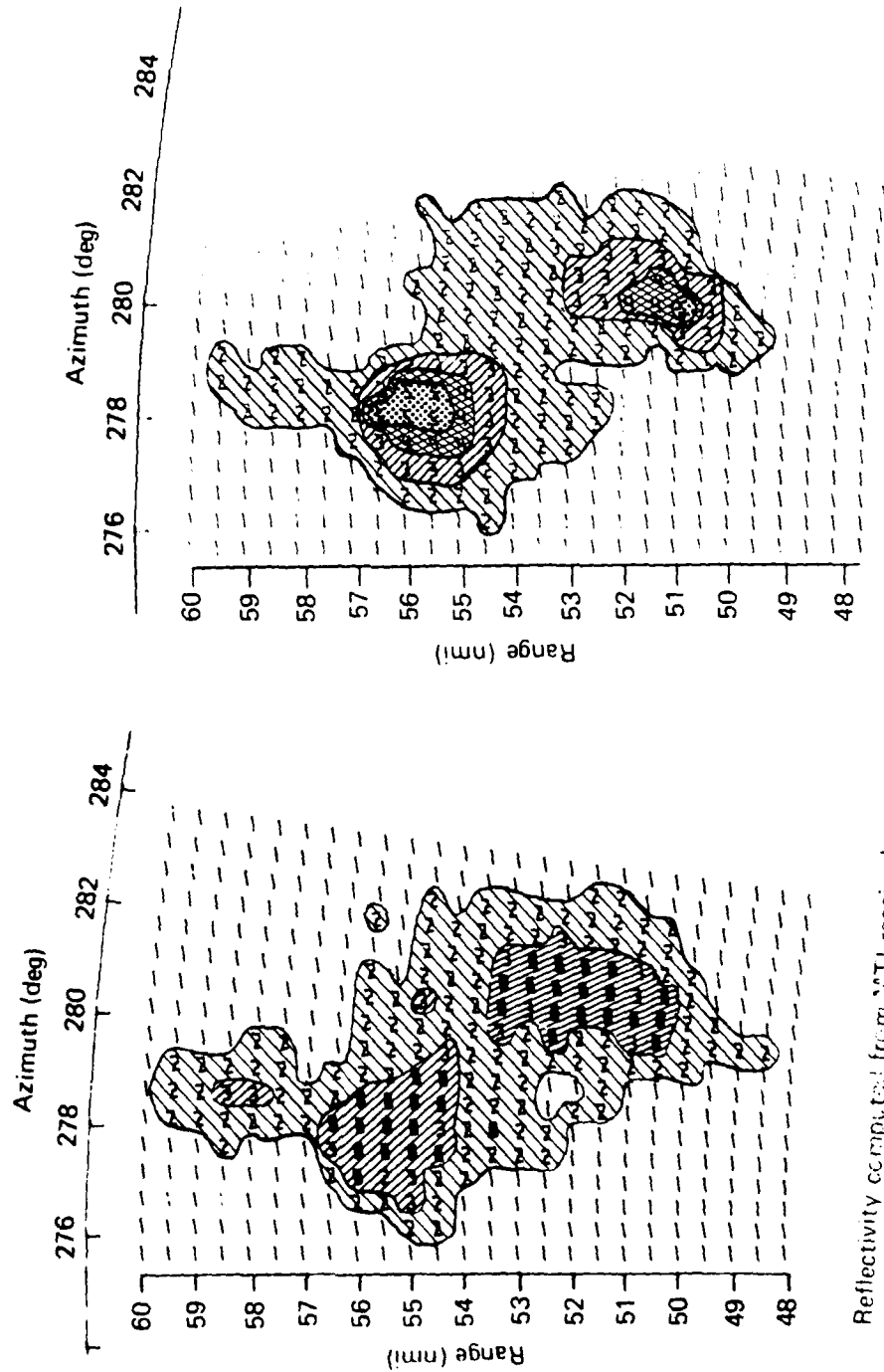
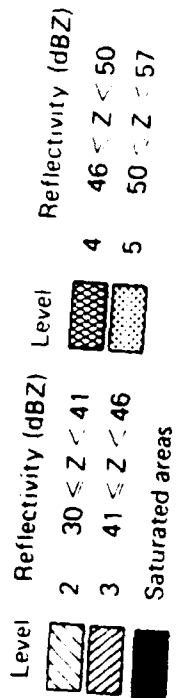


Figure 5-13. ARSR-1D measured reflectivity vs WSR-57 profile maximum at the same azimuth and range as the ARSR-1D measurement for 18 WSR measured profiles.

of reflectivity greater than approximately 30 dBZ, limiting in the MTI receiver caused the signals to saturate so that the maximum reflectivities could not be accurately measured. Figure 5-14 shows an example of how the typical MTI to log video comparison appeared where the solid symbols indicate areas of saturation. This particular cell was one that showed a good pattern at level 2 reflectivity, but reflectivities greater than level 3 could not be accurately measured.

The results indicate that the MTI of the ARSR radar as presently designed is not good for weather reflectivity measurements, due to limiting of the receiver and the zero velocity notch of the filter. The MTI weather reflectivity data analyzed was beyond ground clutter ranges. Over ground clutter MTI weather reflectivities would be further suppressed. Further work may be desirable for determining how to measure MTI weather reflectivities.



Reflectivity computed from MTI received power

Reflectivity computed from log video received power

Figure 5-14. Comparison of MTI and log video contours.

6.0 DATA REDUCTION AND ANALYSIS - TERMINAL

Considerable effort was put into the data reduction phase of data taken in the New Orleans experiment. However, problems were encountered which have not been corrected to this date. These problems were from numerous sources. In some cases calibrations were in error and in others there were spikes in the raw data that could not be removed. All problems pointed to difficulties in the recording of the data and experimental procedures. In no case was there an indication that the problems stemmed from the radars. Due to these problems, no data from the terminal experiment are available for inclusion in this report.

## 7.0 INTERPRETATION OF RESULTS

### 7.1 Enroute Radars

The data analyzed from the Oklahoma experiment and the simulation have indicated that the FAA enroute radars are capable of measuring reflectivity sufficiently accurately to provide a contoured weather display for air traffic controllers. The experimental results presented herein have a bias of approximately 4 dBZ which has not been accounted for to date. Since this is a bias error, the ARSR radars, provided they are properly calibrated, should measure storm intensity and position as well as the NWS WSR-57, at ranges within 185 km (100 nmi).

The simulation indicates that with a  $3/4^\circ$  PMG the ARSR-1D should detect as well as the WSR for convective storms when detecting within 240 km (130 nmi), because within these ranges, heights for severe storms should be sufficient to fill most of the beam. Beyond this range some statistical correction for beamfilling and earth curvature effects could be applied to the received signal to estimate the true reflectivity. The amount of correction will depend on the radar and will be more for the ARSR-1D with its  $6^\circ$  (3 dB) beamwidth, than for the ARSR-2 and ARSR-3 which have a  $4^\circ$  beamwidth. The WSR-57 will also measure signals that are degraded by beamfilling and earth curvature effects if operated beyond 240 km. A statistical correction should also be applied.

It should be emphasized that the experiment in Oklahoma was conducted with the ARSR-1D operated in modes suitable for weather detection. That is, linear polarization was used in all six cell storms analyzed here. Where the STC curve used was equivalent to  $R^{-4}$ , an adjustment was made in the computer program to correct back to an  $R^{-2}$  STC curve. This indicates that the enroute radars must be operated in an optimum weather mode in order to measure reflectivity accurately. This may require modifications and/or adjustment to the radar or correction to the received weather data to produce representative reflectivity estimates.

7.2 Terminal Radar

The simulation has indicated that the terminal radar ASR-8 low beam and ASR-5 should have no problem detecting accurate reflectivity data when operated within conventional 60 nmi range. Although clutter was not addressed in the simulation, the basic assumption is that weather measurements inside of clutter ranges are not accurate.

## 8.0 CONCLUSIONS

The following conclusions are made based on the results from this study.

- (1) All ARSR radars can be used to measure and display meaningful weather data when operated in a mode optimized for weather detection within 240 km. This conclusion is based on both experimental results from the ARSR-1D and simulated results. The 240 km range restriction is imposed because beyond this range, the effects of earth curvature, partially filled beams, and integration greatly degrade the estimates of storm intensity.
- (2) All ARSR radars and the WSR-57 will, in general, underestimate the maximum reflectivity with the amount of underestimation dependent on storm range and position of the maximum in altitude. For storms with maximum reflectivity on the ground the underestimation increases with increasing 3 dB beamwidth. Thus, the WSR-57 with the 2 degree beam should be closer to the maximum. When the maximum is positioned at high altitudes the ARSR radars should detect the storm intensity more accurately than the WSR-57 radar in a normal scan mode (i.e., .5° or 1° elevation angle). This result is significant since there is evidence that severe storms have maximum intensity at higher altitudes during the period of peak development.
- (3) The ARSR and the WSR-57 radars measure a reflectivity closer to an average of the total profile reflectivity (i.e.,  $\langle Z \rangle$ ) than to the maximum.
- (4) The ARSR MTI systems as they are presently configured are not suitable for accurate weather measurement.
- (5) At ranges greater than 240 km the ARSR radars should have a statistical correction factor applied to the received signal to account for partial beamfilling, earth curvature and integration effects. It should be noted that the WSR-57 should also have such correction if operated beyond this range. The exact nature of this statistical correction would have to be

determined based on a study of average heights and profiles of severe storms. Since such a correction factor would be statistical in nature, it would not eliminate all reflectivity measurement errors at long ranges but rather reduce them.

(6) The simulation indicates that the ASR-8 low beam and ASR-5 are capable of detecting weather accurately within their normal operating range and outside the limits of ground clutter (i.e., MTI area). This statement assumes an operating mode which is suitable for detecting weather (i.e., linear polarization and  $R^{-2}$  STC curve).

(7) The ASR-8 high beam is not suitable for weather detection when operated as the sole source of the measurement. However, when it is used in a range gating mode with the low beam and restricted to close-in ranges, it may measure reflectivity as accurately as the low beam. The reason for restriction of the high beam to short ranges is that its maximum gain is positioned at a higher elevation angle which causes it to illuminate the upper portions of storms at shorter ranges than the low beam. The high beam is operationally utilized at close-in ranges to minimize the reception of ground clutter. This improves MTI and weather reflectivity over ground clutter performance.

(8) The location and strength of reflectivity echoes should aid air traffic controllers in determining areas of intense precipitation. It should be noted, however, that research studies concerning turbulence associated with thunderstorms has not established a clear relationship between intense reflectivity areas and turbulent areas. In fact, areas of significant turbulence have been observed to exist in the clear air outside the areas of reflectivity associated with the thunderstorm. Based on such studies, the recommended criteria is for aircraft to avoid higher reflectivity (46 dBZ and above-levels 4, 5, and 6) storm cores by 10 to 15 miles. Also, it can be said that high reflectivity areas (50 dBZ and above-levels 5 and 6) will contain



intense precipitation and often aircraft damaging hail. Therefore, if such reflectivity data is properly interpreted, such displayed information could materially assist the air traffic controllers.

NOTE: Varying amounts of equipment modifications and/or additions would be required (depending on the Model FAA radar) for simultaneously obtaining optimized displays of aircraft and calibrated weather.

9.0 REFERENCE

1. Battan, L. J., 1973, "Radar Observation of the Atmosphere",  
University of Chicago Press.

## Appendix A

### THE COMPUTER PROGRAM

#### 1.0 INTRODUCTION

For the study of severe weather detection, an experiment was conducted in Norman, Oklahoma, during part of September and October of 1977, as described in the body of this report. Weather data were collected by the ARSR radar and the WSR-57 radar simultaneously. In order to compare the ARSR data with the WSR-57 radar, an IBM 360/91 computer program was written to reduce the data from both radars. A description of this computer program is given in this Appendix and the associated flow chart for the program is given in Table A-9. The program described herein is for the enroute data reduction. The program for terminal data reduction is similar with only slight modifications.

#### 2.0 DESCRIPTION OF THE PROGRAM

In order to compare the radar reflectivity factors of the ARSR and those of the WSR-57, overlapping areas of radar video are digitized and recorded on VQR tape by NAFEC. The computer program described here performs the following functions. First, it reads the ARSR data from the VQR digital tape and obtains a data matrix of reflectivity in dBZ. It follows by reading the WSR-57 data from another VQR tape and generates a data matrix of reflectivity in dBZ. The overlapping area between the two radars is selected and a data matrix of WSR-57 reflectivity values with respect to the ARSR coordinate system is obtained.

##### 2.1 Read ARSR Data

The main program first reads in all the necessary input parameters for the ARSR data on IBM cards. A brief description of these parameters is as follows: (1) The ARSR calibration curve of tape units (i.e., digitized voltages) versus power received (dBm) with noise removed. The reason for removing the noise is as follows. Due to the digitization process, the noise

of the data in terms of tape units on the VQR tape is different from the noise in tape units of the calibration. In order to use the calibration curve, the data and the calibration must have the same reference for noise. This is accomplished by removing the respective noise in tape units (TU) from both, so the noise is at 0 TU for both the data and the calibration. The actual procedure for the computation is explained in a later section. (2) The STC curve attenuation in dB versus range (nmi) is the next input item. Either the  $R^{-2}$  or  $R^{-4}$  curve is used. In Figure A-1 note the  $R^{-2}$  curve, the attenuation starts from 32 dB at range 1 nmi and decreases to 1 dB at 80 nmi. And for the  $R^{-4}$  curve, the attenuation starts from 60 dB at 1 nmi and decreases to 1 dB at 50 nmi. The input also includes K, the constant used in the radar equation, and VNOISE, the noise level (tape units) of the data. The neighborhood in terms of azimuth in degrees,  $\epsilon_{Az}$ , and range in nmi,  $\epsilon_{Range}$ , are inputs used to check for overlapping areas. Finally, NO, the number of range bins, and NAR, the number of azimuth sweeps to be averaged, are also read in. In those cases where range exceeds approximately 60 nmi, a range correction, RCORR, is read in to obtain the true range of the window. This step is required because the VQR machine can only digitize 60 nmi of range extent. There is a difference between the true north and the ACP (azimuth change pulse) which was used in recording the video during the experiment. Therefore, this azimuth correction, AZ-REL, is read in to generate the true azimuth for the VQR window. The format and an example of these inputs are given in Table A-1. After all the above parameters are read in, the main program calls the subroutine WSSCAN to read in the digital data.

Before proceeding to the subroutine WSSCAN, we give a brief description of how the data are stored on tape. The data on the VQR tape are from several windows or scans which are separated by end of file marks. The VQR tape format is given in Table A-2. Each scan is made up of a number of VQR azimuth sweeps where each sweep covers from  $R_1$  to  $R_2$  in range. In front of each

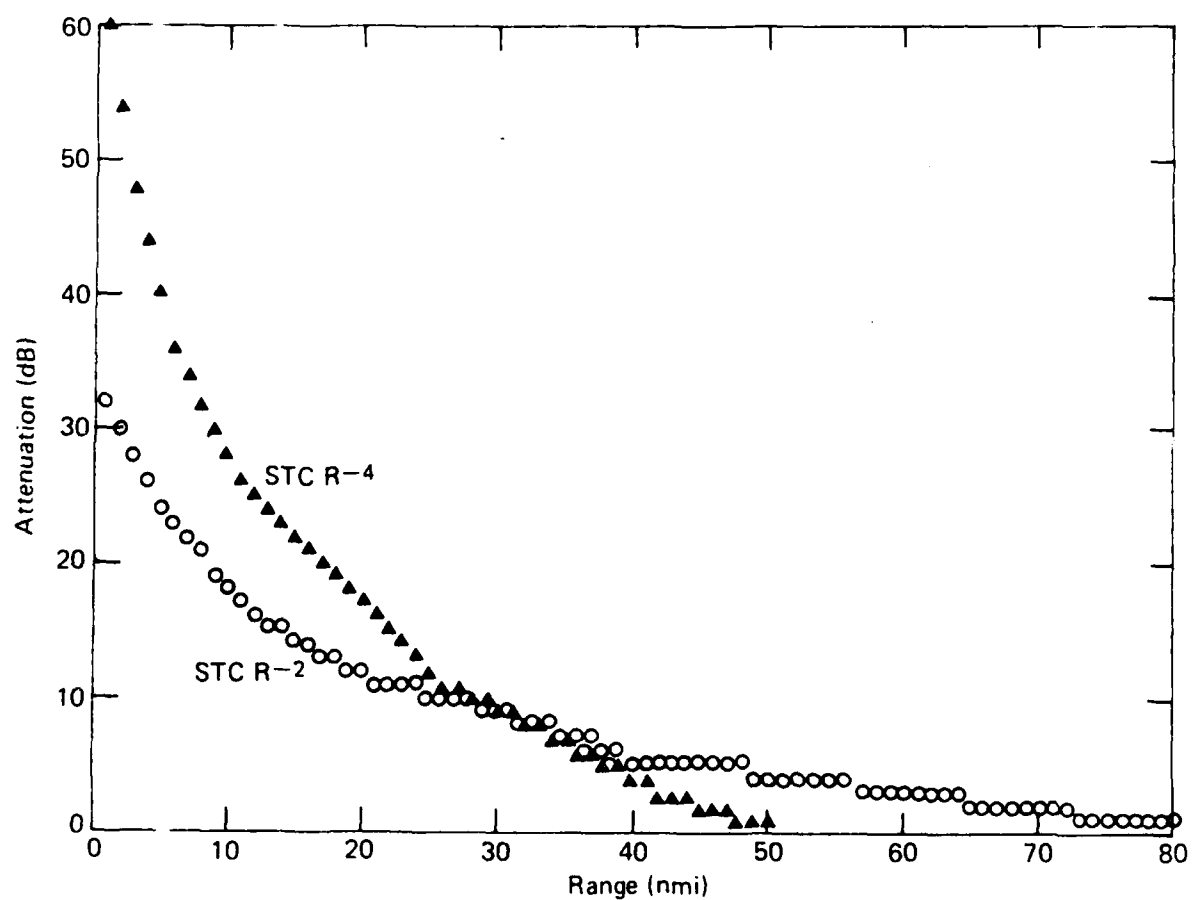


Figure A-1. STC curves measured during Oklahoma experiment.

Table A-1

EXAMPLE INPUT FORMAT AND PARAMETERS FOR THE COMPUTER PROGRAM

Card No.	Input	ARSR	WSR-57
1	Calibration of tape units vs power received (dBm)		
2	File No.	1,1	2,2
3	NO	6	6
4	NAR	5	5
5	$\Delta$ AZ (azimuth sweep resolution)	0.1	0.12
6	AZ-REL (azimuth correction)	13.74°	0.0
7	RCORR (range correction)	0.0 nmi	57.44
8	$\epsilon_{AZ}$	0.3°	.3°
9	$\epsilon_R$	0.5 nmi	.5 nmi
10	$K_p$	1.67E16	4.5E16
11	VNOISE	90 (TU)	233
12(a~)	STC ( $R^{-2}$ ) curve	dB vs range nmi	None
13(a~)	STC ( $R^{-4}$ ) curve	Same	None
14	channel	CHANL = '2'; or '1'	CHANL = '2'; or '1'

Table A-2

VQR TAPE FORMAT

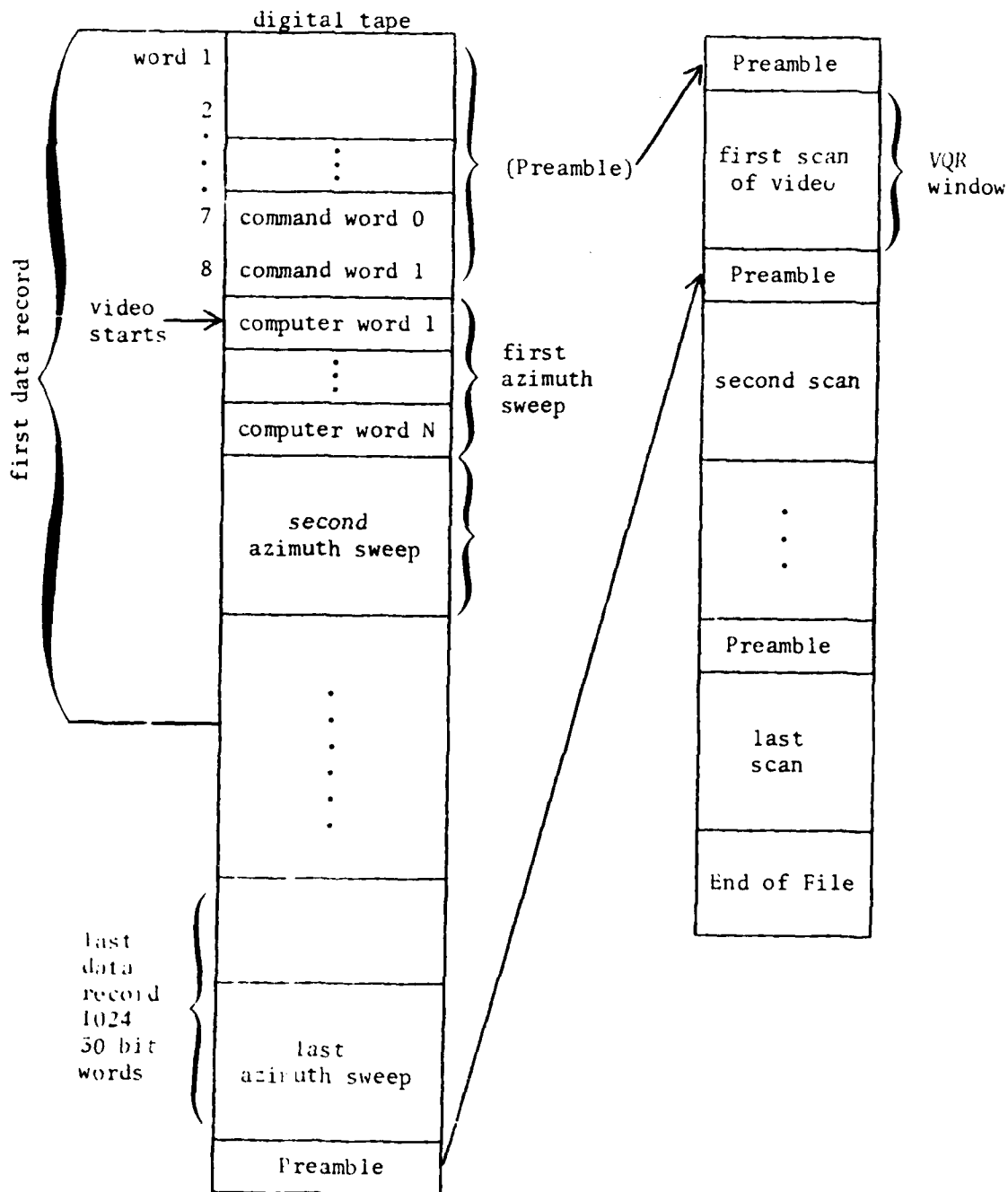


Table A-2 (continued)

## VQR TAPE FORMAT

Preamble:

word 1 Tape identity (digital)  
 2  
 3  
 :  
 6 lower half word contains the scan number  
 7 command word 0  
 8 command word 1

command word 0

29	28	27	26	25	24	23	15	14	1	0
0	SI		C <sub>PD</sub>			no. of computer words per sweep				

C<sub>PD</sub> packing density is 3-10 bit characterSI sample interval 0.869  $\mu$ sec

N = no. of computer words per sweep

command word 1

29		17	12	11	0
1		range start		azimuth start	



 used to check for preamble



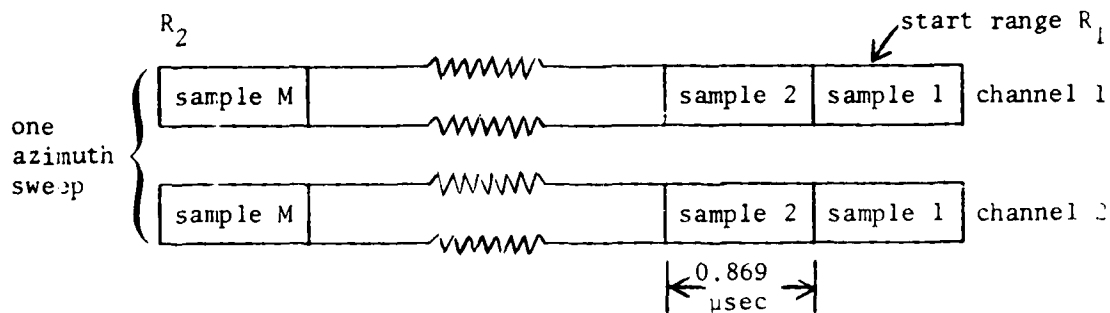
Table A-2 (continued)

## VQR TAPE FORMAT

Video:

computer word 1	29	20	19	10	9	0	bits
	channel 1		channel 2		channel 1		
	sample 2		sample 1				
computer word 2	29	20	19	10	9	0	bits
	channel 2		channel 1		channel 2		
	sample 3		sample 2				

30 bit



where M - total no. of range bins

$$M = N \text{ no. of computer words} \times 3/2$$

$$\Delta S - \text{azimuth sweep} = \left( \frac{1024 \times 3}{2} \right) / N$$

$$R_2 = R_1 + (M-1) \times 0.869 \mu\text{sec} / 12.363 \mu\text{sec per nmi}$$

Each sample of video is a digital number between 0 and 1024.

scan there is a preamble which contains the scan number, start range, start azimuth, and the number of computer words per sweep from which the number of range bins is determined. Each range bin is 0.869  $\mu$ sec long and the azimuth resolution is  $0.1^\circ$  for ARSR data and  $0.12^\circ$  for WSR data. The resolution of the data on tape is too small for comparison of the mean reflectivities from the two radars, therefore, the program averages NO, number of range bins, and NAR, number of sweeps (or azimuths). WSSCAN is the subroutine which reads the data from the digital tape and performs the averaging properly. It returns a data matrix of averaged tape units to the main program.

The computation from tape units to dBZ is performed in the main program in the following manner. Consider a tape unit from the data matrix, the VNOISE in tape units is subtracted from that tape unit, then the power received in dBm corresponding to that tape unit is obtained by interpolation on the input calibration curve. For example, assume that the noise level of the data and the calibration are 88 and 115 tape units, respectively. By subtracting 88 TU from every point in the data and 115 TU from every point in the calibration curve, we bring the noise level of both parameters down to zero. Then the power received for the data is obtained by applying the proper calibration value, which is determined by interpolation from the calibration curve with noise already removed. This power received (dBm) is increased by the amount of attenuation in dB by interpolating the STC curve at the appropriate range. Using this value of power received, the corresponding dBZ value is obtained by using the radar equation. The window of ARSR dBZ values is then constructed. An example of this data matrix is given in Table A-2. The range and azimuth values corresponds to cell center. Notice when the computed dBZ is below 20, the value 11 is printed. When the data is at saturation, the value 99 is printed in its place.

## 2.2 Read WSR-57 Data

The next step is to read in all the input parameters for the WSR-57 data. They are similar to those for the ARSR data.

AD-A142 464

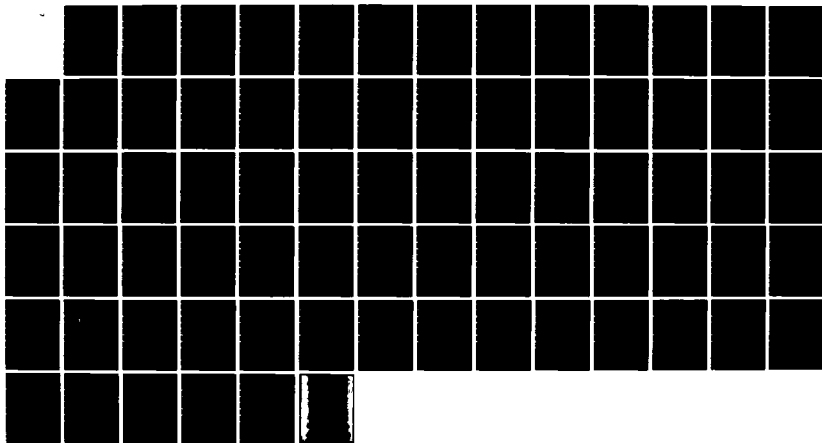
DETECTION OF SEVERE WEATHER BY FAA (FEDERAL AVIATION  
ADMINISTRATION) RADARS(U) JOHNS HOPKINS UNIV LAUREL MD  
APPLIED PHYSICS LAB E B DOBSON ET AL. SEP 79  
FAA-RD-79-91 DOT-FA74WA-3423

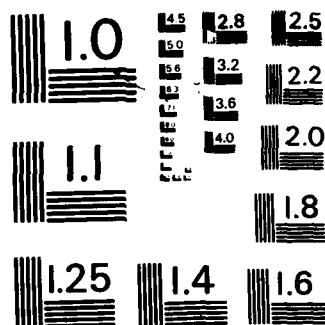
2/2

UNCLASSIFIED

F/G 17/9

NL





MICROCOPY RESOLUTION TEST CHART  
NATIONAL BUREAU OF STANDARDS-1963-A

Table A-3

EXAMPLE OF B-SCAN PRINTOUT OF REFLECTIVITY (dBZ) FOR ARSR-1D

Azimuth (deg)

31.0	31.1	31.2	31.3	31.4	31.5	31.6	31.7	31.8	31.9	32.0	32.1	32.2	32.3	32.4	32.5	32.6	32.7	32.8	32.9	33.0	33.1	33.2	33.3	33.4	33.5	33.6	33.7	33.8	33.9	34.0	34.1	34.2	34.3	34.4	34.5	34.6	34.7	34.8	34.9	35.0	35.1	35.2	35.3	35.4	35.5	35.6	35.7	35.8	35.9	36.0	36.1	36.2	36.3	36.4	36.5	36.6	36.7	36.8	36.9	37.0	37.1	37.2	37.3	37.4	37.5	37.6	37.7	37.8	37.9	38.0	38.1	38.2	38.3	38.4	38.5	38.6	38.7	38.8	38.9	39.0	39.1	39.2	39.3	39.4	39.5	39.6	39.7	39.8	39.9	40.0	40.1	40.2	40.3	40.4	40.5	40.6	40.7	40.8	40.9	41.0	41.1	41.2	41.3	41.4	41.5	41.6	41.7	41.8	41.9	42.0	42.1	42.2	42.3	42.4	42.5	42.6	42.7	42.8	42.9	43.0	43.1	43.2	43.3	43.4	43.5	43.6	43.7	43.8	43.9	44.0	44.1	44.2	44.3	44.4	44.5	44.6	44.7	44.8	44.9	45.0	45.1	45.2	45.3	45.4	45.5	45.6	45.7	45.8	45.9	46.0	46.1	46.2	46.3	46.4	46.5	46.6	46.7	46.8	46.9	47.0	47.1	47.2	47.3	47.4	47.5	47.6	47.7	47.8	47.9	48.0	48.1	48.2	48.3	48.4	48.5	48.6	48.7	48.8	48.9	49.0	49.1	49.2	49.3	49.4	49.5	49.6	49.7	49.8	49.9	50.0	50.1	50.2	50.3	50.4	50.5	50.6	50.7	50.8	50.9	51.0	51.1	51.2	51.3	51.4	51.5	51.6	51.7	51.8	51.9	52.0	52.1	52.2	52.3	52.4	52.5	52.6	52.7	52.8	52.9	53.0	53.1	53.2	53.3	53.4	53.5	53.6	53.7	53.8	53.9	54.0	54.1	54.2	54.3	54.4	54.5	54.6	54.7	54.8	54.9	55.0	55.1	55.2	55.3	55.4	55.5	55.6	55.7	55.8	55.9	56.0	56.1	56.2	56.3	56.4	56.5	56.6	56.7	56.8	56.9	57.0	57.1	57.2	57.3	57.4	57.5	57.6	57.7	57.8	57.9	58.0	58.1	58.2	58.3	58.4	58.5	58.6	58.7	58.8	58.9	59.0	59.1	59.2	59.3	59.4	59.5	59.6	59.7	59.8	59.9	60.0	60.1	60.2	60.3	60.4	60.5	60.6	60.7	60.8	60.9	61.0	61.1	61.2	61.3	61.4	61.5	61.6	61.7	61.8	61.9	62.0	62.1	62.2	62.3	62.4	62.5	62.6	62.7	62.8	62.9	63.0	63.1	63.2	63.3	63.4	63.5	63.6	63.7	63.8	63.9	64.0	64.1	64.2	64.3	64.4	64.5	64.6	64.7	64.8	64.9	65.0	65.1	65.2	65.3	65.4	65.5	65.6	65.7	65.8	65.9	66.0	66.1	66.2	66.3	66.4	66.5	66.6	66.7	66.8	66.9	67.0	67.1	67.2	67.3	67.4	67.5	67.6	67.7	67.8	67.9	68.0	68.1	68.2	68.3	68.4	68.5	68.6	68.7	68.8	68.9	69.0	69.1	69.2	69.3	69.4	69.5	69.6	69.7	69.8	69.9	70.0	70.1	70.2	70.3	70.4	70.5	70.6	70.7	70.8	70.9	71.0	71.1	71.2	71.3	71.4	71.5	71.6	71.7	71.8	71.9	72.0	72.1	72.2	72.3	72.4	72.5	72.6	72.7	72.8	72.9	73.0	73.1	73.2	73.3	73.4	73.5	73.6	73.7	73.8	73.9	74.0	74.1	74.2	74.3	74.4	74.5	74.6	74.7	74.8	74.9	75.0	75.1	75.2	75.3	75.4	75.5	75.6	75.7	75.8	75.9	76.0	76.1	76.2	76.3	76.4	76.5	76.6	76.7	76.8	76.9	77.0	77.1	77.2	77.3	77.4	77.5	77.6	77.7	77.8	77.9	78.0	78.1	78.2	78.3	78.4	78.5	78.6	78.7	78.8	78.9	79.0	79.1	79.2	79.3	79.4	79.5	79.6	79.7	79.8	79.9	80.0	80.1	80.2	80.3	80.4	80.5	80.6	80.7	80.8	80.9	81.0	81.1	81.2	81.3	81.4	81.5	81.6	81.7	81.8	81.9	82.0	82.1	82.2	82.3	82.4	82.5	82.6	82.7	82.8	82.9	83.0	83.1	83.2	83.3	83.4	83.5	83.6	83.7	83.8	83.9	84.0	84.1	84.2	84.3	84.4	84.5	84.6	84.7	84.8	84.9	85.0	85.1	85.2	85.3	85.4	85.5	85.6	85.7	85.8	85.9	86.0	86.1	86.2	86.3	86.4	86.5	86.6	86.7	86.8	86.9	87.0	87.1	87.2	87.3	87.4	87.5	87.6	87.7	87.8	87.9	88.0	88.1	88.2	88.3	88.4	88.5	88.6	88.7	88.8	88.9	89.0	89.1	89.2	89.3	89.4	89.5	89.6	89.7	89.8	89.9	90.0	90.1	90.2	90.3	90.4	90.5	90.6	90.7	90.8	90.9	91.0	91.1	91.2	91.3	91.4	91.5	91.6	91.7	91.8	91.9	92.0	92.1	92.2	92.3	92.4	92.5	92.6	92.7	92.8	92.9	93.0	93.1	93.2	93.3	93.4	93.5	93.6	93.7	93.8	93.9	94.0	94.1	94.2	94.3	94.4	94.5	94.6	94.7	94.8	94.9	95.0	95.1	95.2	95.3	95.4	95.5	95.6	95.7	95.8	95.9	96.0	96.1	96.2	96.3	96.4	96.5	96.6	96.7	96.8	96.9	97.0	97.1	97.2	97.3	97.4	97.5	97.6	97.7	97.8	97.9	98.0	98.1	98.2	98.3	98.4	98.5	98.6	98.7	98.8	98.9	99.0	99.1	99.2	99.3	99.4	99.5	99.6	99.7	99.8	99.9	100.0
------	------	------	------	------	------	------	------	------	------	------	------	------	------	------	------	------	------	------	------	------	------	------	------	------	------	------	------	------	------	------	------	------	------	------	------	------	------	------	------	------	------	------	------	------	------	------	------	------	------	------	------	------	------	------	------	------	------	------	------	------	------	------	------	------	------	------	------	------	------	------	------	------	------	------	------	------	------	------	------	------	------	------	------	------	------	------	------	------	------	------	------	------	------	------	------	------	------	------	------	------	------	------	------	------	------	------	------	------	------	------	------	------	------	------	------	------	------	------	------	------	------	------	------	------	------	------	------	------	------	------	------	------	------	------	------	------	------	------	------	------	------	------	------	------	------	------	------	------	------	------	------	------	------	------	------	------	------	------	------	------	------	------	------	------	------	------	------	------	------	------	------	------	------	------	------	------	------	------	------	------	------	------	------	------	------	------	------	------	------	------	------	------	------	------	------	------	------	------	------	------	------	------	------	------	------	------	------	------	------	------	------	------	------	------	------	------	------	------	------	------	------	------	------	------	------	------	------	------	------	------	------	------	------	------	------	------	------	------	------	------	------	------	------	------	------	------	------	------	------	------	------	------	------	------	------	------	------	------	------	------	------	------	------	------	------	------	------	------	------	------	------	------	------	------	------	------	------	------	------	------	------	------	------	------	------	------	------	------	------	------	------	------	------	------	------	------	------	------	------	------	------	------	------	------	------	------	------	------	------	------	------	------	------	------	------	------	------	------	------	------	------	------	------	------	------	------	------	------	------	------	------	------	------	------	------	------	------	------	------	------	------	------	------	------	------	------	------	------	------	------	------	------	------	------	------	------	------	------	------	------	------	------	------	------	------	------	------	------	------	------	------	------	------	------	------	------	------	------	------	------	------	------	------	------	------	------	------	------	------	------	------	------	------	------	------	------	------	------	------	------	------	------	------	------	------	------	------	------	------	------	------	------	------	------	------	------	------	------	------	------	------	------	------	------	------	------	------	------	------	------	------	------	------	------	------	------	------	------	------	------	------	------	------	------	------	------	------	------	------	------	------	------	------	------	------	------	------	------	------	------	------	------	------	------	------	------	------	------	------	------	------	------	------	------	------	------	------	------	------	------	------	------	------	------	------	------	------	------	------	------	------	------	------	------	------	------	------	------	------	------	------	------	------	------	------	------	------	------	------	------	------	------	------	------	------	------	------	------	------	------	------	------	------	------	------	------	------	------	------	------	------	------	------	------	------	------	------	------	------	------	------	------	------	------	------	------	------	------	------	------	------	------	------	------	------	------	------	------	------	------	------	------	------	------	------	------	------	------	------	------	------	------	------	------	------	------	------	------	------	------	------	------	------	------	------	------	------	------	------	------	------	------	------	------	------	------	------	------	------	------	------	------	------	------	------	------	------	------	------	------	------	------	------	------	------	------	------	------	------	------	------	------	------	------	------	------	------	------	------	------	------	------	------	------	------	------	------	------	------	------	------	------	------	------	------	------	------	------	------	------	------	------	------	------	------	------	------	------	------	------	------	------	------	------	------	------	------	------	------	------	------	------	------	------	------	------	------	------	------	------	------	------	------	------	------	------	------	------	------	-------

Range (nmi)

The subroutine WSSCAN again reads the WSR data in and averages properly and returns with a data matrix of tape units. The VNOISF in tape units is removed from each of the elements of the data matrix. By using the proper WSR calibration curve and radar equation, we obtain the window of WSR-57 dBZ values. In the following section, the method of obtaining the overlapping area of the two radars is described.

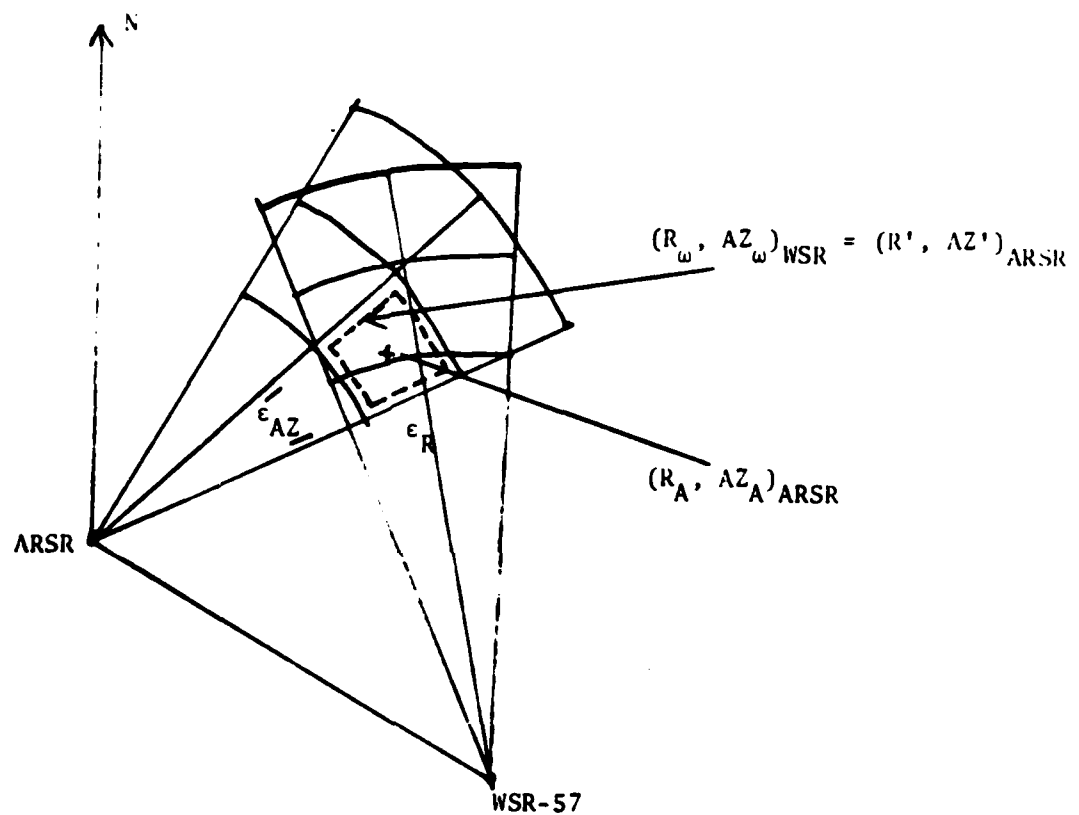
### 2.3 Find Overlapping Area of ARSR and WSR Windows

Each of the windows of data is given with respect to its own radar in terms of range and azimuth. See Figure A-2 for the sketch of the ARSR and WSR windows. In order to compare the mean radar reflectivity of the ARSR and WSR-57 using the ARSR radar position as reference, the coordinates ( $R_w, AZ_w$ ) of the center of a WSR-57 cell must be transformed into ( $R', AZ'$ ) the new coordinates with respect to the ARSR radar. The equations used for the conversion of coordinates are given in Figure A-3. The new coordinates ( $R', AZ'$ ) are then used to check if the position in question fell within the neighborhood ( $\epsilon_{Az}, \epsilon_{Range}$ ) of any ARSR cell indicated by ( $R_A, AZ_A$ ). If it does, the radar reflectivity of that WSR cell is placed in the position of the data matrix of that ARSR cell. Hence, a data matrix with ARSR coordinates is filled by a scan of overlapping WSR reflectivity values. An example of this is given in Table A-4. When there is no overlap, zero is placed in the data matrix. Table A-5 gives the rms values within an averaged area for a single scan.

### 2.4 Example of Printout

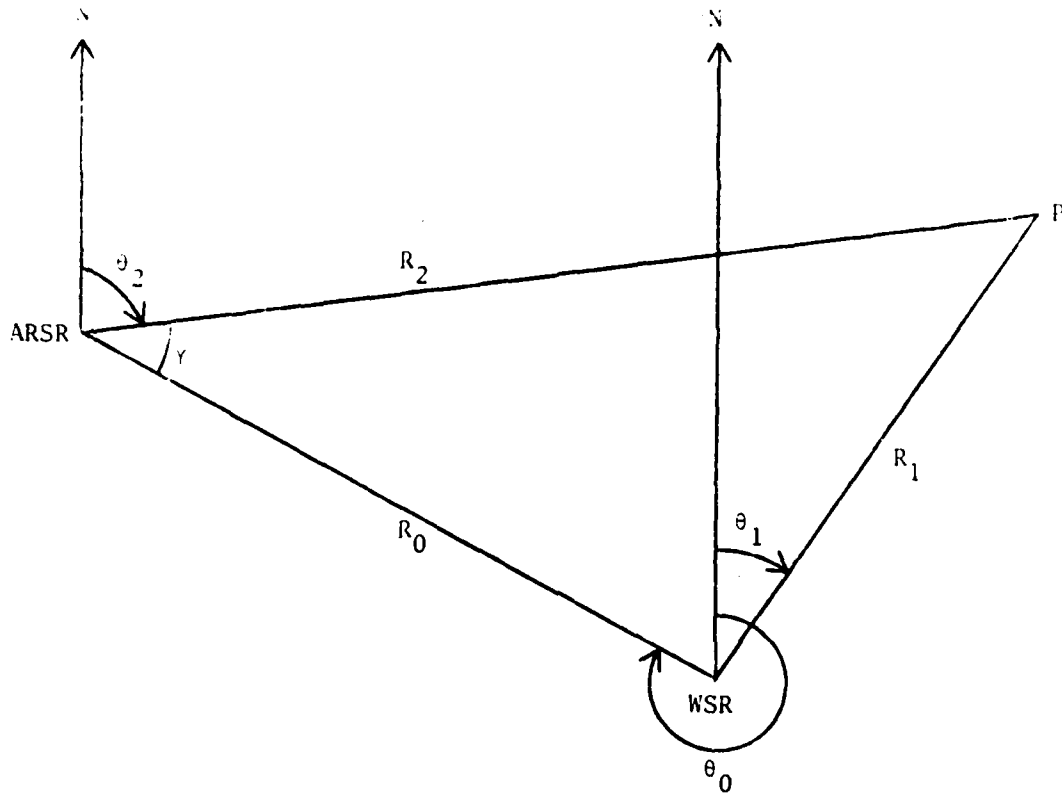
The program continues by reading the next elevation scan of the WSR-57 data. After printing out the data matrix of that WSR-57 scan, the average of the mean WSR radar reflectivity for these scans and previous scans is computed and the average of the rms of these scans is also computed (see Tables A-6 and A-7). As each scan is read in and processed, the average of the mean and the rms of the radar reflectivity factors of the cumulative scans

Figure A-2. Sketch of ARSR and WSR Windows.



- $(R_w, AZ_w)$  range & azimuth with respect to WSR-57
- $(R_A, AZ_A)$  range & azimuth with respect to ARSR
- $(R', AZ')$  is range & azimuth with respect to ARSR
- $\epsilon_{AZ}, \epsilon_R$  neighborhood of ARSR cell

Figure A-3.



$$R_2^2 = R_1^2 + R_0^2 - 2 R_1 R_0 \cos(360 - \theta_0 + \theta_1)$$

$$R_2^2 = R_1^2 + R_0^2 - 2 R_1 R_0 \cos(\theta_1 - \theta_0)$$

$$\gamma = \sin^{-1} \sqrt{\frac{(S - R_0)(S - R_2)}{R_0 R_2}}, \text{ where } S = 1/2(R_0 + R_1 + R_2)$$

If \$\theta\_0 = \theta\_1 = 360\$ or \$0 \leq \theta\_1 < \theta\_0 - 180\$ ; then \$\theta\_2 = \theta\_0 + \pi - \gamma\$ .

If \$\theta\_0 = 180 + \theta\_1 < \pi\$ or \$\pi < \theta\_1 < \theta\_0\$ ; then \$\theta\_2 = \theta\_0 - \pi + \gamma\$ .





Table A-5

EXAMPLE OF ROOT MEAN SQUARE (RMS) REFLECTIVITY (dBZ) WITHIN AN AVERAGED AREA

[illegible]



are printed out. This continues until all the desired WSR elevation scans have been presented. Finally, a data matrix of the differences between the ARSR dBZ values and the WSR-57 dBZ values is printed. An example of this is shown in Table A-8. This completes the description of the program.

### 3.0 THE FLOW CHART

The flow chart of the program is given in Table A-9. It is divided into four parts: Read ARSR data, Read WSR-57 data, Find overlap area of WSR-57, and ARSR data and printout data matrices. The details of the flow chart follow the description of the program very closely. Finally, the listing of the program is given at the end of this Appendix.



Table A-9

## FLOW CHART OF THE COMPUTER PROGRAM TO PROCESS FAA VQR DATA

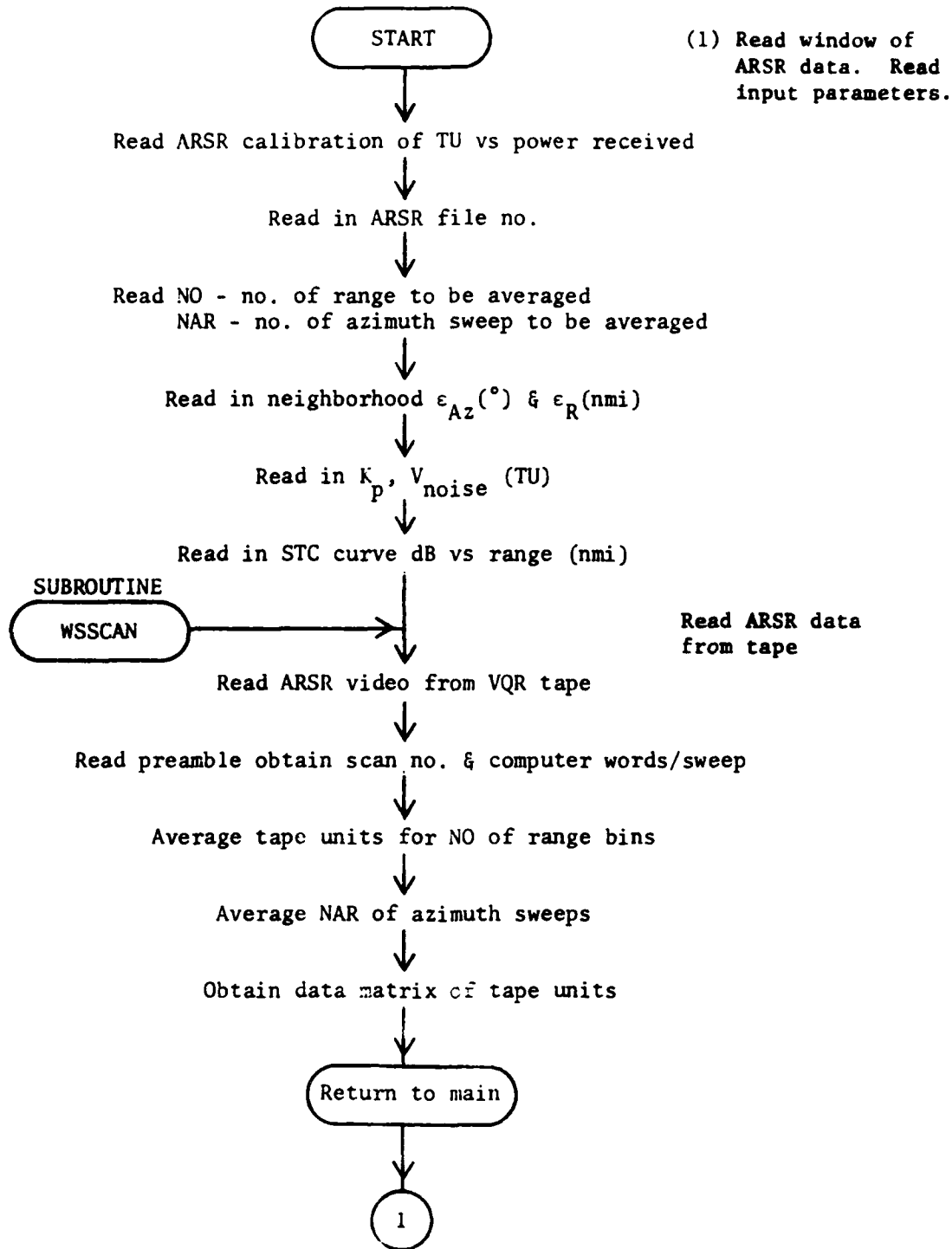


Table A-9 (continued)

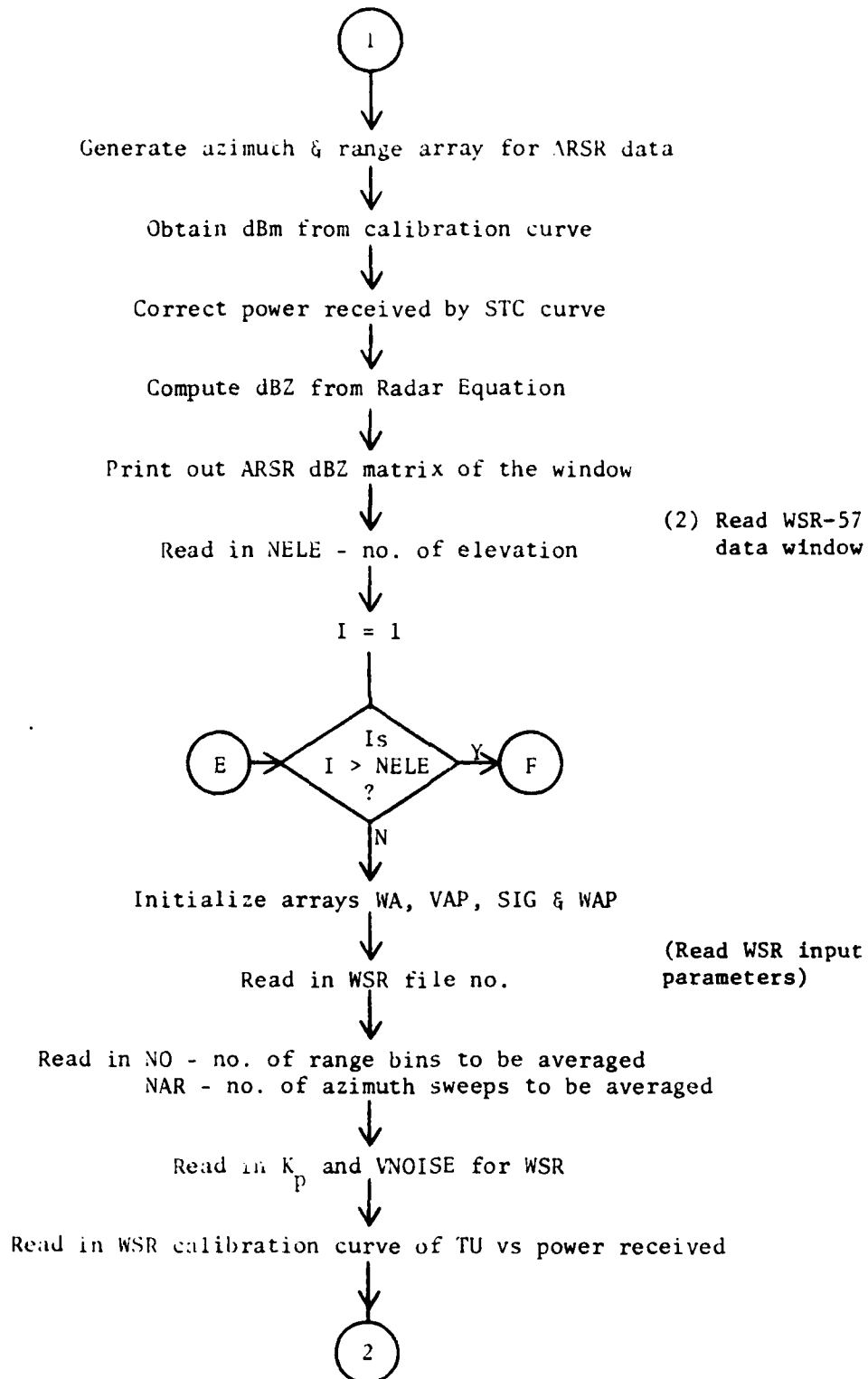


Table A-9 (continued)

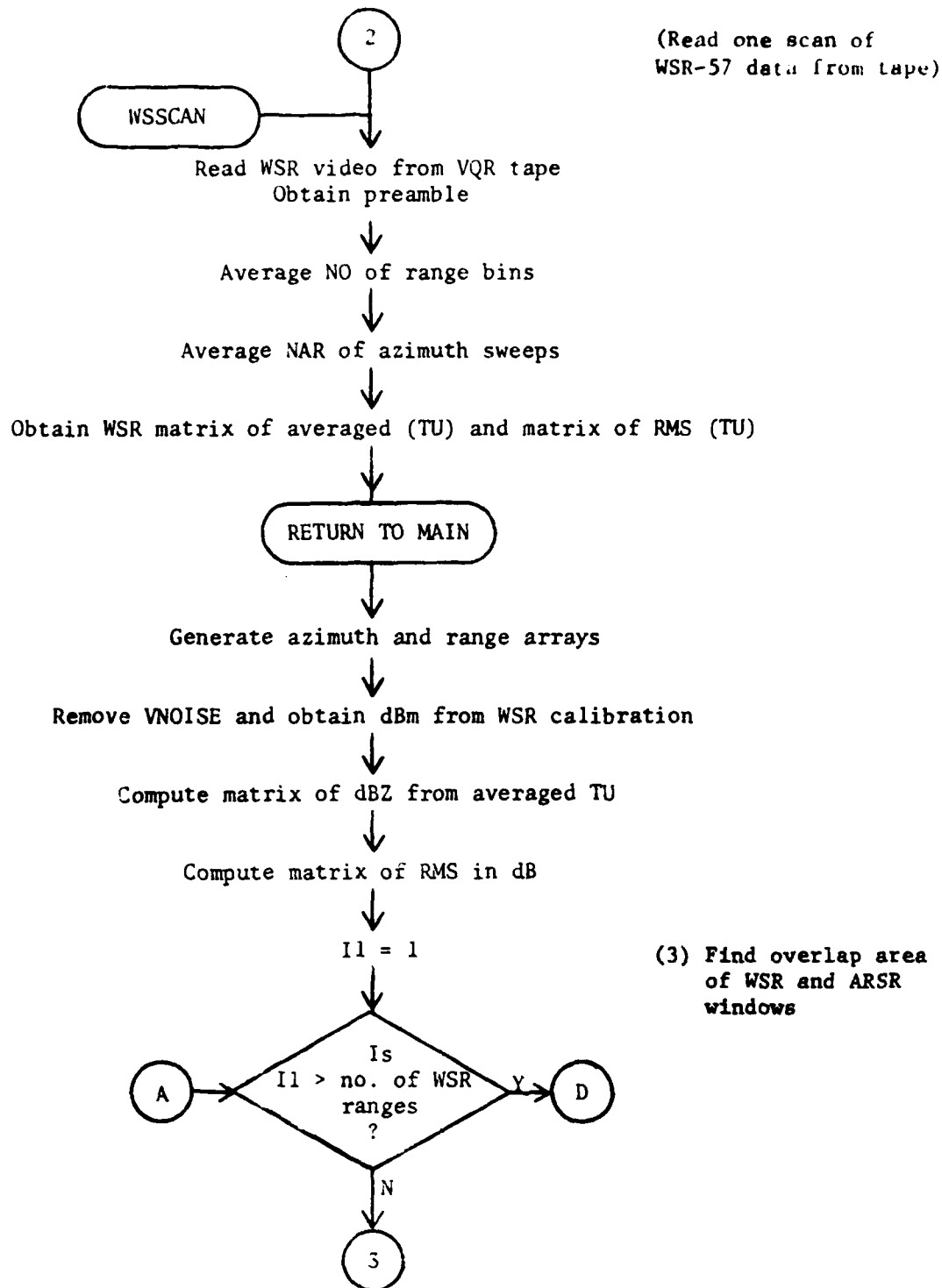




Table A-9 (continued)

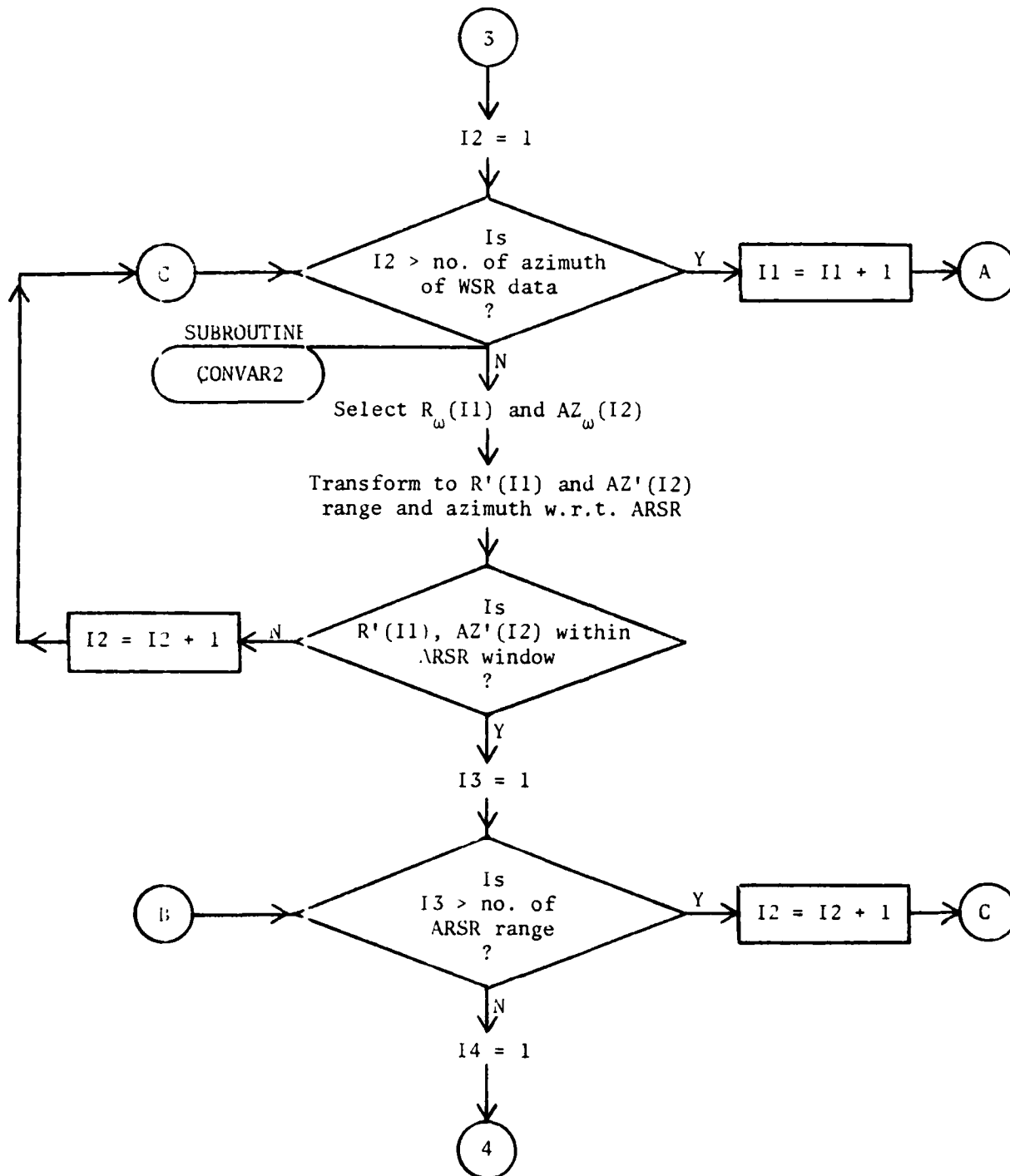


Table A-9 (continued)

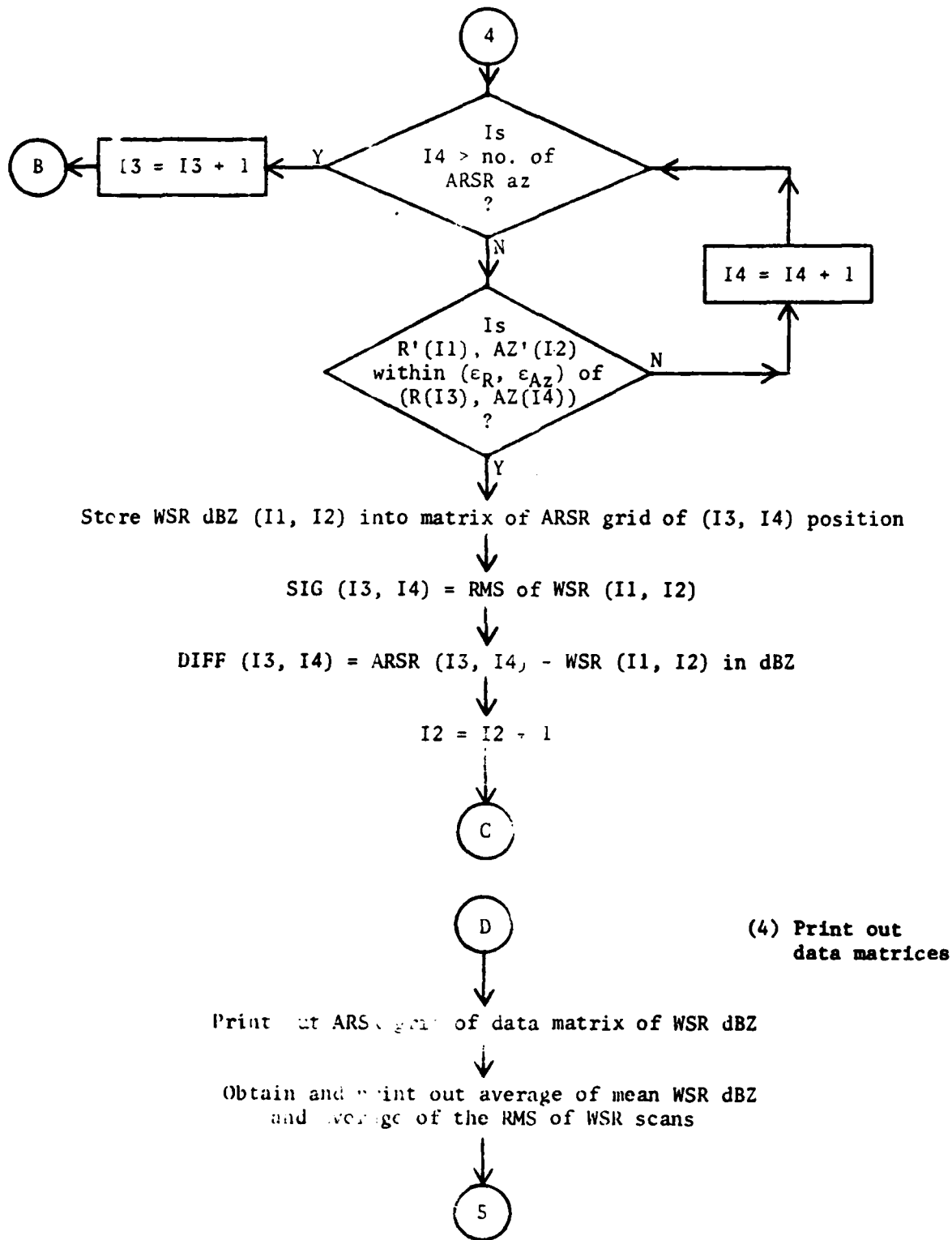
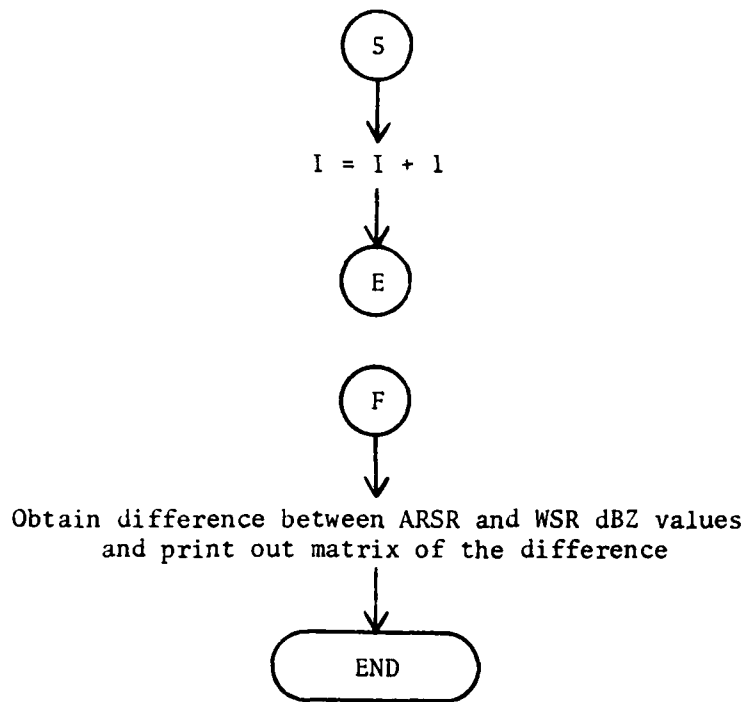


Table A 9 (continued)



## COMPUTER LISTING

COMPILE

\*CALL: PROC OPTIONS(MAIN):

## SOURCE LISTING

```

*CALL: PROC OPTIONS(MAIN):
/* FAAG1 */
DCL VNOISE FLOAT BIN EXTERNAL:
DCL FLAG BIT (1) INIT('1'B):
DCL (TEMPR, TEMPA, APS, AAS) FLOAT BIN:
DCL CH(120) CHAR(1) INIT('120'('1'-1)):
DCL CHANI CHAR(1) EXTERNAL:
DCL (R0 INIT (12.44),
    TH INIT (321.6),
    AZEP INIT (.2), /* EPSTON ROUND IN AZ */
    DEP INIT (0.5) /* EPSTON ROUND IN RANGE */
) FLOAT BIN(21):
DCL CONVAD2 ENTRY:
    FLOAT BIN(21), FLOAT BIN(21), FLOAT BIN (21),
    FLOAT BIN(21), FLOAT BIN(21), FLOAT BIN (21)
)
DCL (TEMP FIXED BIN:
    DCL (RA(60),
        D(50,50),
        DTEF(50,50),
        X(50),Y(50),
        H(50,50),
        HD(50,50),
        AZA(50),
        AVTD(30),
        APP(30)) FLOAT BIN:
DCL CORR ENTRY ( (*)FLOAT BIN, (*)FLOAT BIN, FIXED BIN,
    FLOAT BIN:
    DCL (I1 INIT(1))
        FIXED BIN:
DCL (IFLAG, MFLAG, IFLAG, MFLAG) BIT(1) EXTERNAL:
    DCL (RCOR), RCOR) FLOAT BIN:
DCL DOF FLOAT BIN:

DCL (NAW) FIXED BIN:
DCL (LASR, MASR, MA, MAST) FIXED BIN:
DCL (NST2, NST4) FIXED BIN:
DCL (STC2(42), RS2(42),
    STC4(42), RS4(42)) FLOAT BIN:
ON ENDFILE (SYSIN) BEGIN:
PUT SKIP(4) LIST ('END OF DATA CARDS -HALT'):
STOP:
END:
/* GET ASR-R DATA AND POSITION */
GET LIST (NAW, (AVTD(1), APP(1) D=1 TO NAW)) COPY:
GET LIST (AFILE, AEFIL) COPY:

```

COMPILER

NCALL: PROC OPTIONS(MAIN):

```

      GET LIST ( NO, NAR) COPY:
      GET LIST ( AZPR, REF) COPY:
      DCL ( AZ_DEL1, AZREF1, XKR1) FLOAT BIN:
      DCL ( TASPR, TASRAZ) FLOAT BIN (2):
      GET LIST ( AZ_DEL1, AZREF1, RCOR1) COPY:
      GET LIST ( XKR1) COPY:
      GET LIST ( VNOISE) COPY:
      GET LIST ( NST2, ( RS2(I), STC2(I) DO I=1 TO NST2)) COPY:
      GET LIST ( NST4, ( RS4(I), STC4(I) DO I=1 TO NST4)) COPY:
      GET DATA ( CHAN1):
GETTASR: GET LIST ( MAST, MA, IFLAG, MFLAG) COPY:
      NW=NAW:
      AVID=AVID:
      WOR=APR:
      RADAR=111R:
      CALL WSSCAN( AFILE, AREFL, MAST, MA, NO, NAR, U, UR, LASZ,
      MASR):
      IF (LASZ > 50) | (MASR > 50) THEN DO:
        PUT EDIT ('  ASR  ARRAY STORAGE EXCEEDED') (X(10),A):
        STOP:
      END:
/*  GENERATE AZIMUTHS AND RANGE ARRAY  */
      SUM = AZZ + 0.5 * AZ_DEL1 * (NAR-1) + AZREF1:
      DO I=1 TO (ASR:
        AZA(I) = SUM:
        SUM = SUM + ( NAR -1) * AZ_DEL1:
      END:
      SUM = RANGE + 0.5 * RANGE_DEL * (NO-1) + RCOR1:
      DO I=1 TO (MASR:
        RA(I) = SUM:
        SUM = SUM + (NO-1) *RANGE_DEL:
      END:
/* PRINT OUT ASR-R POWER RECEIVED OR REFLECTIVITY */
      DO I= 1 TO (ASR:
        DO J= 1 TO (MASR:
          IF U(I,J) > AVID(NAW) THEN DO:
            U(I,J) = 99.9
            GO TO NEXTI:
          END:
          U(I,J) = PIF1(U(I,J), AVID, NAW, APR):
          TEMPA = PIF1(RA(J),RS4,NST4,STC4):
          TEMPR = U(I,J) + TEMPA:
          TEMPR = TEMPR /10.0:
          TEMPR = 10. ** ( TEMPR):
          U(I,J) = (RA(J)**2* TEMPR/XKR1)*1.F18*1.43*1.F6:
          U(I,J) = 10. * LOG10(U(I,J)):
          IF U(I,J) <20. THEN U(I,J) = 11.:
        NEXTJ:
      END:
      END:

```

COMPILE

WCALL: PROC OPTIONS(MAIN):

```

1      LTEMP = LASR:
2      IF LASR > 30 THEN LASR = 30:
3      PUT LIST ( '          ASD-R DATA          ' ):
4      PUT SKIP EDIT ( ' -P-1. (AZA(1) DO I=1 TO LASR))
5          (X(2), A, 30 F(4.0), SKIP):
6      DO J=1 TO MASH:
7          PUT SKIP EDIT ( RA(J), ( U(I,J) DO I=1 TO LASR))
8          (X(2), F(6.1), 30 F(4.0), SKIP):
9      END:
10     LACO = LTEMP:
11         DO J = 1 TO MASH:
12             DO I = 1 TO LASR:
13                 D(I,J) = U(I,J):
14                 U(I,J) = -120:
15                 JP(I,J) = -120:
16             END:
17         END:
18     PUT PAGE LIST ( '          ' ):
19     FLAG = '11R:
20     GET LIST ( NELE):
21     DCL ( AFILE, AENFI)    FIXED BIN (31):
22     DCL ( RANGE1(50),
23         AZ1(50))FLOAT BIN:
24     DCL WADR BIT (1) EXTERNAL INIT ('0'B):
25     GET LIST ( NA, NR):
26     DCL ( WA(NA, NR),
27         WAP( NA, NR),
28         SIG ( NA, NR),
29         VAP( NA, NR)) CONTROLLED FLOAT BIN:
30     ALLOCATE WA(NA, NR),
31         WAP( NA, NR),
32         SIG ( NA, NR),
33         VAP( NA, NR):
34     DCL ( WVID(30), WPR(30)) FLOAT BIN EXTERNAL:
35     DCL ( RANGE_DEL INIT(0.07),
36         AZ_DEL INIT (0.07),
37         AZREL,
38         R,
39         SUM) FLOAT BIN:
40     DCL NW FIXED BIN EXTERNAL:
41     DCL ( WFILE , WENFI) FIXED BIN(31):
42     DCL ( MSTART , M, NA1, NA7, NAZEN, NRAN) FIXED BIN:
43     DCL WSSCAN ENTRY ( FIXED BIN (31), FIXED BIN(31),
44         FIXED BIN, FIXED BIN, FIXED BIN, FIXED BIN,
45         (*,*) FLOAT BIN, (*,*) FLOAT BIN,
46         FIXED BIN, FIXED BIN):
47     WA=11:
48     SIG=0.01:
49     VAP=0.01:

```

COMPILER

WCALL: PROC OPTIONS(MAIN):

```

      WAP=0.0;
      GET LIST ( WFILE, WENFL) COPY;
      GET LIST ( NA1, NAZ) COPY;
      GET LIST ( AZ_DEL, AZVEL, PCOR) COPY;
      GET LIST ( XKP) COPY;
      GET LIST ( VNOISE);
      GET LIST ( NW, ( WVID(I3), WPR(I3) DO I3=1 TO NW)) COPY;
      I1=1;
      ONE: DO IM=1 TO NEFL;
      EXTRA: GET LIST ( MSTART, M, IFLAG, MFLAG) COPY;
      ON ENDFILE ( SYSIN) BEGIN;
      PUT SKIP(4) LIST ( 'END DATA CARDS-HALT');
      STOP;
      END;
      RADAR=101R;
      CALL WSSCAN(WFILE, WENFL, MSTART, M, NA1, NAZ, WAP, VAP,
      NAZEN, NRAN);
      IF NAZEN > 50 | NRAN > 50 THEN DO;
      PUT EDIT ('WSH ARRAY STORAGE EXCEEDED') (X(10),A);
      STOP;
      END;
      DCL ( RANGE , AZ2) FLOAT BIN EXTERNAL;
      IF FLAG THEN DO;
      SUM= AZ2 + 0.5 *AZ_DEL*(NAZ-1) + AZVEL;
      DO I=1 TO NAZEN;
      AZ1(I) = SUM;
      SUM = SUM + AZ_DEL *(NAZ-1);
      END;
      SUM = RANGE + 0.5 * RANGE_DEL *(NA1-1) + PCOR;
      DO I=1 TO NRAN;
      RANGE1(I) = SUM;
      SUM = SUM + RANGE_DEL *(NA1 -1);
      END;
      END;
      FLAG = 101R;
      DCL PIF1 ENTRY ( FLOAT BIN, (*) FLOAT BIN, FIXED BIN,
      (*) FLOAT BIN) RETURNS ( FLOAT BIN);
      DCL ( XKP) FLOAT BIN;
      DCL ( XIM) FLOAT BIN;
      XIM=IM;
      DO J=1 TO NRAN;
      DO I=1 TO NAZEN;
      Q= RANGE1(J);
      IF WAP(I,J) > WVID(NW) THEN DO;
      WAP(I,J)=WQ.;
      GO TO NEXTI;
      END;
      WAP(I,J) = PIF1 (WAP(I,J), WVID,NW,WPR);
      TEMPA = WAP(I,J) /10.0;

```

COMPILER

WCALL: PROC OPTIONS(MAIN):

```

      WAP(I,J) = 10. ** (TEMPA);
      WAP(I,J) = ((R**2 * WAP(I,J)) / XKP) * 1.E18 * 3.43 * 1.F6;
      WAP(I,J) = 10. * LOG10(WAP(I,J));
      IF WAP(I,J) < 20 THEN WAP(I,J) = 11.;
      VAP(I,J) = PIF1( VAP(I,J), WVID, NW, WPR);
      TEMPA = VAP(I,J) / 10.0;
      VAP(I,J) = 10. ** (TEMPA);
      VAP(I,J) = ((R**2 * VAP(I,J)) / XKP) * 1.E18 * 3.43 * 1.F6;
      VAP(I,J) = 10. * LOG10(VAP(I,J));
NEXTL:  FND:
      K1 = NAZFN;
      K2 = MRAN;
DO  J=1 TO K2:
      TEMPR = RANGE1(J); /* WSP RANGE */
DO  I = 1 TO K1:
      TEMPA = AZ1(I); /* WSP AZIMUTH */
      CALL CONVAR2(RD,TH,TEMPR,TEMPA,ARS,AAS);
      DO ICON = 1 TO MASR:
        DO ION = 1 TO LASR:
          IF AAS <= AZA(ION) & AAS > AZA(1) THEN DO:
            IF ARS(AAS-AZA(ION)) <= AZEP THEN DO:
              JA=ION;
              IF ARS(ARS - RA(ICON)) <= REP THEN DO:
                JR = ICON;
                WA(JA,JR) = WAP(I,J);
                SIG(JA,JR) = VAP(I,J);
                DTF(JA,JR) = D(JA,JR) - WA(JA,JR);
                IF D(JA,JR) < 20 & WA(JA,JR) < 20. THEN DTF(JA,JR) = 11.;
                FND:
              FND:
            FND:
          FND:
        FND:
      FND:
      FND:
      FND:
      FND:
      IF LASR > 30 THEN LASR = 30;
      PRINT PAGE LIST ( ' WSP57 DATA ' );
      PRINT SKIP EDIT ( ' MEAN VALUES ' ) (X(20),A);
      PRINT LIST ( ' AZIMUTH --->' );
      PRINT SKIP EDIT ( ' -R- ' , (AZA(I) DO I=1 TO LASR))
        ( X(2),A, 30 F(4,0), SKIP);
      DO J= 1 TO MASR:
        PRINT SKIP EDIT ( RA(I), ( WA(I,J)
          DO I= 1 TO LASR))
          (X(2), F(6,1), 30 F(4,0), SKIP);
        FND:
      PRINT SKIP EDIT ( ' RMS VALUES ' ) ( SKIP ,X(20), A ,SKIP);

```



COMPILER

\*CALL : PROC OPTIONS(MAIN):

```

      PUT SKIP EDIT ( ' -R- ', (AZA(I) DO I=1 TO LASR))
      (X(2), A, 30 F(4.0), SKIP);
    DO J=1 TO MASR;
      PUT SKIP EDIT ( RA(J), ( SIG(I,J) DO I=1 TO LASR))
      (X(2), F(6.1), 30 F(4.0), SKIP);
    END;
    XIM=IM;
    DO I=1 TO LASR;
    DO J=1 TO MASR;
      IF XIM=1 THEN TEMPA = 10. **((U(I,J)/10.));
      ELSE TEMPA = 10.**((U(I,J)/10.)*(XIM-1));
      TEMPR = WA(I,J) /10.0;
      TEMPA = TEMPA + 10.**(TEMPR);
      TEMPA = TEMPA / XIM;
      IF TEMPA <=0.0 THEN TEMPA=1.0;
      U(I,J) = TEMPA;
      U(I,J) = 10.*LOG10(U(I,J));
      IF XIM=1 THEN TEMPA=10.**((UP(I,J)/10.));
      ELSE TEMPA = 10.**((UP(I,J)/10.)*(XIM-1));
      TEMPR = SIG (I,J) /10.0;
      TEMPA = TEMPA + 10.0 ** (TEMPR);
      TEMPA = TEMPA / XIM;
      UP (I,J) = TEMPA;
      UP(I,J) = 10. *LOG10(UP(I,J));
    END;
  END;
  PUT SKIP EDIT ( ' AVERAGE OF SCANS' )(X(20),A);
  PUT SKIP EDIT ( ' -R- ', (AZA(I) DO I=1 TO LASR))
  (X(2), A, 30 F(4.0), SKIP);
  DO J=1 TO MASR;
    PUT SKIP EDIT ( RA(J), (U(I,J) DO I=1 TO LASR))
    (X(2), F(6.1), 30 F(4.0), SKIP);
  END;
  PUT SKIP EDIT ( ' RMS OF SCANS ' ) (X(20), A);
  PUT SKIP EDIT ( ' -R- ', (AZA(I) DO I=1 TO LASR))
  (X(2), A, 30 F(4.0), SKIP);
  DO J=1 TO MASR;
    PUT SKIP EDIT(RA(J), ( UP(I,J) DO I=1 TO LASR))
    (X(2), F(6.1), 30 F(4.0), SKIP);
  END;
  PUT PAGE EDIT ( ' FAA RADAR MINUS WSR' )
  (X(10),A);
  DO J=1 TO MASR;
    PUT SKIP EDIT ( RA(J), (DIFF(I,J) DO I=1 TO LASR))
    (X(2),F(6.1), 30 F(4.0), SKIP);
  END;
  PUT PAGE EDIT ( ' CORRELATION IN AZIMUTH ' ) (X(10), A);
  DO J=1 TO MASR;
    DO I=1 TO LASR;

```

COMPILE

WCALL : PROC OPTIONS(MAIN) :

```
|      X(I) = H(T,J) :  
|      Y(I) = D(T,J) :  
|      END :  
|      CALL CORR ( X, Y, LASH, ROF) :  
|      OUT SKID EDIT ( HA(1), ROF) ( X(20), / F(10,3)) :  
|      END :  
|      END :  
|      GO TO GETASR :  
|      END :
```

COMPILED

SSCAN: PROC (AFILE#, ENFILE, NSTART, M, NA1, NA7, WAS, VADS,

## SOURCE LISTING

```

SSCAN: PROC (AFILE#, ENFILE, NSTART, M, NA1, NA7, WAS, VADS,
    NAZEN, NRAM):
    DCL ( WAS(*.*), VADS(*.*) ) FLOAT RIN:
    DCL ( WVID(30), WDR(30)) FLOAT RIN EXTERNAL :
    DCL ( AFILE ) FIXED RIN(31):
    DCL ( PX(30), PY(30)) FLOAT RIN:
    DCL ( NO FIXE ) RIN:
    DCL RADAR BIT(1) EXTERNAL INIT (0.0H):
    DCL ( NW FIXE ) RIN EXTERNAL :
    DCL ( WA(26, 58)) FLOAT RIN:
    DCL ( VAP(26, 58)) FLOAT RIN:
    DCL ( NA1, NA7) FIXED RIN:
    DCL ( AZENTH INIT(0),
        RENTH INIT(0)) FIXED RIN:
    DCL (SUM, SUM1) FLOAT RIN:
    DCL RFI ENTRY (FLOAT RIN, (*) FLOAT RIN, FIXED RIN,
        (*) FLOAT RIN) RETURNS (FLOAT RIN):
    DCL CHANL CHAR(1) EXTERNAL:
    DCL TEMPI FLOAT RIN:
    DCL (HRS, MONTH, DAY, YEAR, HPM, PRF, VI_TYPE, SCAN_NO, ST) FIXED RIN:
    DCL (M) FIXED RIN:
    DCL V1(1542) FLOAT RIN:
    DCL VIDEO BIT(32000) VAR:
    DCL TAPE FILE INPUT :
    DCL ( ENFILE) FIXED RIN(31):
    DCL ( RANGE , A72) FLOAT RIN EXTERNAL:
    DCL TAPE FILE INPUT:
    DCL ( AFILE#) FIXED RIN(31):
    DCL ZPSENS ENTRY(FILE, FIXED RIN(31), CHAR(12)):
    DCL CODE FIXED RIN(31), SENSEWORD CHAR (12):
    DCL (NRUN, NREC, ICODE) FIXED RIN(31):
    DCL (11) FIXED RIN EXTERNAL:
    DCL ( K17, K18, IX, IX1, IX2,
        I7, I9, J, J1, K1, K19, K2, K20, K3, K4, K5, K7, I18, I4,
        I6, LENTH, ISAN, ISTART, IK5, IAV2, IAV3, IFX ) INIT(0)
    FIXED RIN:
    DCL OPENFI ENTRY(CHAR(5), FIXED RIN(31), FIXED RIN(31)):
    DCL ( A7,
        NO_PTS,          /* NO OF VIDEO PTS PRINTED OUT      */
        NO_WORDS,       /* NO OF COMPUTER WORDS PER SWEEP  */
        INCR,
        MESAD,          /* MEMORY START ADDRESS            */
        NO_SWEEP,       /* NO OF SWEEPS IN A WINDOW        */
        AZDEL,         /* AZIMUTH DELTA                   */
        RANGE_DEL,     /* RANGE DELTA                      */
        MAXMEM,        /* MAX MEMORY ADDRESS              */

```

COMPILED

WSSCAN: 0000 (AFILE#, ENFILE#, MSTART, MEND, NA7, WAS, VAL

```

      MILE_SWEEP      /* MILE DEB SWEEP      */
      ) FIXED RIN (21):
      DO ( MSTART) FIXED RIN:
/* MSTART IS THE STARTING RECORD */
/* M IS THE STOP RECORD */
      NOPTS=1536:
      DX=MVID:
      PY=WPD:
      NP=NP:
      ON ENDFILE (SYSTEM) BEGIN:
        PUT SKIP(4) LIST ('END DATA CARDS-HALT'):
        STOP:
      END:
      ON TRANSMIT(TAPE) BEGIN:
        CALL TRSENS(TAPE, CODE, SENSEWORD):
        IF CODE=1 ICODE=3 ICODE=4 THEN GO TO L3:
        PUT SKIP(1) LIST('TRANSMIT FOR CODE=' || ICODE || 'INDEF&NRIN='
          'SENSE-ORD IS ' || SENSEWORD):
        GO TO L0:
      END:
      ON TRANSMIT(TAPEW) BEGIN:
        CALL TRSENS(TAPEW, CODE, SENSEWORD):
        IF CODE=1 ICODE=3 ICODE=4 THEN GO TO L3:
        PUT SKIP(1) LIST('TRANSMIT FOR CODE=' || ICODE || 'INDEF&NRIN='
          'SENSEWORD IS ' || SENSEWORD):
        GO TO L0:
      END:
      ON ENDFILE (TAPEW) BEGIN:
        PUT SKIP (2) LIST ('END OF FILE REACHED'):
        STOP:
      END:
      ON ENDFILE (TAPE) BEGIN:
        PUT SKIP (2) LIST ('END OF FILE REACHED'):
        STOP:
      END:
      AFILE = AFILE#:
      IF AFILE > ENFILE THEN
        DO:
        PUT SKIP (2) LIST ( ' ALL RECORDS READ '):
        RETURN:
      END:
      IF RADAR THEN DO:
      CLOSE FILE (TAPE):
      CALL OPENFIL( 'TAPE', AFILE, ICODE):
      IF ICODE =1 THEN
        DO:
        PUT SKIP(2) LIST ('RAD READ IN OPEN FILE -HALT'):
        STOP:
      END:

```

COMPILE

WSSCAN: PROC (AFILE#, ENFILE, MSTART, MEND, NAZ, WAS, VARS,

```

1      IF IFLAG THEN I1=1:
2      TYPE=0:
3      ISAM=1:
4      GO TO ONE:
5      END:
6      CLOSE FILE ( TAPEW):
7      CALL OPENFILE ( TAPEW, AFILE, ICODE):
8      IF ICODE =1 THEN
9      GO:
10     PUT SKIP(2) LIST ('RAD READ IN OPEN FILE -HALT'):
11     STOP:
12     END:
13     IF IFLAG THEN I1=1:
14     TYPE=0:
15     ISAM = 1:
16     DO VNOISE FLOAT HIM EXTERNAL:
17     ONE: IF RADAR THEN READ FILE(TAPE) INTO (VIDEO):
18           ELSE READ FILE ( TAPEW) INTO ( VIDEO):
19     IF I1< MSTART THEN GO TO L2:
20     Y012: DO I=1 TO NO_PTS:
21     K1 = 20*(I-1) + 1:
22     K2 = 20*(I-1) + 11:
23     IF RADAR & CHANL=11 THEN V1(I)= SUBSTR(VIDEO,K1,10):
24           ELSE V1(I) = SUBSTR(VIDEO, K2, 10):
25     TEMP1 = V1(I):
26     TEMP1 = TEMP1 - VNOISE:
27     V1(I) = TEMP1:
28     END:
29     AZ= SUBSTR(VIDEO,229,12) * .037912:
30     NUM= SUBSTR(VIDEO,211,1):
31     NO_WORDS= SUBSTR(VIDEO,157,4):
32     IF TYPE =0 THEN DO:
33     IF NUM=1 THEN GO TO L:
34     GO TO I050:
35     END:
36     IF IWOOD = NO_WORDS & NUM=1 THEN GO TO I050:
37           ELSE GO TO L:
38     I050: MESAD = SUBSTR( VIDEO, 212, 6) *(2**4):
39     ISAM = 1:
40     RANGE = SUBSTR(VIDEO,223,6):
41     HRS= SUBSTR(VIDEO,1,9):
42     MONTH = SUBSTR(VIDEO,10,6):
43     DAY= SUBSTR(VIDEO,16,6):
44     YEAR= SUBSTR(VIDEO,21,9):
45     RMV = SUBSTR(VIDEO,67,6):
46     PRE = SUBSTR(VIDEO,73,11):
47     VI_TYPE = SUBSTR(VIDEO,74,6):
48     SCAN_NO = SUBSTR(VIDEO,166,15):
49     SI = SUBSTR(VIDEO,182,2):

```

COMPILER

WSSCAN: DDOP (ASTIFH, ENFILE, \*START, \*NA), NA7, WAS, VAP

```

      IWORD = NO_WORDS:
      MAXHEAD = SUBSTR ( VIDEO , 195 , 13):
      NO_SWEEP = 1527 / (NO_WORDS * 3/2):
      DCL (SUM2) FLOAT BIN:
      SUM2 = 0.0:
      TFX=0:
      DCL ( TLEFT INIT(0),
      NFLAG INIT(0)) FIXED BIN:
      NFLAG=0:
      TLEFT=0:
      TAV3=0:
      IF RPM = 0.0 THEN DO:
        PUT SKIP(2) LIST ( ' RPM=0.0 ):
        RPM = 5.0:
      END:
      DEG_SWEEP = 360. / RPM / 1030.:
      AZDEL = DEG_SWEEP * NO_SWEEP:
      SI = (2**4)*(2**SI):
      RANGE_DEL = 1. / SI:
      MILE_SWEEP = NO_WORDS * RANGE_DEL:
      RANGE_STOP = RANGE + MILE_SWEEP:
      AZ_STOP = AZ + AZDEL:
      AZ2 = AZ:
      PUT SKIP EDIT('RECORD NO.,1,1) (A,F(10.0)):
      PUT SKIP(2) EDIT('TIME:',HRS,'MONTH:',MONTH,'DAY:',DAY,
        'YEAR:',YEAR,'RPM:',RPM,'DRF:',DRF,
        'VIDEO TYPE:',VT_TYPE,'SCAN:',SCAN_NO,
        'SAMPLING INTERVAL',SI,'RANGE:',RANGE,
        'NO. OF COMPUTER WORDS/SWEEP',NO_WORDS,'AZIMUTH:',AZ)
        (3(X(2),A,F(10.2),X(2),A,F(10.2),X(2),A,F(10.2),
        X(2),A,F(10.2))):
      PUT PAGE EDIT (
        ' MEMORY START ADDRESS = ', MESAD,
        ' NO OF SWEEP = ', NO_SWEEP,
        ' DEGREE EXTENT ', DEG_SWEEP,
        ' STOP RANGE ', RANGE_STOP,
        ' MILES PER SWEEP ', MILE_SWEEP,
        ' RANGE _ DEL ', RANGE_DEL,
        ' AZ STOP ', AZ_STOP) ( X(20), A, F(5), SKIP, X(20),
        A, F(5.0), SKIP, X(20), A, F(5.2), SKIP, X(20), A, F(5.0),
        SKIP, X(20), A, F(5.2),
        SKIP, X(20), A, F(5.0)):
      YDRF = 1:
      YSTART=9:
      VAP = 0.0:
      WA=0.0:
      AZENTH = NO_SWEEP / NA7:
      LENTH = IWORD * 3/2:
      RENTH = LENTH / NA7:

```

COMPILE

WSSCAN: P200 (AFILE, ENFILE, MSTART, MNA), NAZ, WAS, VAPS.

```

      TAV2 = ILENTH;
L:    IK5 = 1;
      IF NFLAG = 0 THEN DO:
          TAV3 = 0;
          ILEFT = 1536 - NO_SWEEP * ILENTH - ISTART;
          GO TO P20;
          END;
      TAV3 = ILEFT + IFX;
      ILEFT = 1536 + ILEFT - NO_SWEEP * ILENTH;
      NFLAG = 0;
      IK5 = 1;
      IF IFX = 0 THEN DO:
      IF IFX > ILENTH THEN DO:
          PUT LIST (IFX);
          IFX = 0;
          GO TO P20;
          END;
      DO K7 = 1 TO IFX;
      TEMP1 = V1(K7);
      SUM2 = SUM2 + TEMP1;
      SUM1 = SUM1 + TEMP1 ** 2;
      END;
      IF IX > 50 THEN DO:
          PUT SKIP EDIT (IX, ' ')
            (X/10, F(6.0), A);
          GO TO P20;
          END;
      NA(1, IX) = SUM2 / NA1;
      VAP(1, IX) = SUM1;
      IK5 = K7;
      END;
P20: DO I7 = 1 TO NO_SWEEP;
      IX = (1 + TAV3) / NA1 + 1;
      DO I = 1 TO ILENTH BY NA1;
      IF (I + TAV3) > ILENTH THEN GO TO P25;
      I18 = I;
      I4 = I + NA1 - 1;
      SUM = 0.;
      SUM1 = 0.0;
      DO I6 = I18 TO I4;
          K5 = IK5 + ISTART;
          IF K5 > 1536 THEN GO TO P21;
          IF (I6 + TAV3) > ILENTH THEN GO TO P25;
          TEMP1 = V1(K5);
          SUM = SUM + TEMP1;
          SUM1 = SUM1 + TEMP1 ** 2;
          IK5 = IK5 + 1;
          END;
      IF IX > 50 THEN DO:

```

COMPILEP

VSSCAN: PBOC (AFTER#, ENFILE, MSTART, M, NA1, NA7, WAS, VAPS,

```

      PUT SKIP EXIT ( TX, 121)
      (Y(10), F(6,0), A1)
      GO TO Q56:
      END:
      WA(17, IX) = SUM/NA1:
      VAP(17, IX) = SUM1:
      IX = IX + 1:
Q56: END:
P25: TAV3=0:
      END:
Q21: DO IX1 = 1 TO RENTH:
      DO J=1 TO NO_SWEEP BY NA7:
      K3 = J:
      K4 = J+NA7 - 1:
      IX2 = J/NA7 + 1:
      SUM=0.0:
      SUM1 = 0.0:
      DO J1 = K3 TO K4:
      IF J1 > NO_SWEEP THEN GO TO Q25:
      SUM = SUM+WA(J1, IX1):
      SUM1 = SUM1 + VAP( J1, IX1):
      END:
      WA(IX2, IX1) = SUM/NA7:
      SUM1 = SUM1 / (NA1*NA7) - WA(IX2, IX1) **2:
      IF SUM1 < 0.0 THEN DO:
      VAP( IX2, IX1) = 0.0:
      GO TO Q26:
      END:
      VAP( IX2, IX1) = SORT(SUM1):
Q26: IX2 = IX2 + 1:
Q25: END:
      END:
      NAZEN = ISAN * A7ENTH:
      NRAM = RENTH:
      K17 = (ISAN - 1) * A7ENTH + 1:
      K18 = K17 + A7ENTH - 1:
      K19 = 1:
      DO I4=K17 TO K18:
      DO J=1 TO RENTH:
      WAS (I9, I) = WA(K14, I):
      END:
      K19 = K14 + 1:
      END:
      K20 = 1:
      DO I4 = K17 TO K18:
      DO J=1 TO RENTH:
      VAPS (I9, I) = VAP(K20, I):
      END:
      K20 = K20 + 1:

```



COMPILE

WSSCAN: PROC (AFTER, ENFILE, NSTART, M, NA1, NA2, WAS, VAPS,

```

      END:
P21: ISTART = 0:
      IF ILEFT = 0 THEN GO TO I2:
      IF ILEFT > LENTH THEN DO:
        DO I=1 TO LENTH BY NA1:
          IX = I/NA1 + 1:
          IIR=I:
          L4 = I+NA1 - 1:
          SUM=0.0:
          SUM1 = 0.0:
          DO L6=IIR TO L4:
            K5=IX5:
            IF K5 > 1536 THEN GO TO P19:
            IF L6 > LENTH THEN GO TO P19:
            TEMP1 = V1(K5):
            SUM = SUM + TEMP1:
            SUM1 = SUM1 + TEMP1 **2:
            IX5 = IX5 + 1:
          END:
          IF IX > 50 THEN DO:
            PUT SKIP EDIT ( IX, '3')
              (X(10), F(6,0), A):
            GO TO P19:
          END:
          WA(1, IX) = SUM / NA1:
          VAP (1, IX) = SUM1:
P19: ILEFT = 1536 - K5 + 1:
      END:
      END:
      IFX=0:
      DO I=1 TO ILEFT BY NA1:
        IX = I/NA1 + 1:
        IIR=I:
        L4 = I+NA1 - 1:
        SUM=0.0:
        SUM1 = 0.0:
        DO L6=IIR TO L4:
          K5=IX5:
          IF L6 > ILEFT THEN DO:
            IFX = L4 - L6 + 1:
            SUM2 = SUM:
            GO TO Q68:
          END:
          IF K5 > 1536 THEN GO TO Q68:
          TEMP1 = V1(K5):
          SUM = SUM + TEMP1:
          SUM1 = SUM1 + TEMP1 **2:
          IX5 = IX5 + 1:
        END:

```

COMPILE

USSCAN: 0000 (AFTECH, ENFILE, MSTDY, J, NAL, '87, WAS, VAP

```

1      IF IX > 50 THEN DO:
2          PUT SKIP EDIT ( IX, '4')
3              (X(10), F(6.0), A):
4          GO TO Q6R:
5          END:
6      WA(1, IX) = SUM / NA:
7      VAP (1, IX) = SUM:
8      END:
9      Q6R: AFLAG=1:
10     NEXT: GO TO L2:
11     L0: PUT SKIP EDIT ( 'ERROR') (A):
12         I1=I1+1:
13         GO TO L3:
14     L2: I) = I1+1:
15         ISAM = ISAM +1:
16     L3: IF I1<4 THEN GO TO ONE:
17         AFILE = AFILE +1:
18         GO TO TWO:
19     L1: END:

```

SOURCE LISTING

```

CONVAR2: PROC( R0, TH, RS, AS, AAS, AAS1):
    DCL ( RS, AS, AAS, AAS1) FLOAT MIN(2);
    DCL ( R0, TH, TEMP1, 2, S,
           TEMP ) FLOAT MIN(2);
    TEMP1 = RS**2 + R0**2 - 2*RS * R0* COSD(AS -TH);
    TEMP1 = ABS( TEMP1);
    TEMP1 = SQRT ( TEMP1);
    AAS = TEMP1;
    S = (RS +R0 +AAS)/2.0;
    W = SQRT((S-RS)*(S-R0)*(S-AAS)/S);
    TEMP = SQRT (( S-R0)*(S-AAS)/(R0*AAS));
    TEMP = ASIN ( TEMP);
    TEMP=TEMP*2;
    TEMP = TEMP * 57.1;
    IF ( TH -180.) <=AS & AS<TH THEN DO;
        AAS = TH -180. + TEMP;
        GO TO L1;
    END;
    AAS = TH + 180. - TEMP;
L1: IF AAS >360. THEN AAS=AAS -360.;
    RETURN;
END;

```

## SOURCE LISTING

```
I PIF:PROCEDURE ( X, XLIST, N, FLIST) RETURNS(FLOAT RIN);
I   /*
I   FIRST ORDER POLYNOMIAL INTERPOLATION IN ONE VARIABLE.
I   X = POINT TO BE INTERPOLATED.
I   XLIST = INDEPENDENT VARIABLE LIST, (XLIST(1), XLIST(2), ...).
I   N = NUMBER OF ELEMENTS IN XLIST.
I   FLIST = DEPENDENT VARIABLE LIST CORRESPONDING TO INDEPENDENT
I   VALUES IN XLIST.
I   */
I   DECLARE ((XLIST, FLIST) (*), X) FLOAT RIN,
I   (I, N) FIXED BIN;
I   IF X >= XLIST(N) THEN I = N;
I   ELSE IF X <= XLIST(1) THEN I = 2;
I   ELSE DO I = 1 TO N;
I       IF X<=XLIST(I) THEN GO TO PIF;
I   END;
I   PIF:RETURN((XLIST(I-1) - X) *(FLIST(I-1)-FLIST(I))
I       /(XLIST(I) - XLIST(I-1))+FLIST(I-1));
I   END PIF;
```

## Appendix B

### FAA RADAR GAIN PATTERNS

The antenna gain patterns for the ARSR-1D, ARSR-2/1E, ARSR-3, ASR-8, and ASR-4/5/6/7 are shown in Figures B-1 through B-5. The curves are shown plotted as gain versus relative elevation angle. The actual gain at a given elevation angle depends on the positioning of the antenna in elevation. The plotted curves represent data points read at .5° elevation increments from curves furnished by the FAA.

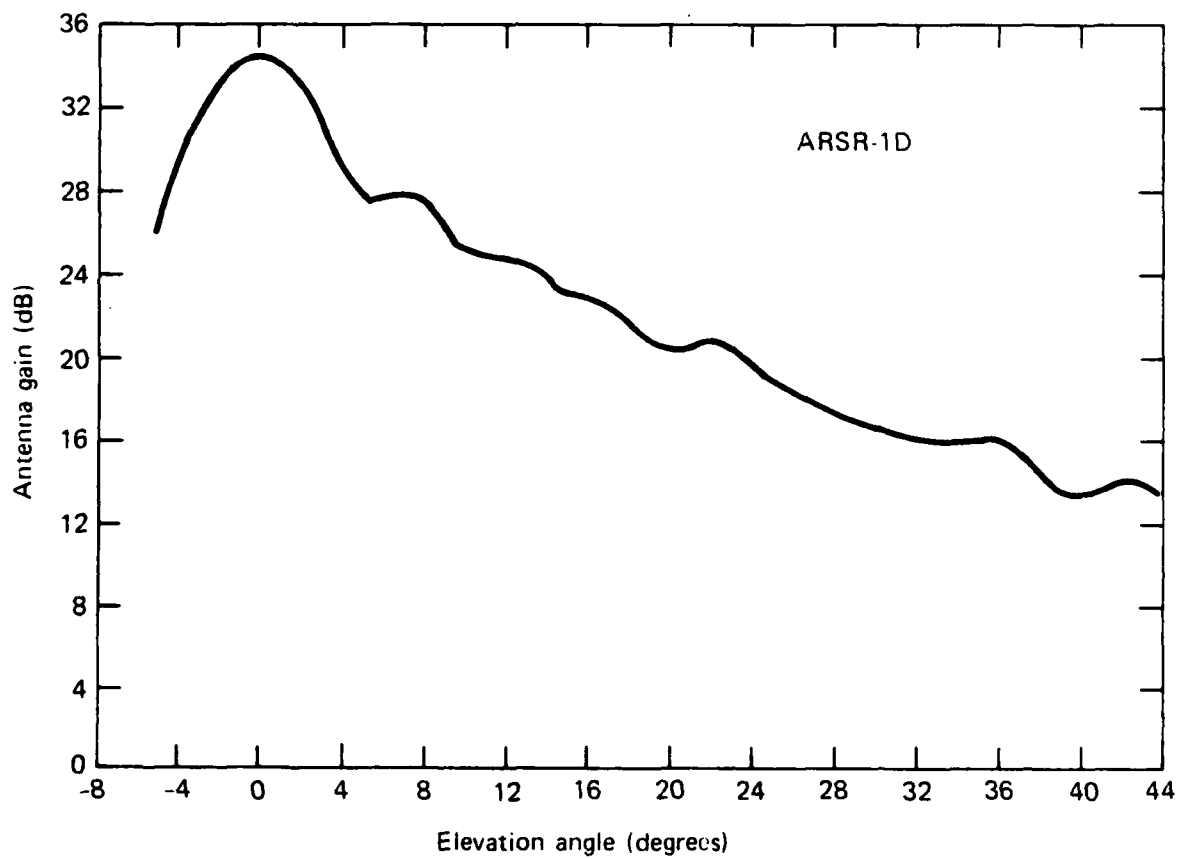


Figure B-1. Antenna gain pattern for ARSR-1D versus relative elevation angle.

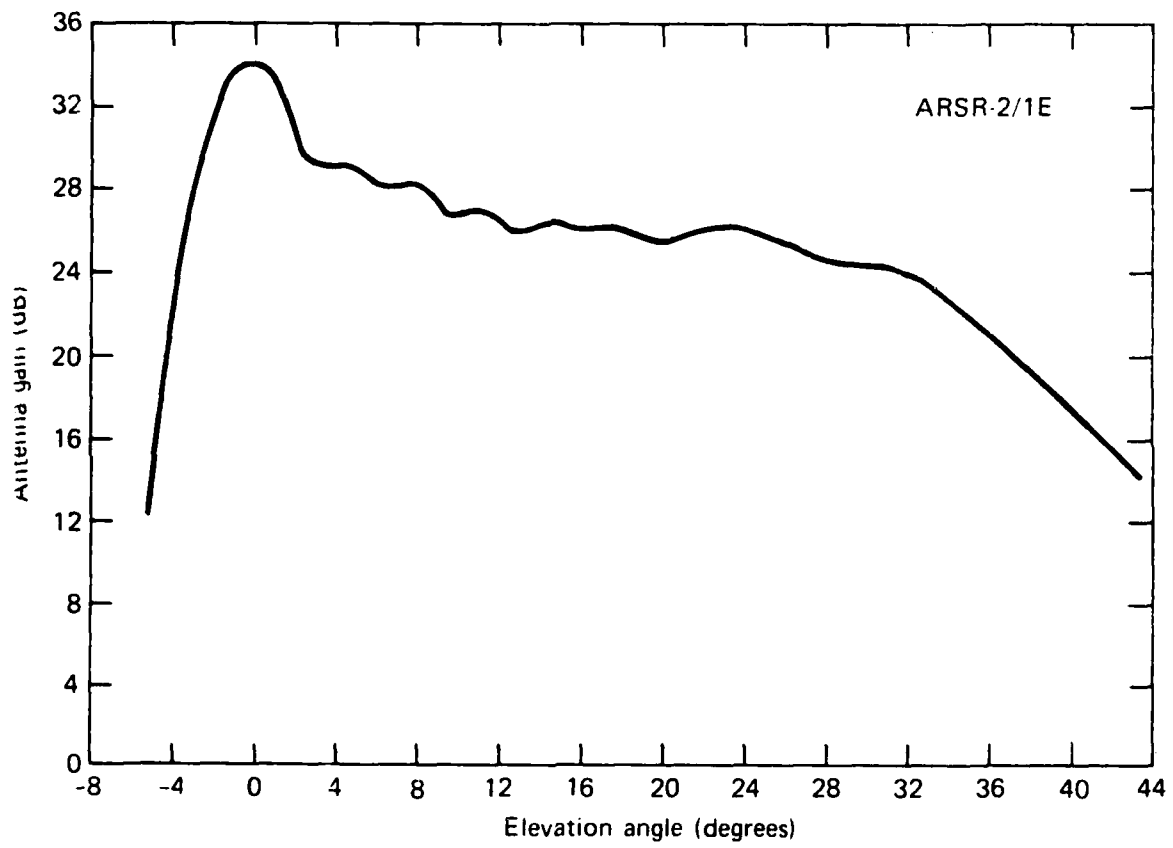


Figure B-2. Antenna gain pattern for ARSR-2/1E versus relative elevation angle.

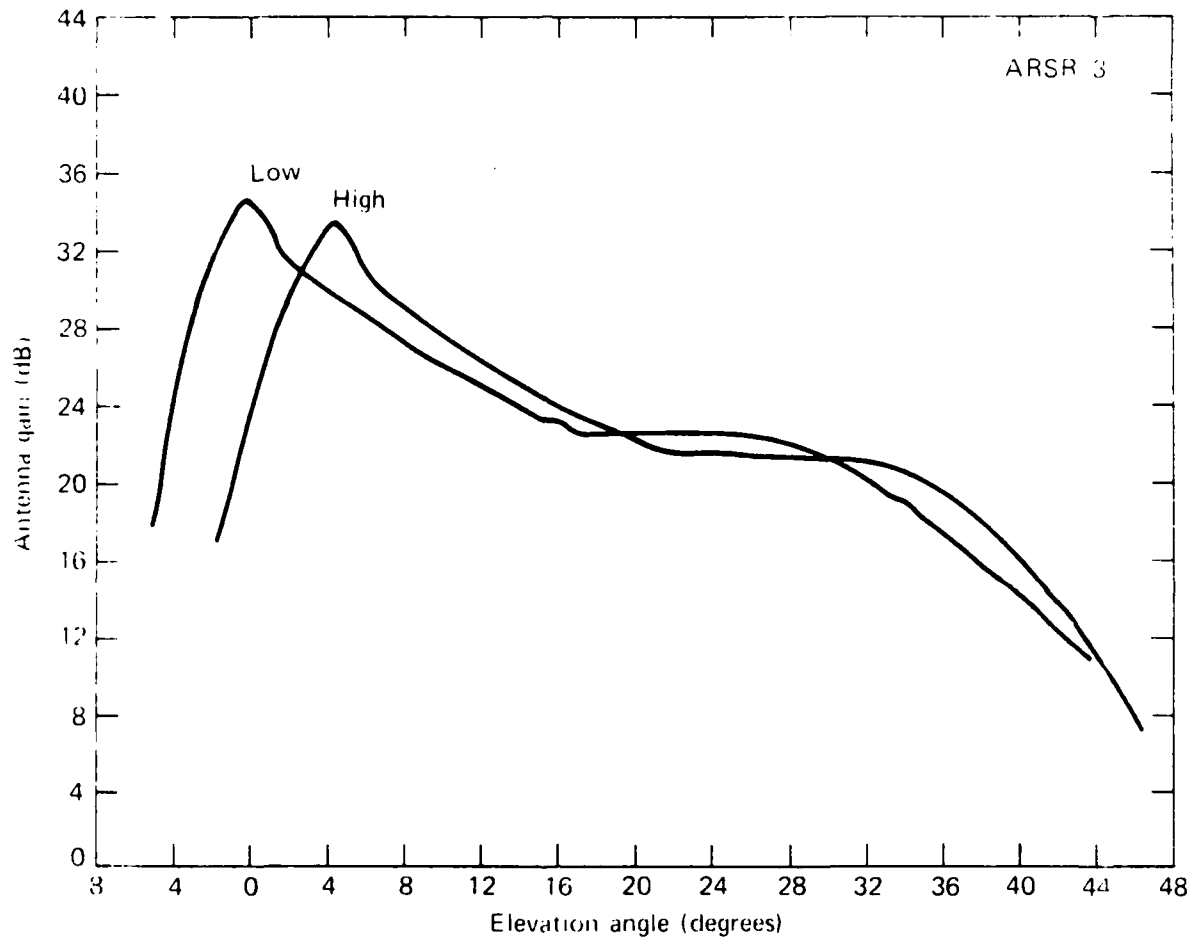


Figure B-3. Antenna gain pattern for ARSR-3 versus relative elevation angle. High and low beams shown.



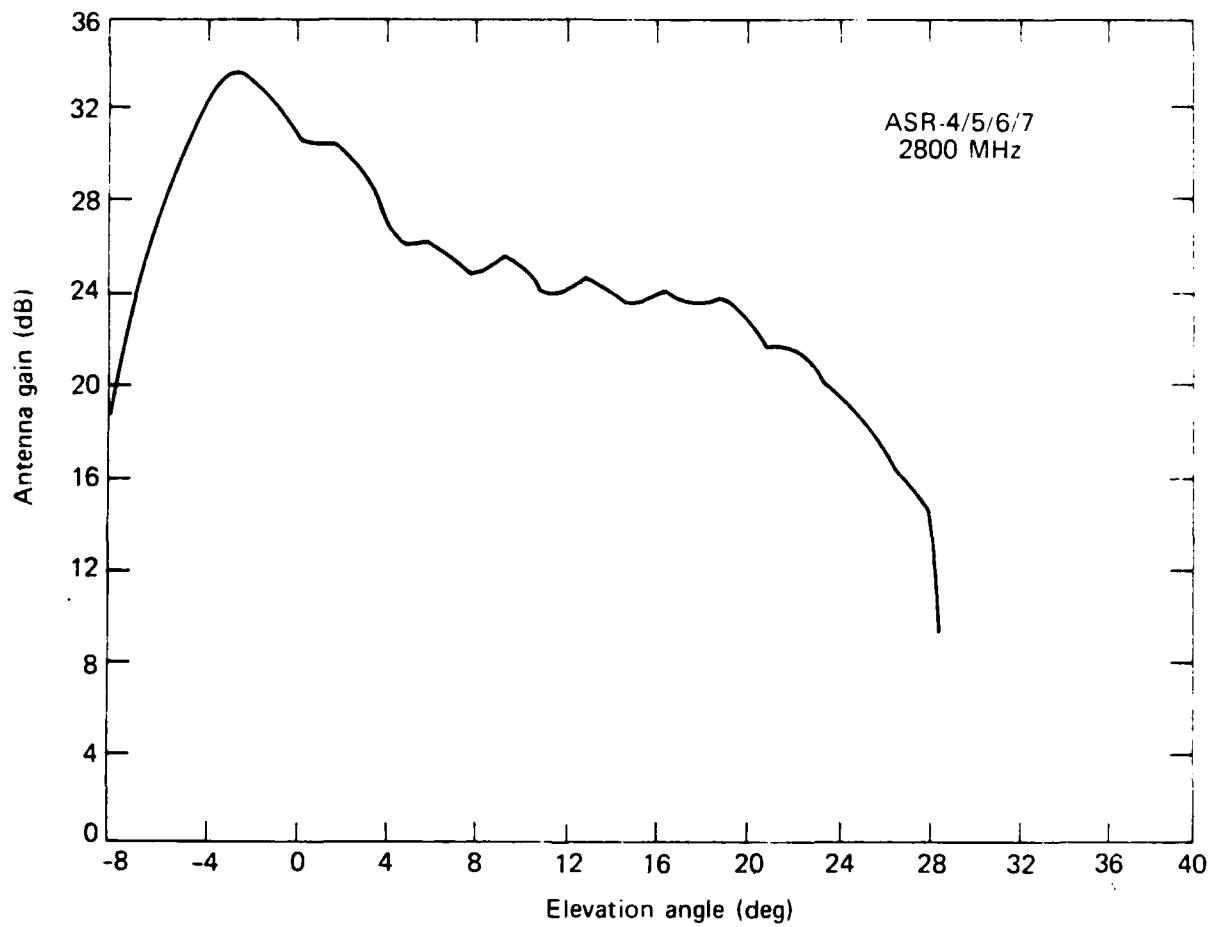


Figure B-4. Antenna gain pattern for ASR-4/5/6/7 versus relative elevation angle.

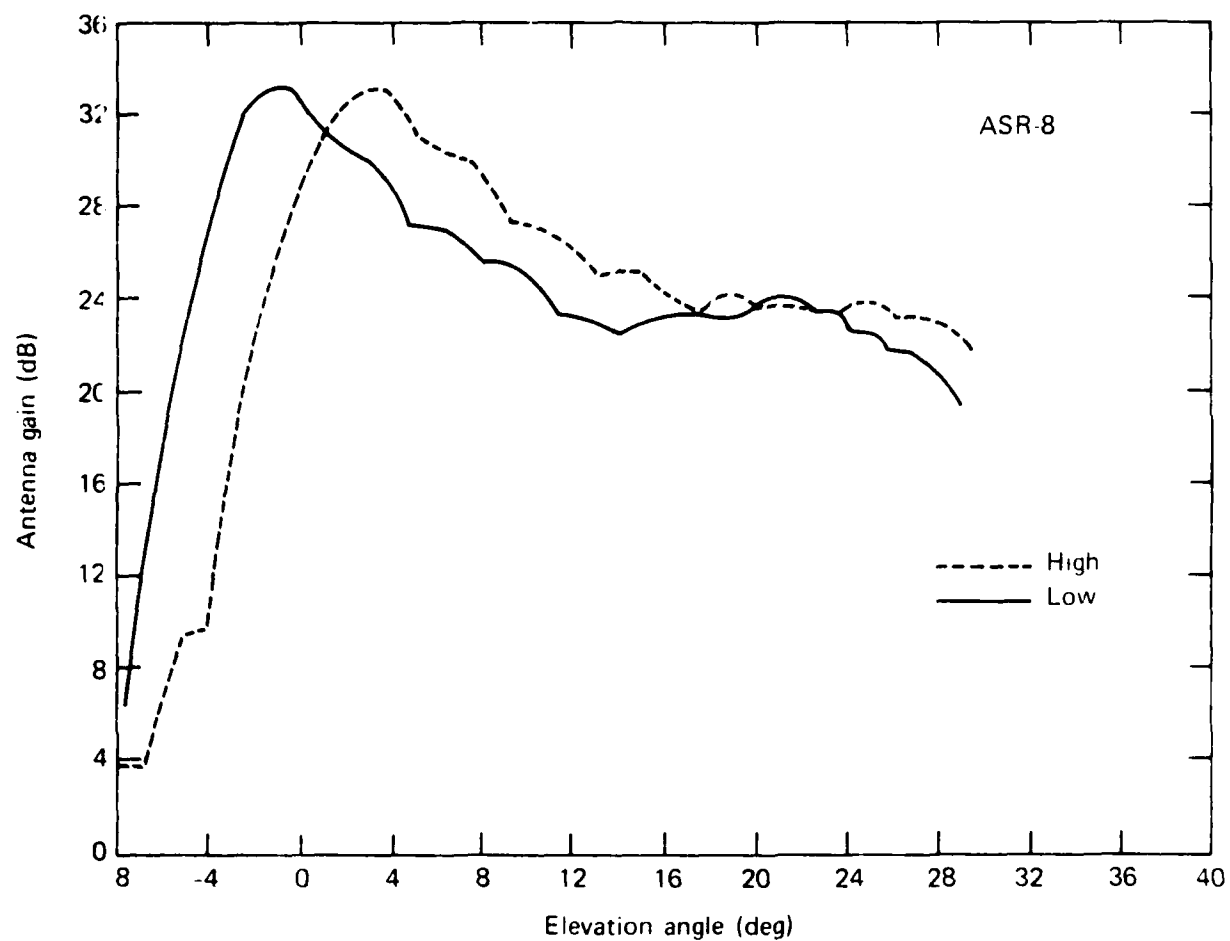


Figure B-5. Antenna gain pattern for ASR-8 versus relative elevation angle. High and low beams shown.

Appendix C

ATC ENROUTE WEATHER DETECTION

This appendix is a report written by W. Goodchild of NAFEC which documents the weather measurement experiment performed in Oklahoma during September and October 1977.

DATA REPORT

ATC ENROUTE WEATHER DETECTION

PROJECT NO. 021-241-130

By

W. Goodchild, ANA-180

SEPTEMBER 1978

# TABLE OF CONTENTS

	Page
DISCUSSION	1
TEST CONDUCTED	2
General	2
Antenna Polarization	2
Sensitivity Time Control	3
Signal Attenuation (MTI dynamic range)	3
MTI Velocity Response	4
Data Forwarded to APL for Analysis	4
RESULTS	4

DISCUSSION

From late August 1977 to November 1, 1977, simultaneous comparative radar weather data was collected by NAFEC and National Severe Storm Laboratory (NSSL) personnel. This data was collected from a typical WSR-57 radar which is used extensively by National Weather Service (NWS) for severe weather detection, etc., and from a typical ARSR-1 radar which is used by FAA primarily for aircraft surveillance. The WSR-57 was situated at NSSL in Norman, Oklahoma and the ARSR-1 was located at FAA Aeronautical Center in Oklahoma City. The Aeronautical Center is located approximately 12 nautical miles northwest of NSSL.

Both the WSR-57 and ARSR-1 radars were operated with established radar parameters. A dual channel video recorder was added to the instrumentation already available at both sites for simultaneous data collection. Channel 1 of both recorders recorded the intensity of the weather (log video output of the radar). The log video output of the ARSR-1 was recorded at the output of the Cardion modification. The log video output of both radars had at least 65 dB of linear dynamic range. Channel 2 of the recorder at NSSL recorded the elevation of the WSR-57 antenna. This information was recorded so that the vertical profile of weather cells could be determined. On channel 2 of the recorder at the ARSR-1 site, the moving target indicator (MTI) video was recorded. The dynamic range of the MTI video was 25 dB. The auxiliary channels of both recorders recorded time (for simultaneous comparisons), range, and azimuth information. Photographs were also taken at both sites as secondary data. At NSSL, the output of the Video Integrator Processor (VIP) was photographed. This provided six levels of weather intensity information on photographs. At the ARSR-1 site, photographs were also taken but since no VIP was available there was no level information on the photographs. Figures 1 and 2 are block diagram of data collection configurations.

Approximately 20 hours of weather data were gathered at both sites. Weather information was recorded on a total of six different days. The weather data that was collected was observed to be from different types of precipitation structures, including isolated air mass showers, squall lines accompanying a front, thunderstorms, and stratiform rain.

In an attempt to determine if the ARSR-1 can be used simultaneously for weather and aircraft detection without degradation to either, the ARSR-1 was operated in several different modes during the weather data collection. The weather data collected under these different conditions was recorded for a comparison with the weather data collected simultaneously at NSSL.

Standard calibration procedures were performed on both radar systems throughout the test period. Sunstroke data was collected to permit accurate registration of the data from the two radar sites. Receiver sensitivity data was collected using the video tape recorders to provide accurate calibration of the video radar data tapes.

Upon completion of the data collection, the video recordings were returned to NAFEC for digitizing. The video recordings were played back into a dual channel Video Quantizer and Recorder (VQR) with the output being recorded on a high speed digital recorder. These digital recordings were then sent to the Applied Physics Laboratory (APL) for analysis. The analog video recordings were also used at NAFEC to determine the capability of the Weather and Fixed Map Unit (WFMU) to accurately depict weather under the phase 2 portion of this project.

### TESTS CONDUCTED

#### GENERAL

Several radar parameters greatly effect the display of weather versus aircraft targets. Antenna polarization, MTI velocity response, sensitivity time control, and weather detection over ground clutter were each the subject of individual and combined data collection efforts under this project. Table 1 lists the various test combinations for which data was collected. Each of the above parameters/tests is discussed below. A further chronological breakdown of data taken and available for analysis is given in table 2.

Comparative WSR-57 weather data was collected for each of the ARSR-1 data segments listed in table 2 and is retrievable using the same data/tape/time information.

#### ANTENNA POLARIZATION

This test was performed for determination of the effects of polarization on weather detection and to investigate use of the orthogonal circular polarization (OCP) signal to provide dedicated weather information.

The effects of antenna polarization on aircraft and weather detection are well known. If weather conditions are present, it is common practice to use circular polarization (CP) which will reduce the weather signal level by approximately 16 dB (the amount of decrease depends upon the sphericity of the rain drops) while to a lesser degree (2 to 6 dB) reducing the signal returns from aircraft. The level and real extent of weather returns (desired for weather formatting and display) thus become unknown when using CP. However, it is possible in the case of the ARSR-1 polarizer to use the OCP (reverse polarized) signal component to provide dedicated weather information of the same amplitude as that available using linear polarization.

Since CP was originally derived to eliminate weather from the radar display, the OCP signal was dissipated into a matched termination. Use of the OCP signal requires that a low power RF path be provided to transmit the OCP signal from the polarizer to the radar receiver. This path includes an extra channel in the rotary joint.

SENSITIVITY TIME CONTROL

This test was designed to determine the optimum STC characteristic for the detection of aircraft versus weather. Two different STC values were used. They were the inverse of the second power of the range ( $R^{-2}$ ) extending to 80 nautical miles (nmi) and the inverse of the fourth power of the range ( $R^{-4}$ ) extending to 50 nmi. An  $R^{-4}$  curve provides range normalization for discrete targets signals since their signal power decreases in a fourth power relationship with range. However, since weather exhibits an antenna beam filling characteristic, its return signal power decreases in a second power manner with range. Thus, an inverse fourth power curve, while providing optimum discrete target range normalization and detection, overly attenuates weather signals. A second power curve while providing optimum weather detection doesn't correctly normalize aircraft signals and, in addition, allows excessive ground clutter signals into the radar receiver/processor. This excessive input of spurious signals will ultimately result in a higher false alarm rate into the common digitizer.

The  $R^{-2}$  maximum range value (80 nmi) was chosen due to the effect of the curvature of the earth on the detection of radar signals. That is, while in some cases the most intense portion of a weather cell is close to the ground, for a weather cell at 100 nmi only those portions above 6000 ft elevation could be observed with the radar. This problem gets worse with increased range making such long range weather data unreliable. Therefore, only the data within approximately 100 nmi of the radar site was used and the STC curve was adjusted accordingly. The  $R^{-4}$  curve is representative of those in general use in the FAA.

An additional feature of this data collection sequence is that the  $R^{-2}$  curve for weather extends further in range than the typical  $R^{-4}$  curve. This results in a crossover phenomenon resulting in the  $R^{-2}$  curve having greater attenuation than the  $R^{-4}$  curve at long ranges and less at short ranges. Table 1 lists the various tests conducted to collect data relative to the two STC curves and other pertinent radar parameters.

SIGNAL ATTENUATION

The next category of data listed in table 1 relates to signal attenuation. This test was designed to enhance detection of weather over ground clutter. MTI systems in use with current FAA radars utilize limiting of the intermediate frequency signals prior to phase detection. This is done to keep the signals within the dynamic range of the cancellers thereby keeping ground clutter residue to a minimum. However, this limiting also reduces the amount of weather available for display. By attenuating the radar receiver signals prior to limiting, additional useful weather information may be available. The tests listed in table 1 show the various configurations tested and the amount of attenuation used to provide the desired data for analysis.



#### MTI VELOCITY RESPONSE

The last category of data in table 1 was taken with respect to system MTI velocity response. The maximum setting shown provided the greatest possible narrowing of the MTI filter low radial velocity band reject notch. This provided the maximum amount of weather information for analysis while still rejecting ground clutter. Data was collected for analysis for the related configurations shown in table 1.

#### DATA FORWARDED TO APL FOR ANALYSIS

The above lists of data collected were forwarded to APL along with the weather cell photographs taken at the time of data collection. Based on this information, the weather data windows shown in table 3 were selected for digitizing at NAFEC. The data reduction configuration shown in figure 3 was used to provide the desired digital tapes. The data shown in table 3 were forwarded to APL. Calibration data from both radars, azimuth correction (offset) data, and ground clutter levels with STC 1 (R-4) and STC 2 (R-2) were furnished.

#### RESULTS

1. Seven comparative ARSR-1/WSR-57 weather window data tape pairs were forwarded to APL for analysis along with the necessary calibration information.
2. Video data tapes were made for studies of the weather quantization and display capabilities of the WFMU at NAFEC.

This evaluation was conducted in response to 9550-AAT-100-33 "Provide Improved Display of Weather Data on Radar Displays," dated August 29, 1975; Subprogram 021-241, sponsored by ARD-243, Mr. Kenneth Coonley. This project number is 021-241-130, the NAFEC Program Manager is Ronald Bassford. Further information can be obtained from William D. Goodchild, ANA-180 (609) 641-8200, extension 2396.

### TABLE 1. ARSR-1 TEST CONFIGURATIONS

[illegible]

**Darkened area indicates test conducted.**

TABLE 2. ARSR-1 WEATHER DATA

Date	Tape Number	Test Number	Time
9/13/77	1	6	1111
		14	1122
		15	1126
		16	1130
		2	1132
9/13/77	2	6	1207
		3	1211
		2	1217
		3	1221
		3	1226
9/22/77	1	1	1530
		2	1534
		3	1539
		1	1544
		2	1548
9/22/77	2	3	1552
		10	1636
		10	1640
		10	1644
		10	1648
		10	1653
		10	1657
9/23/77	1	10	1700
		1	1335
		6	1339
		12	1344
		17	1348
		17	1352
9/23/77	2	18	1356
		1	1412
		6	1416
		15	1420
		10	1424
		12	1428
		18	1432
		6	1437

TABLE 2. ARSR-1 WEATHER DATA (CONTINUED)

Date	Tape Number	Test Number	Time
9/23/77	3	6	1458
		1	1502
		2	1506
		3	1511
		1	1515
		6	1518
		10	1522
9/23/77	4	6	1546
		1	1550
		12	1554
		18	1558
		1	1602
		6	1604
		1	1608
9/28/77	1	7	931
		8	932
		9	933
		1	937
		1.5	937
		12	939
		1	941
		1.5	943
		1	945
		12	948
		10	949
		1	953
		1.5	954
9/28/77	2	1	1012
		1.5	1014
		12	1016
		1	1019
		1.5	1021
		12	1023
		3	1026
		1	1030
		1.5	1032
		12	1034
		1	1037

TABLE 2. ARSR-1 WEATHER DATA (CONTINUED)

Date	Tape Number	Test Number	Time
9/28/77	3	Calibration	-
9/28/77	4	1	1506
		7	1509
		8	1512
		9	1515
		6	1518
		1.5	1523
		12	1527
9/28/77	5	1	1554
		7	1557
		8	1600
		9	1603
		1.5	1606
		12	1610
9/28/77	6	1	1634
		7	1637
		8	1640
		15	1643
		1	1646
		1.5	1649
		7	1653
		1	1656
		6	1700
9/28/77	7	1	2100
		2	2103
		1.5	2106
		10	2109
		14	2113
		1	2116
		1.5	2119
		12	2122
9/28/77	8	1	2142
		14	2145
		2	2147
		1.5	2150
		10	2152
		1	2156
		3	2159
		14	2201
		1.5	2204
		12	2207

TABLE 2. ARSR-1 WEATHER DATA (CONTINUED)

Date	Tape Number	Test Number	Time
9/28/77	9	7	2220
		8	2223
		9	2226
		6	2229
		15	2232
		12	2235
		1	2239
		1.5	2242
		1	2246
9/28/77	10	1	2332
		7	2339
		8	2341
		9	2344
		1	2346
		1.5	2351
		1	2355
10/4/77	1	1	1247
		7	1251
		8	1254
		9	1257
		1	1300
		1.5	1303
		12	1306
		12	1309
		7	1312
10/4/77	2	8	1320
		9	1323
		1	1326
		7	1329
		8	1331
		9	1334
		1	1337
		1.5	1340
10/4/77	3	1	1356
		7	1359
		8	1402
		9	1406
		1	1409
		3	1412
		8	1418
		7	1421

TABLE 2. ARSR-1 WEATHER DATA (CONTINUED)

Date	Tape Number	Test Number	Time
10/7/77	1	7	1901
		8	1903
		9	1905
		1	1907
		1.5	1910
		7	1912
		8	1914
		9	1916
		7	1918
		1	1920
10/7/77	2	7	1935
		8	1937
		9	1939
		1	1941
		1.5	1943
		12	1947
		7	1950
		8	1952
		9	1954
		1	1956
		7	1958
10/7/77	3	7	2007
		8	2011
		9	2014
		1	2017
		7	2020
		7	2023
		8	2026
		9	2029
		1	2032
10/7/77	4	1	2049
		7	2052
		8	2055
		9	2058
		1.5	2103
		12	2107
		1	2113

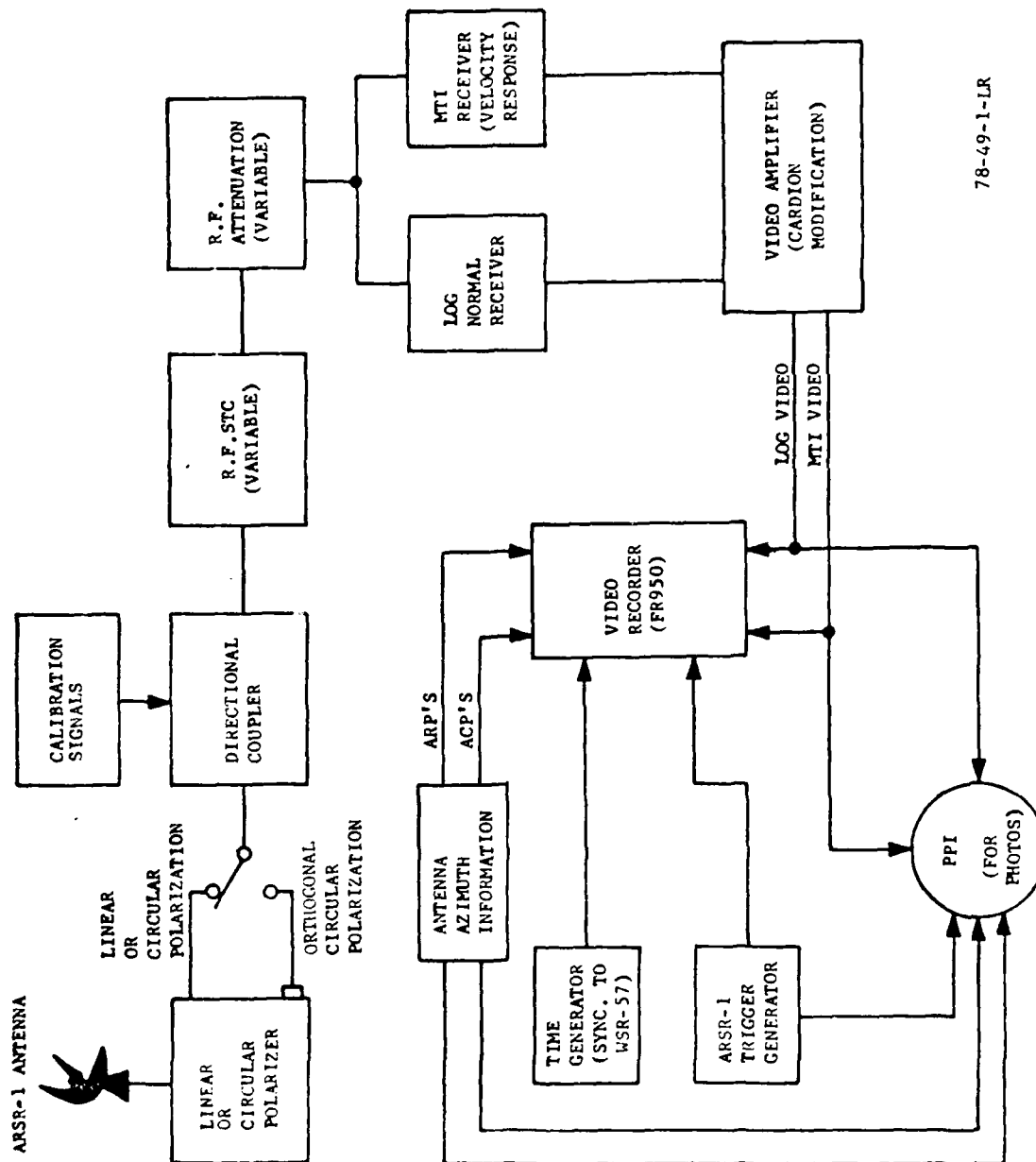


TABLE 2. ARSR-1 WEATHER DATA (CONTINUED)

Date	Tape Number	Test Number	Time
10/7/77	5	7	2131
		8	2135
		9	2138
		1	2141
		1.5	2144
		12	2147
		8	2154

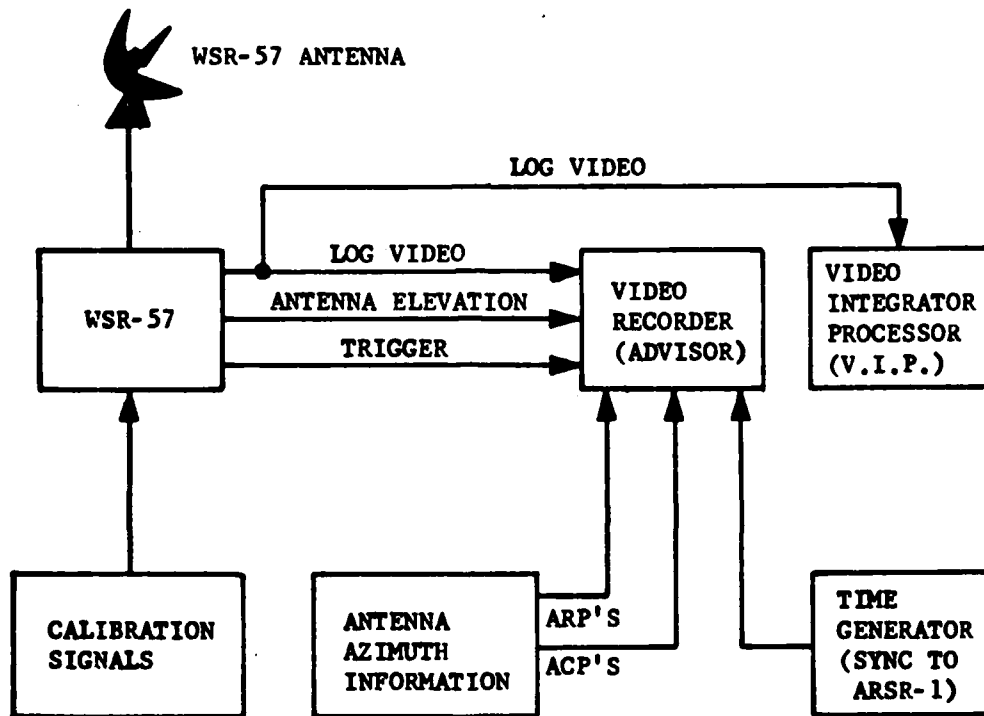
TABLE 3. DATA PROVIDED TO APPLIED PHYSICS LABORATORY

VQR Window (Number)	Date	Time	ARSR-1 Range Azimuth	WSR-57 Range Azimuth	Test Number
1	9/28/77	2142	31 miles 266°	40 miles 274°	1
2	9/28/77	2142	98 miles 34°	100 miles 28°	1
3	10/7/77	1936	58 miles 18°	64 miles 10°	7
		1942	59 miles 19°	64 miles 10°	1
4	9/28/77	2109	45 miles 276°	55 miles 283°	10
5	10/4/77	1326	34 miles 238°	40 miles 254°	1
6	9/28/77	2220	6 miles 270°	17 miles 300°	7
7	10/4/77	1329	6 miles 270°	17 miles 299°	7



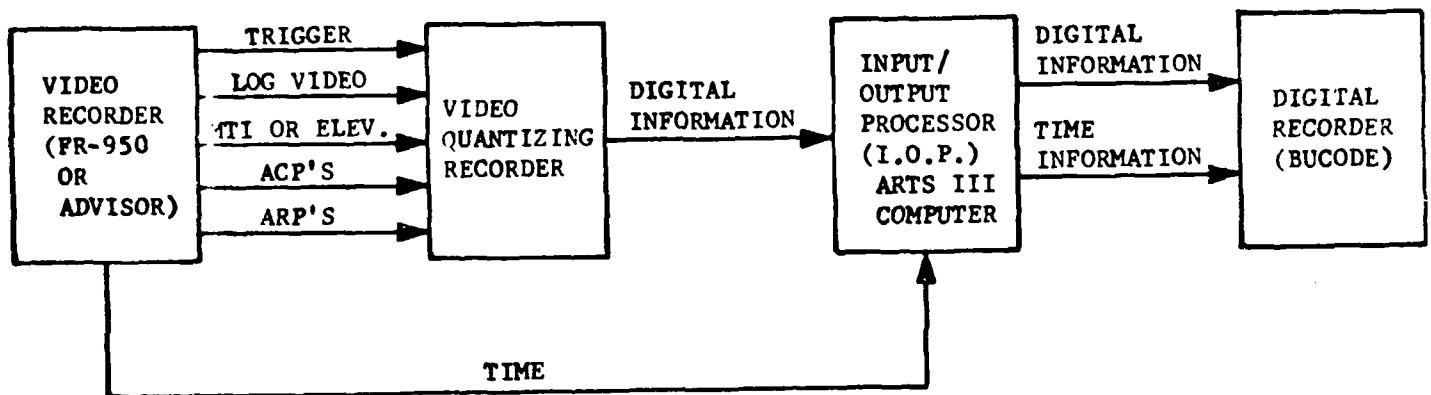
78-49-1-LR

FIGURE 1. ARSR-1 DATA COLLECTION CONFIGURATION



78-49-2-LR

FIGURE 2. WSR-57 DATA COLLECTION CONFIGURATION



78-49-3-LR

FIGURE 3. NAFEC DATA REDUCTION CONFIGURATION

## Appendix D

### THE EFFECT OF GROUND REFLECTIONS ON WEATHER REFLECTIVITY MEASUREMENTS

#### INTRODUCTION

During 1977, an experiment was run in Oklahoma where a Federal Aviation Administration (FAA) ARSR-1D was used to measure storm reflectivity simultaneously with a National Weather Service (NWS) WSR-57, as described previously in the body of this report. The purpose of the experiment was to evaluate the ARSR-1D's capability to measure weather. The analysis of the experimental data indicated that the ARSR-1D reflectivity values were, on the average, 4 dBZ higher than the WSR-57 for six storms located at ranges between 55 (29.7) and 180 km (97 nmi). In searching for the source of this difference, Ken Coonley of the FAA suggested that the ARSR-1D signal may have been enhanced due to reflected energy from the surface. Reflected energy was a consideration since the ARSR-1D was positioned with maximum gain at 3/4° elevation during the experiment. This positioning directs a considerable amount of energy to the ground.

The analysis reported herein was performed to determine whether ground reflected power could account for a portion of the 4 dBZ enhancement of the ARSR-1D measured values.

#### THEORY

The electric field illuminating an object at some slant range  $R$  from a transmitter can be expressed as (see Figure D-1)

$$E = \frac{k \sqrt{G_t P_t}}{R} \cos \left[ \omega \left( t - \frac{R}{c} \right) \right] \quad (D.1)$$

where

$G_t$  = transmitted gain

$R$  = direct path length

$P_t$  = transmitted power

$K$  = a constant which depends on the radiating source

$c$  = speed of light

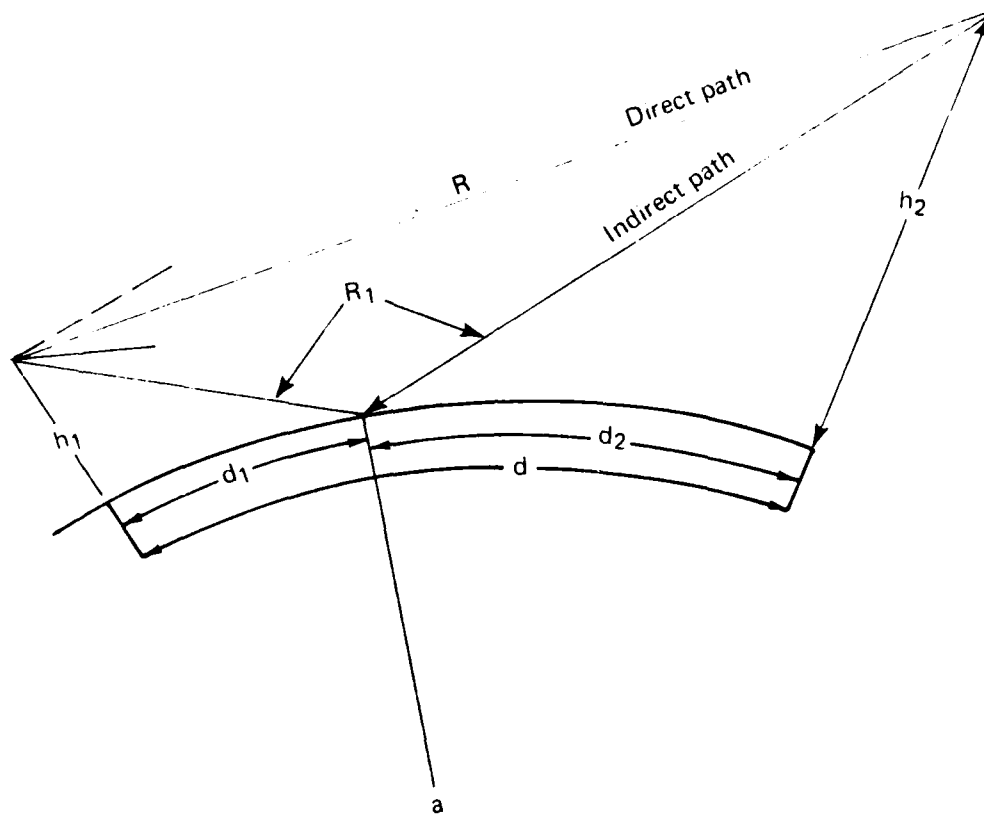


Figure D-1. Geometry showing direct and indirect ray paths.

If the transmitter has a beam shape such that a portion of the transmitted beam illuminates the surface, then the power incident at the target is the sum of the energy transmitted along R and that transmitted along  $R_1$  (i.e., reflected from the ground). This combined field is

$$E = \frac{K \sqrt{G_T P_t}}{R} \sqrt{(1-R')^2 + 4R' \cos^2\left(\frac{\theta}{2}\right)} \quad (D.2)$$

where

$$R' = \frac{R}{R_1} \sqrt{G_T'/G_T} \rho D$$

$G_T'$  = gain transmitted along indirect path

$\rho$  = surface reflection coefficient

D = divergence factor (to be discussed)

R = direct path length

$R_1$  = indirect path length

$$\theta = \frac{2\pi f \Delta}{c} + \psi = \frac{2\pi \Delta}{\lambda} + \psi \quad (D.3)$$

where

$\lambda$  = wavelength

$\psi$  = phase angle

$\Delta$  = path length difference for a curved earth

f = frequency

In order to determine  $\Delta$  for a curved earth we use the following approach from References D-1 and D-2.

$$\text{Let } u = \frac{h_2}{h_1} \quad \text{and} \quad v = \frac{d}{\sqrt{2a h_1}}$$

where

a = a modified earth's radius (i.e., 4/3 earth was used in this analysis)

$h_1$  = height of the antenna



$h_2$  = height of some point in a storm

$d$  = ground range to the storm

Consider a parameter  $S$  which is defined as

$$S = \frac{d_1}{d} \quad (\text{see Figure D-1 for } d_1) \quad (D.4)$$

This parameter  $S$  is the root of the equation

$$S^3 - \frac{3}{2} S^2 - \frac{S}{2} \left( \frac{1+u}{v^2} - 1 \right) + \frac{1}{2v^2} = 0 \quad (D.5)$$

Solving this equation for  $S$  we can find the path difference

$$\Delta = \frac{h_1 \sqrt{2a h_1}}{a} \left[ (1-S) \frac{(1-S^2 v^2)^2}{S v} \right] \quad (D.6)$$

$S$  is also used to compute a divergence factor. When a ray illuminates the surface the beam may spread depending on the geometry, causing a decrease in the intensity of energy reflected from the surface. We must, therefore, multiply the reflection coefficient,  $\rho$ , by a parameter  $D$ .  $D$  is given by the equation

$$D = \frac{1}{\sqrt{1 + \frac{4(S v)^2 (1-S)}{1 - (S v)^2}}} \quad (D.7)$$

Having  $\Delta$  and  $D$ , the field in Eq. (D.2) can be computed. The pattern of energy that would be incident on a storm at 40 km (21.6 nmi) is shown in Figure D-2. Plotted in that figure is the quantity under the square root in Eq. (D.2). This field is called the interference pattern. One should observe that at certain altitudes the direct and indirect paths add to give twice the amplitude and in other cases they subtract to create a null

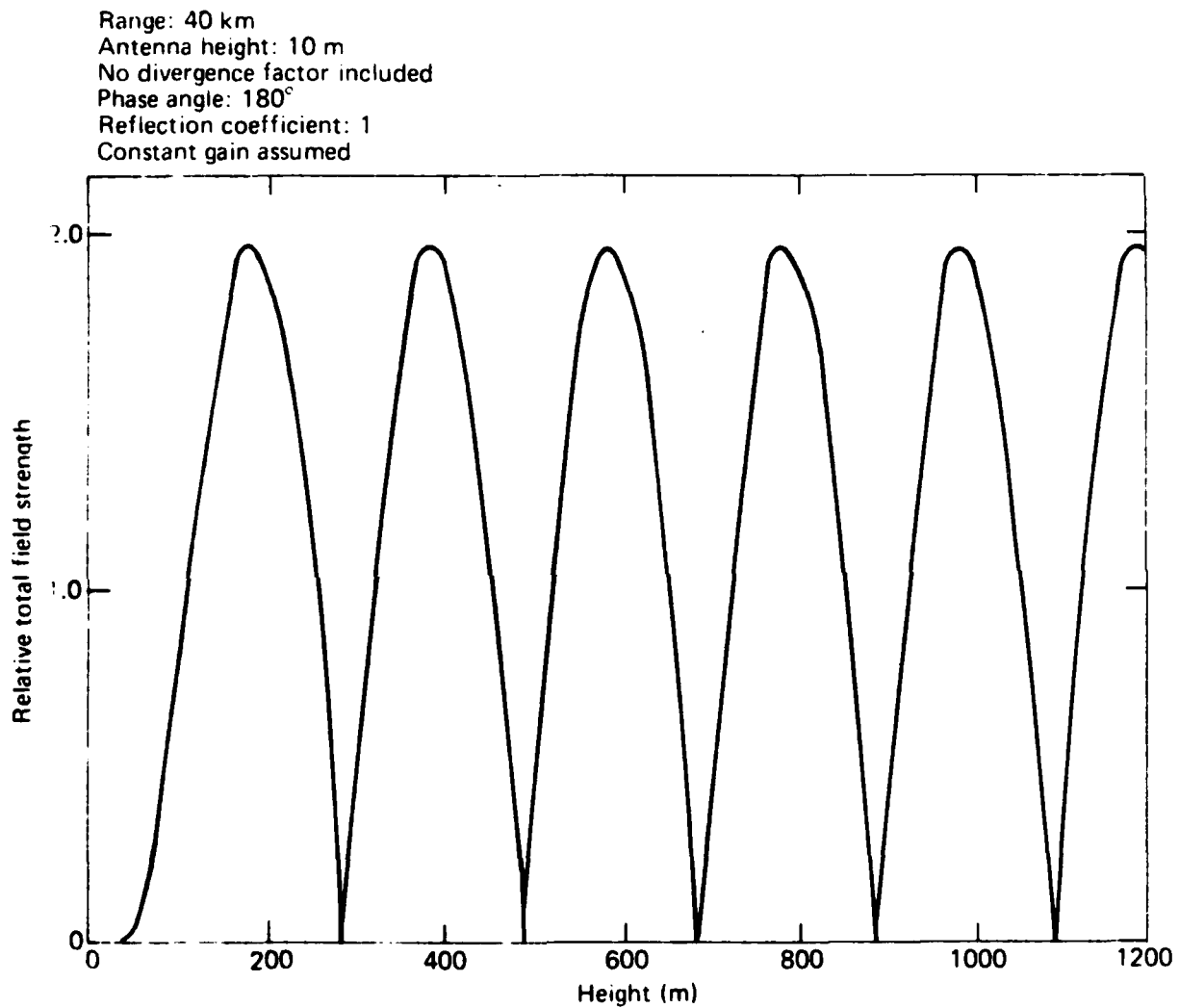


Figure D-2. Relative field strength of the sum of direct and indirect rays illuminating a storm at 40 km for the ARSR-1D positioned with maximum gain at  $3/4^\circ$  elevation.

field at that altitude. Figure D-2 is meant to show the lobing pattern and assumes equal gain along both paths with no divergence.

We wish to investigate the effect this interference pattern may have on a storm positioned at various ranges.

#### TOTAL POWER

Let us position a storm at ground range,  $d$ , and examine the total power received from a slice of the storm such as that pictured in Figure D-3. In the computation we divide the storm cell into height intervals  $\Delta h$  and compute the power received from each small pulse volume. The power received from only the direct path can be expressed as

$$P_r(h)_{\text{direct}} = \frac{K_p Z(h) G_T(h) G_R(h)}{R^2} \quad (\text{D.8})$$

where

$$K_p = \frac{P_t \pi^3 \theta c\tau |K|^2 L_T}{512 \lambda^2}$$

and  $P_t$  is the transmitted power,  $\theta$  is the horizontal beamwidth,  $c\tau/2$  is the range resolution,  $|K|^2$  is a function of the complex index of refraction and  $L_T$  is the radar losses.

The power received from the combined direct and indirect path is Eq. (D.8) multiplied by the square of the quantity under the square root sign in Eq. (D.2).

$$P_r(h)_{\text{total}} = \frac{K_p}{R^2} Z(h) G_T(h) G_R(h) \left\{ (1-R')^2 + 4R' \cos^2\left(\frac{\theta}{2}\right) \right\} \quad (\text{D.9})$$

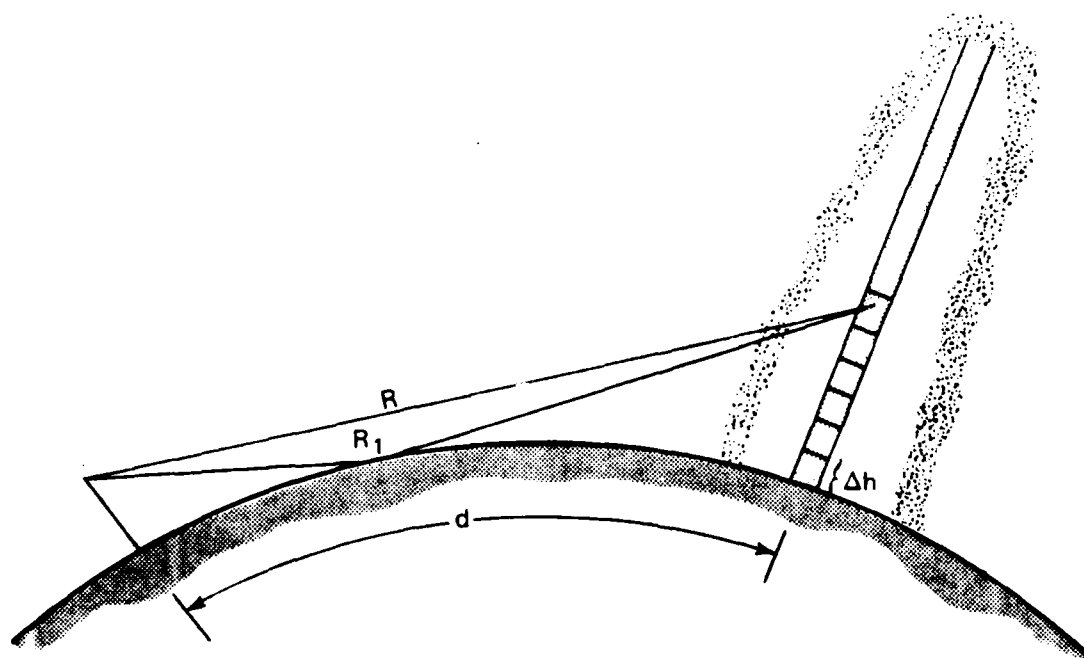


Figure D-3. Sketch showing direct and indirect rays illuminating a storm cell at ground range  $d$ .

Eq. (D.9) represents the total power that would be received from the two paths and includes the effect of the reflected ray. This effect is controlled in the equation by the quantity in brackets.

#### DISCUSSION

Eqs. (D.8) and (D.9) were computed for a profile by positioning the profile at various ranges. Since the interest in this analysis lies in the difference between the total and direct power, the shape and magnitude of the Z profile is of no importance as will be seen later.

Throughout the analysis a ground reflection coefficient  $\rho = 1$  has been used along with a phase angle of  $180^\circ$ . The  $\rho$  value represents a worst case, which means that the difference between the total power and the direct power will not be greater for any other reflection coefficient. Since an integrated power effect is being sought here, the phase angle simply acts as a reference angle for the lobing structure. A value of  $180^\circ$  was used throughout the analysis. It appears that at the ARSR-1D frequency and horizontal polarization a reflection coefficient close to 1 and phase angle of  $180^\circ$  may be expected.

Figures D-4 through D-6 show plots of

$$\sum_h P_r(h)_{\text{direct}} \Delta h \quad \text{and} \quad \sum_h P_r(h)_{\text{total}} \Delta h$$

at three ranges 40, 80, and 120 km. These curves were computed for  $\Delta h = 10$  meters and to the altitude for which the difference  $\sum P_{r_{\text{total}}} - \sum P_{r_{\text{direct}}}$  became constant.

Consider Figure D-4, the difference in the two curves is small, below 130 m (426 ft). The difference then increases up to 210 meters (689 ft). Note that the summed power for the

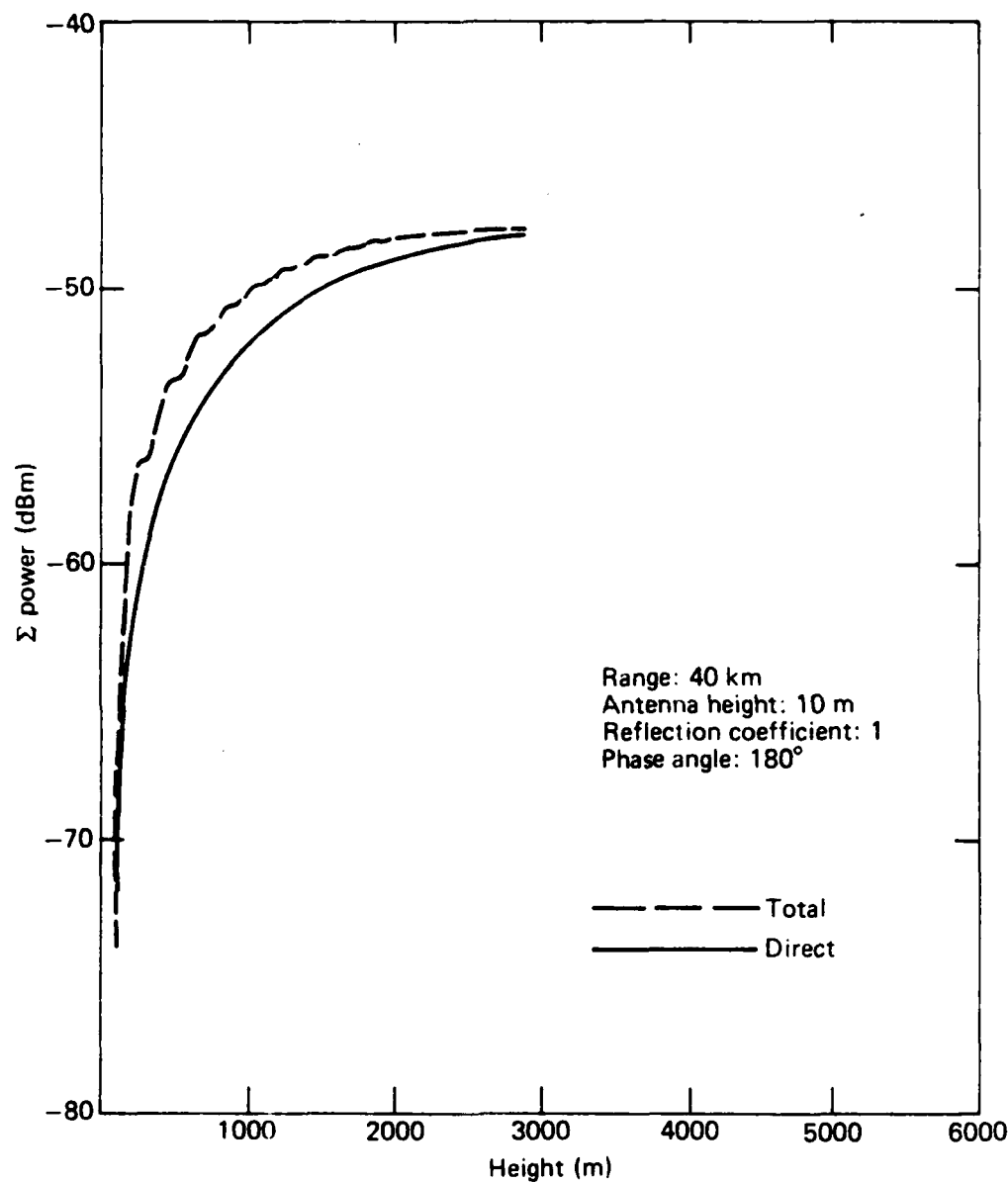


Figure D-4. Integrated power at 40 km range versus Z height for ARSR-1D radar positioned with maximum gain at 3/4° elevation. Direct and total (direct plus indirect) paths are shown.

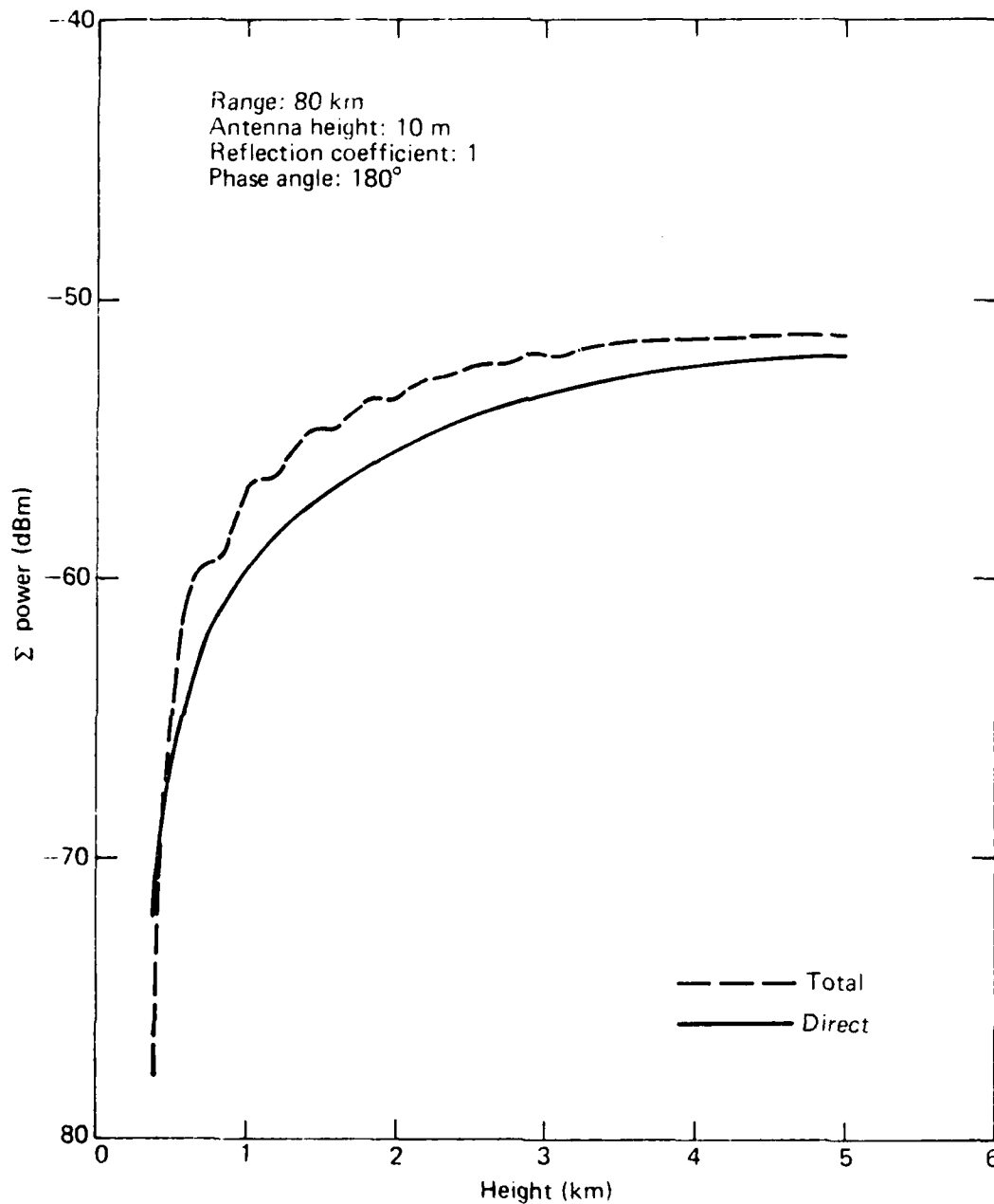


Figure D-5. Integrated power at 80 km range versus  $z$  height for ARSR-1D radar positioned with maximum gain at  $3/4^\circ$  elevation. Direct and total (direct plus indirect) paths are shown.

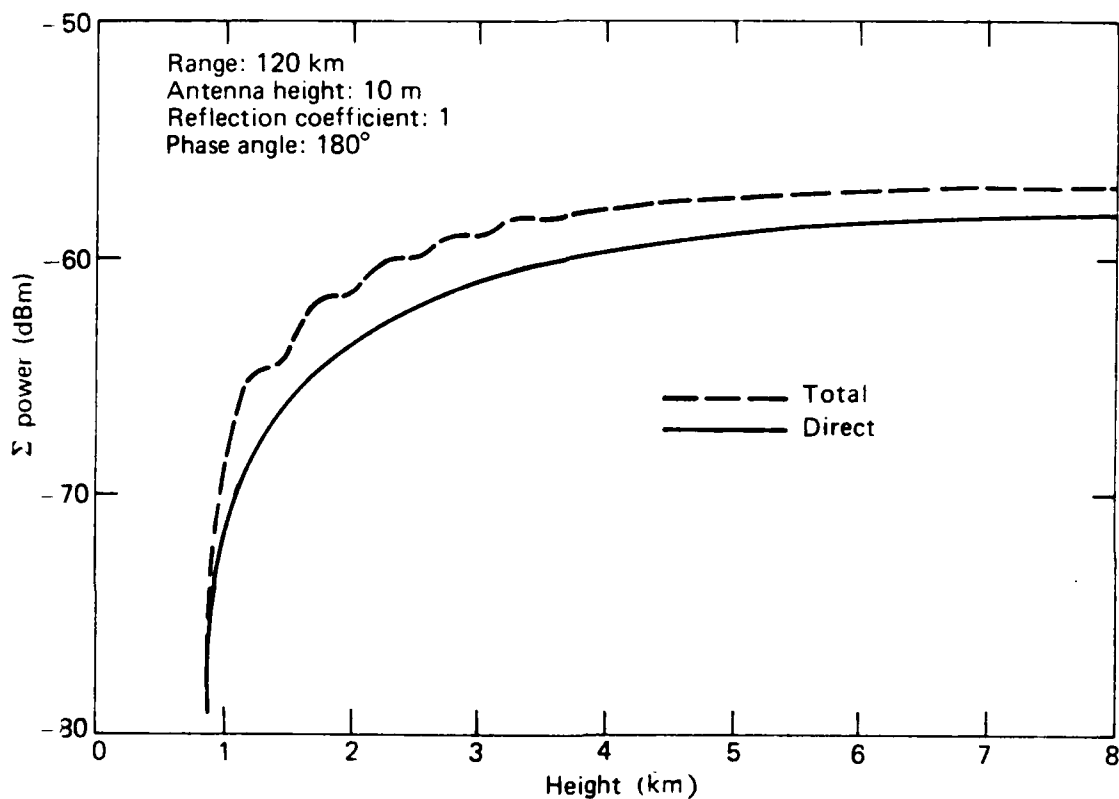


Figure D-6. Integrated power at 120 km range versus  $z$  height for ARSR-1D radar positioned with maximum gain at  $3/4^\circ$  elevation. Direct and total (direct plus indirect) paths are shown.



total has an oscillation in it. This oscillation is due to the interference pattern. That is, when the altitude interval is in a null no power is added to the summation. When a peak is within the altitude interval, power is added to the summation. Therefore, the flattened portions of the total power curve correspond to the nulls of the interference pattern.

As the power is summed higher in altitude, the indirect path no longer affects the power and the difference between the two becomes nearly constant. The same general trend is seen for 80 (43) and 120 km (65 nmi) except that the maximum difference is greater and occurs at different altitudes.

The ratio of the  $\sum$ total power to  $\sum$ direct power is

$$P' = \frac{\sum G_T'(h)}{\sum G_T(h)} \left\{ (1-R')^2 + 4R' \cos^2 \frac{\theta}{2} \right\}$$

This ratio is independent of reflectivity,  $Z$ . It is, however, dependent on range and storm height since these parameters are included in the computation of the quantities in brackets. The quantity  $10 \log P'$ , power difference, is shown plotted in Figure D-7 for four ground ranges. The curves for each range start at the radar horizon.

At 40 km (21.6 nmi), if a storm is present which is greater than 2800 m in height, the curve indicates that the power received from the storm will be .45 dB greater than it would be without reflected signals. The curve reaches its maximum at 210 m (689 ft) and decreases with oscillations above that altitude. This maximum at 40 km (21.6 nmi) range would never be measured in the received power unless the storm height were less than 210 m (689 ft) which is highly unlikely. Considering the fact that most severe storms are greater than 5 km in height, the curves indicate that the potential increase in received power would range between .5 and 2.4 dB for ranges up to 200 km (108 nmi).

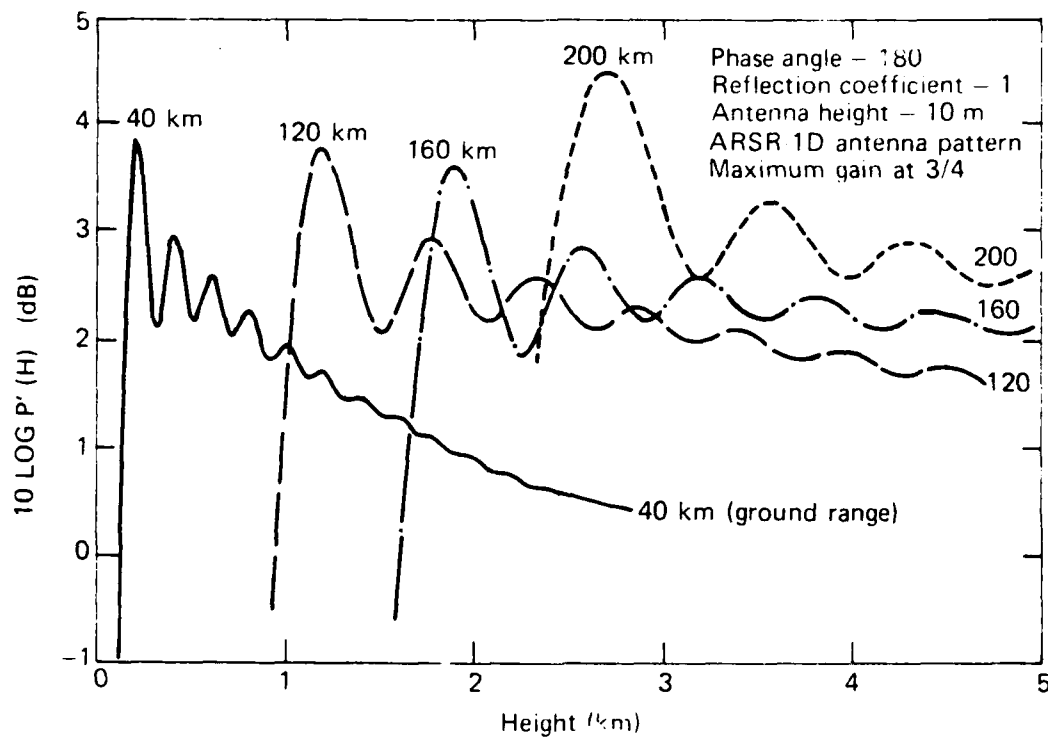


Figure D-7. The power difference  $10 \log P'(H)$  versus height of storm for the ARSR-1D radar.

The difference plotted in Figure D-7 increases with range. This effect is due to the fact that as the range increases the depression angle of the reflected ray becomes smaller and thus the portion of the gain pattern incident on the rain would be closer to the maximum gain. The result of this is that the quantity  $P'$  in Eq. (D.2) is closer to 1 and the difference between the direct and total integrated power at 5 km height increases.

Figures D-4 through D-7 were computed for the ARSR-1D antenna. It is expected that other ARSR radars with narrower beamwidths would show less increase in signal, with the magnitude depending upon antenna tilt.

For comparison, the antenna pattern for the WSR-57 was run through the program with its maximum gain positioned at  $1/2^\circ$  and  $0^\circ$ . These results are shown in Figure D-8 and indicate that for  $1/2^\circ$  positioning of the maximum there would be a small increase in power for profiles at 40 (21.6) or 160 km (86 nmi). However, with maximum gain at  $0^\circ$ , a 3 dB increase in received power would be experienced. This is probably of little consequence in WSR operational modes since  $0^\circ$  positioning is probably never used. However, in research radar situations, this increase may be of importance when operating near the horizon.

#### CONCLUSIONS

As pointed out earlier, this analysis was performed to determine whether the 4 dB discrepancy in the Oklahoma experiment could be explained by ground reflections. The discrepancy can only be partially explained in this way for two reasons: (1) The increase in received power due to ground reflected rays is range dependent and no range dependency was evident in the Oklahoma data. However, it is possible that a 1 or 1.5 dB range dependence would not be recognizable. (2) All the Oklahoma data were taken at less than 180 km (97 nmi) range and the largest increase calculated from the analysis is 2.4 dB at 200 km (108 nmi). It is possible that of the 4 dB discrepancy, approximately 2 dB could be explained for the ARSR in this manner.

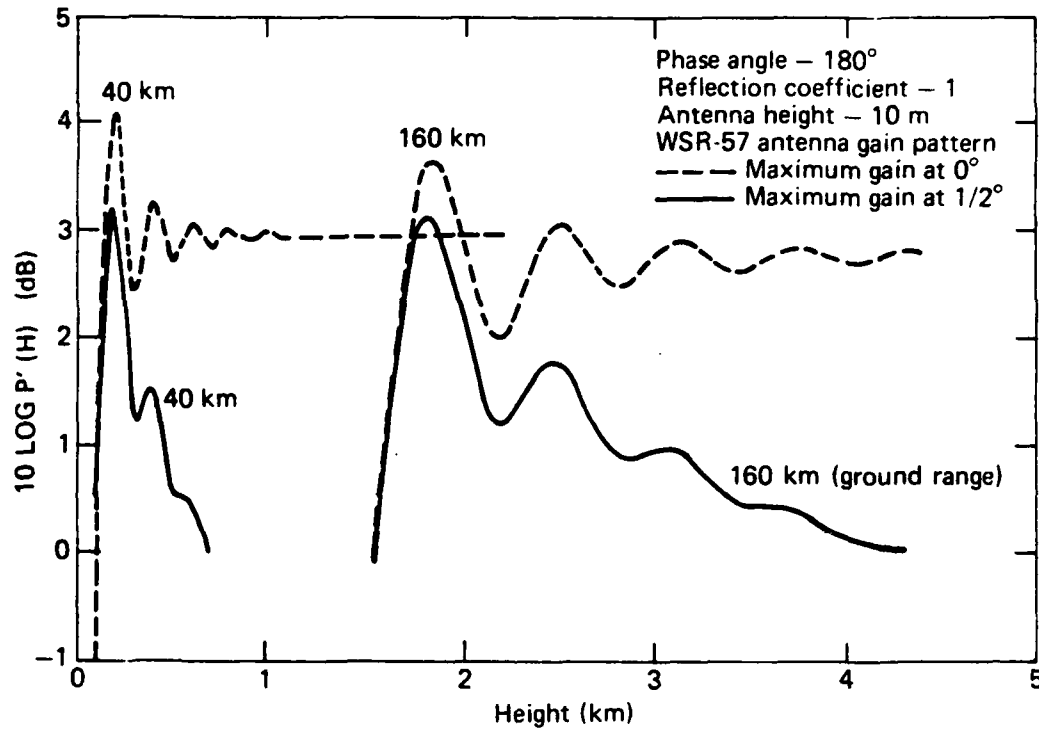


Figure D-8. The power difference  $10 \log P'(H)$  versus height of storm for the WSR-57 radar.

Although this analysis was performed for a specific reason, it should be heeded by those operating radar with maximum gain near the horizon when observing diffuse targets. The potential should be considered. In some cases where the diffuse targets are weak this enhancement may aid in detection capability. In cases where high accuracy is required, a potential error may exist.

REFERENCES

- D-1 David, P. and J. Voge, "Propagation of Waves", Pergamon Press, 1969.
- D-2 "The Propagation of Radio Waves through the Standard Atmosphere", Volume 3, Summary Technical Report of National Defense Research Committee, Washington, D. C., 1946.

REPROD

FILMED

8